BEAM COLLIMATION AND INTENSITY UNIFORMIZATION OF LASER DIODE ARRAY USING LENSLETS

by

Ming Zhang

A thesis submitted to the Graduate Faculty of
Auburn University
in partial fulfillment of the
requirements for the Degree of
Master of Science

Auburn, Alabama
May 5, 2013

Approved by

Hulya Kirkici, Chair, Professor of Electrical and Computer Engineering
Lloyd Stephen Riggs, Professor of Electrical and Computer Engineering
Stanley Reeves, Professor of Electrical and Computer Engineering

Abstract

With the advent of the laser, its applications have been extended to many areas including material processing, such as welding, cutting and drilling; and medical procedures, such as eye surgery and cosmetic skin treatments; and other applications such as lithography, semiconductor manufacturing, optical data processing. Among the many kinds, laser diodes have been the most developed in recent years, due to its multiple features like low cost, compactness, electronic compatibility, broad range of wavelengths, and high Pulse Repetition Frequency values. However, the beams from the laser diodes must be shaped before they can be widely used commercially. This is because the beams produced by the laser diodes are characterized as having elliptical beam spot shape along the transverse directions. Also, the intensity profile is Gaussian, not evenly distributed energy profile as commonly preferred in industry applications.

In this work, a system that reshapes the beams of an array of laser diodes from elliptical shaped to rectangular shaped and from Gaussian energy distribution to uniform energy distribution. The output beam is also collimated. This system employs 4 sets of lenses, either aspheric, cylindrical or lenslets, which treat the light rays respectively in both perpendicular and parallel planes to achieve the goal. Besides, this lenslet technology used in this system can also be applied to multi laser diode sources to generate a single bunch of high-energy and collimated beam with rectangular beam spot shape. In this way, the disadvantage of the low-energy output of the laser diode will be

overcome. In addition, the resultant ray bunches are highly adjustable and can be applied to many more different areas of industrial world. In addition, a detailed derivation process designing the proposed system is shown in this thesis. A series of MATLAB codes are developed to calculate the system parameters according to the derived equations and to simulate the resultant system performance. ZEMAX is also employed to verify the simulation results. A comparison between the simulation results of MATLAB and that of ZEMAX is discussed.

Acknowledgments

The author would like to thank his advisor Dr. Hulya Kirkici, who has been giving so much patience and guidance during the past two and half years that allows the author to finally finish this project. Without her support this project could not come to the current level of performance. The author would like to thank the other two committee members, Dr. Riggs who taught him a lot of knowledge of electromagnetic fields and Dr. Reeves who guided him to gain the knowledge of using MATLAB to do the simulation during the classes. The author also would like to express appreciation to his research group members, thanks for all the helps that they have given to support him. Finally, the author wishes to thank his parents, Guohua Zhang and Jvfen Li, for their consistent encouragement and care, and thank his wife, XiaLi, for her concern and love.

Style manual or journal used Graduate School's Thesis and Dissertation Guide

Computer software used Microsoft Office 2007

Table of Contents

List of Tables

List of Figures

CHAPTER 1

INTRODUCTION & LASER DIODE BEAM

1.1 Introduction

Laser diode is a semiconductor-based coherent light emitting device used to generate analog signals or digital pulses for transmission through optical fibers. Laser emission follows the same principle as other gas or solid-state lasers, except laser diodes are much smaller. The most common type of laser diode is formed from a p-n junction and powered by current injection. In fact, laser diode can be classified as a member of the family of semiconductor p-n junction diodes, and it is fabricated using semiconductor processes just like any other microelectronic chips. A semiconductor laser diode is shown schematically in Figure 1.1, where the gain medium in the middle is surrounded by the guiding layers. The refractive index of the guiding layers is somewhat greater than that of the surrounding regions (substrate and cladding) so that the light can be confined to a relatively narrow region by total internal reflection. The two ends of the diode in the cross direction (x-y plane) are cleaved to form perfectly smooth, parallel edges, forming a Fabry-Perot resonator, and thus an optical cavity is formed. When the electrical current is injected through the positive electrode and collected at the base-plate on the bottom side of the junction (ground electrode), the original stable state of thermal equilibrium of the junction will be disturbed, and electrons can absorb energy either from heat caused by

the collision among the massively increased amount of electrons or from the photons caused by the spontaneous emission which is necessary to initiate the laser oscillation. As a result, there are more electrons in higher energy states than in lower energy states, thus population inversion is achieved in the gain medium within the optical cavity.

When an electron is excited from a lower to a higher energy level, it will not stay that way forever; instead it will go back to the stable state and emit photons. These photons will travel along the waveguide and be reflected several times from each end face before they are emitted out. As the light wave passes through the cavity, it is amplified by the stimulated emission which generates another photon of the same frequency, travelling in the same direction, with the same polarization and phase as the first photon. This is how laser diode works and generates laser light.

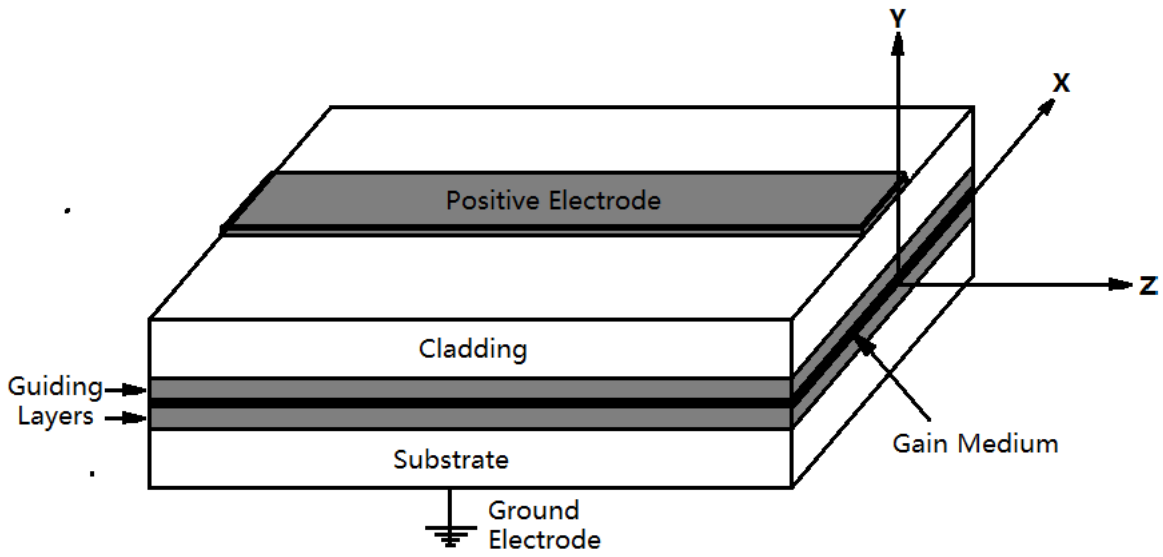

Figure 1.1: A semiconductor laser diode with the p-n junction structure.

1.2 The characteristics of the laser diode beam

One important characteristics of the laser diode beam is the Gaussian irradiance distribution, as shown in Figure 1.2. One difference is that, for laser diodes, the beam has Gaussian distribution with different beam radius in two different transverse directions, as shown in Figure 1.2. The basic principles and characteristics of the laser beams will be discussed in detail in section 3.1.

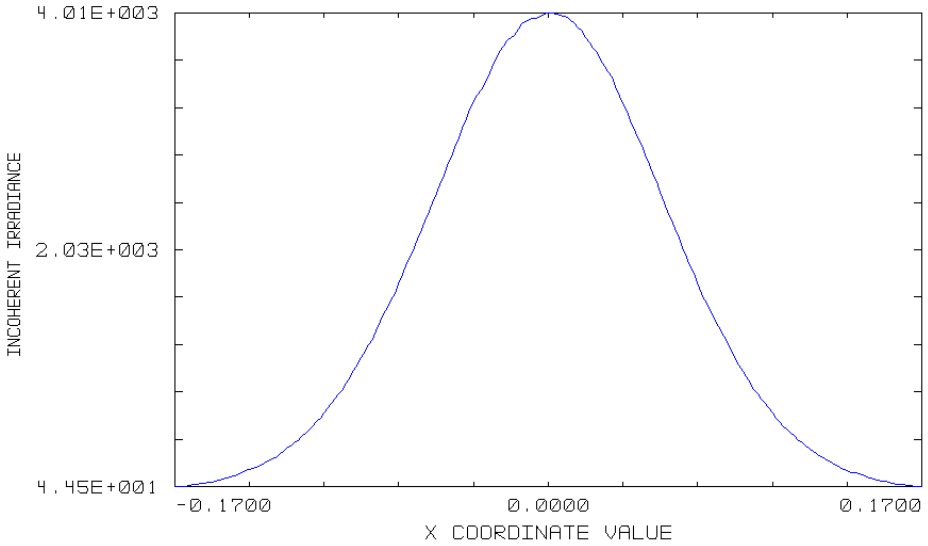

Figure 1.2 (a): Illustration of Gaussian irradiance distribution in x direction at $z = z_0$

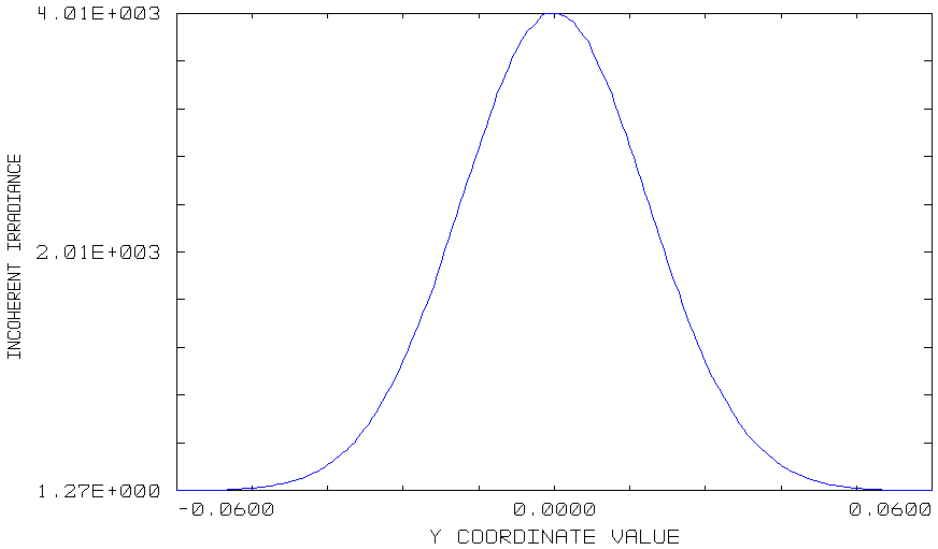

Figure 1.2 (b): Illustration of Gaussian irradiance distribution in y direction at $z = z_0$

The second characteristic of the laser diode beam is the elliptical beam spot shape as shown in Figure 1.4. The divergent angles along the perpendicular transverse direction and along the parallel transverse direction are not same for laser diodes; therefore the beam profile was an elliptical shape. This phenomenon is caused by the structure of the laser diode itself. The working region of the laser diode is actually a thin and wide strip of p-n junction, limiting the active area in the perpendicular transverse direction and allowing a wider active area along the parallel transverse direction.

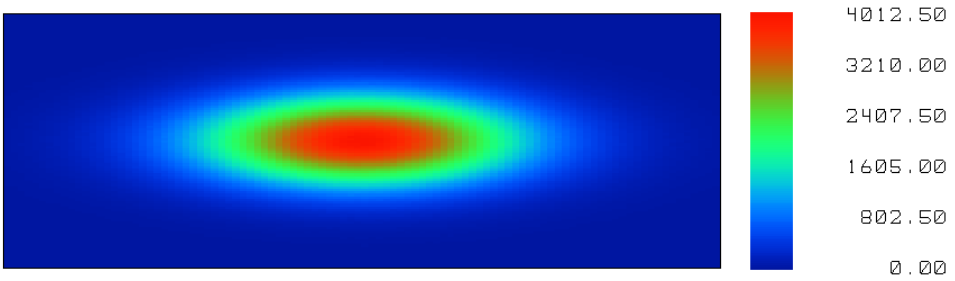

Figure 1.3: Illustration of the elliptical beam spot shape generated by ZEMAX

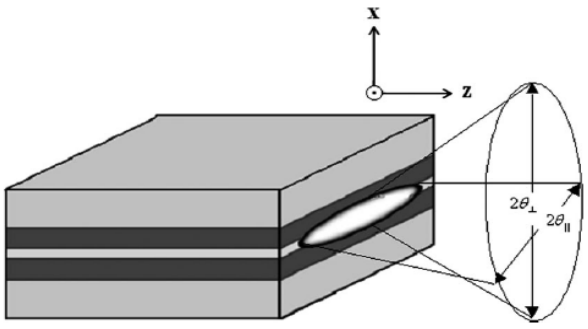

Figure 1.4: Illustration of different divergent angle in x-z and y-z planes [3]

The third characteristic of the laser diode beam is the astigmatism. The cause of astigmatism is the non-uniform gain profile along the y-axis within the active region. As the gain is the strongest near the cavity's central axis, the beam, while propagating along z, in the cavity experiences a "gain focusing" effect resulting a stronger amplification on axis than in the wings [1]. Astigmatism is important for the optical systems designed to

focus the laser beam to a small spot. On the contrary, for most applications where the beam is expanded to cm to m levels and collimated, astigmatism μm levels can be neglected [3].

1.3 The applications of the laser diode and the necessity of beam shaping

Laser diodes are semiconductor lasers and come in many different structures and sizes with laser powers ranging from a few mW to hundreds of watts. The emitted wavelength depends mainly on the semiconductor material of the laser diode cavity. Earlier laser diodes operated in the infrared, but most recent ones cover the full visible spectrum range from blue to red and beyond. Compared to other lasers such as CO_2 and Nd-YAG, semiconductor lasers have the advantages of low cost, compactness, electronic compatibility, broad range of wavelengths, and high Pulse Repetition Frequency (PRF) values. Therefore, they are used in many scientific and commercial applications.

A few of the primary applications include material processing, such as welding, cutting, and drilling. In medical procedures, They are used in corneal surgery and cosmetic skin treatments. Other applications include laser/material interaction studies, lithography, semiconductor manufacturing, graphic arts, optical data processing, and military uses. In addition, laser diode is a perfect source for compact Light Detection and Ranging (LIDAR) systems [2].

However, many of these applications require a certain beam shape such as circular or rectangular, rather than the elliptical beam shape. They also require uniform intensity profile rather than Gaussian intensity profile; and collimated light beams rather than divergent light beams. For example, a very important objective in optical

lithography is to obtain uniform control of the intended critical dimension over the whole imaging field, so the irradiance uniformity are needed to maintain the same exposure latitude at the wafer, the same thing also happens in many other semiconductor manufacture processes [24]. Applications such as nonlinear optics, and optical data (image) processing may require beams with uniform phase as well as amplitude, because they need large depth of field so that the beams can propagate for a considerable distance and remain the same energy profile during the period; LIDAR systems prefer the beams to be collimated and have a circular beam profile. Otherwise at the far field the difference between the radii of the beam in the two directions causes highly elliptical beam shape after long-range propagation and thus reduces the efficiency and accuracy of the LIDAR detection [3].

In some application, a single laser diode may not have the required power level. To increase the beam power, beams from several laser sources o be combined to form a single beam. This is called the power scaling. In this case the uniformity of each beam and how they are combined is important to maximize the output power.

Therefore, the diode laser beams must be reshaped before they are utilized commercially. In fact, beam characteristics of collimation, uniform energy profile and regular beam shape such as circular or rectangular are highly preferable in the beam shaping applications. Inspired by these requirements, this thesis concentrates on how to simultaneously achieve these characteristics and makes the semiconductor laser diode more applicable in the industrial world.

CHAPTER 2

RESEARCH OBJECTIVES AND DISCUSSION OF CHAPTERS

The laser diode example shown in the last chapter is the basic edge-emitting semiconductor laser, only one of three kinds of laser diodes. The other two includes double heterostructure laser diode and vertical cavity surface emitting laser diode (VCSEL), as shown in Figure 2.1. Though different from each other in the structure, these laser diodes work on the same principle, functioning as an optical oscillator by stimulating a chain reaction of photon emission inside a tiny chamber. Thus they produce the same beam characteristics and can share the same beam shaping methods. Throughout this thesis, edge-emitting laser diodes will be referred to as an example by the author to demonstrate how to design and analyze the beam shaping systems involved.

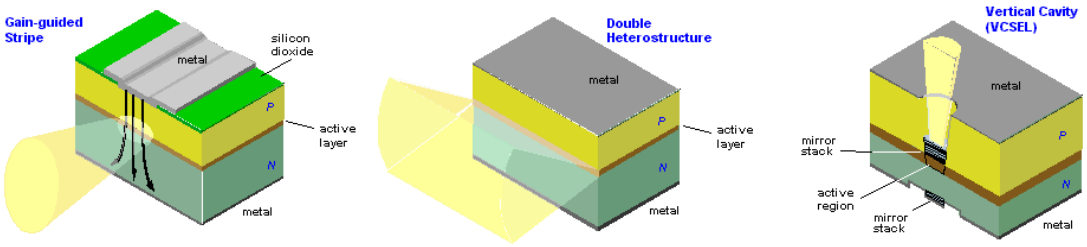

Figure 2.1: Three different structures of laser diodes [4]

As mentioned earlier, collimation, uniform intensity and pre-determined beam shape are the three main features in the regions of laser beam shaping applications. There are many papers presenting either to collimate the beam, to make it circular or rectangular, or to bring the irradiance profile to a uniform irradiance. For example, in a

dissertation [3], the author proposed several design methods using lens or mirrors to collimate and circularize the laser beams, this work also developed a two lens systems that can achieve the uniform phase as well as amplitude. In the paper [5], the author introduced a beam profile named the multi-tilted Gaussian beam which has the advantage of nearly uniform distribution throughout its far-field propagation. In [6], the author demonstrated how to manipulate multi-Gaussian beams to a beam with a flat-topped shape. In paper [7], the author talked about using converging blades to collimate the beams. In a book [8], the authors summarized many types of beam shaping theory and techniques. However, there is little work engaging in to achieve all of the above features simultaneously. The difficulty stems from the complexity of the problem itself.

Once the laser beams possess these features, they become highly adjustable, applicable and preferable in the industrial and commercial world. But during the process of the practical applications, people often find that high power densities must be provided on the targets and that only one laser diode source usually cannot meet the energy requirements. Therefore, using high-power laser diode arrays (LDAs) is necessary. Laser diode arrays are composed of multiple separate beams of laser-diode pitches. The beam quality of the high-power laser diode stack is poor because of its large beam size and great divergence. Generally, on the fast axis, the beam divergence is 40 degree; in the slow axis, which is parallel to the array direction, the beam divergence is 6 to 8 degree. At this point, the complexity of the problem is increased to a new level, involving beam shaping techniques of Multi-laser diode sources.

Many sophisticated beam collimation techniques have been developed to improve output power, coupling efficiency, and simplicity. Generally, the beam divergence in the

fast axis can be collimated to several miliradians by using a microcylindrical lens for each high-power laser-diode, while the beam quality in the slow axis is very poor and requires special treatments. The slow-axis correction usually involves beam reshaping and rearrangement [9], such as using microstage mirrors [10], prism arrays [11] and refractive gratings [12] to divide, rotate and rearrange the beam along the slow axis. Another approach does not require beam rearrangement, and the light from each emitter is collimated separately by microlens arrays [13] or a phase mask [14]. Graded-index fiber lens array can also be used to collimate the beams of high-power laser array [15]. Each of the above techniques has its own advantages and strong points.

Inspired by these works, this thesis will propose a new optical system which employs four sets of lenslets, either aspheric or cylindrical, and treat the light rays respectively in both perpendicular and parallel planes. The goal of this system is to transform the irradiance distribution of such laser diodes form Gaussian to uniform in addition to collimation and expansion of the beams, and to combine the beams from different laser diode into a single laser beam with a rectangular beam shape. In this way, the disadvantage of the low-energy output of a single laser diode is overcome, and the resultant beam can be applied to many different areas of industrial world. The author presents the principles and tools used to design this system explicitly in order to create a guideline for the ones working with similar problems or further improving the proposed designs. The equations specific to this system are derived analytically based on ray optics principles and geometrical relationships. Electromagnetic principles used to derive the governing equations. Then MATLAB is used to solve these equations. MATLAB codes are written to calculate and determine the parameters of the optical components, while

considering the governing equations of beam propagation. Computer package program ZEMAX is utilized to optimize and simulate the optical designs. The author expects that this beam-shaping system can be used and easily modified to address the issues related to the laser beam shaping and the analysis methods developed in this thesis will be a valuable resource for the scientific community interested in beam shaper systems.

Chapter 3 talks about the background and mathematical development for this research project, concerning about the characteristics of the laser beam, the lenslet technology, the mathematical preliminaries, and ZEMAX implementation. Chapter 4 begins to design each lenslet and its surfaces and derive the equations to determine them. Chapter 5 gives the design examples. In this chapter, the author will use MATLAB to solve the derived equations and to simulate the results. Additionally, ZEMAX will also be used to simulate the designed system and a comparison of the results from MATLAB and ZEMAX is shown. The conclusions are discussed in Chapter 6.

CHAPTER 3

BACKGROUND AND MATHEMATICAL DEVELOPMENT

In this chapter, the background of lasers and some basic knowledge of the laser beam shaping are given. The complete mathematical expression of the laser beam propagation and the fundamental mode is derived, showing the characteristics and the parameters of a laser beam analytically. The knowledge about the lenslet technology and ZEMAX implementation is introduced also. Finally, some of the necessary mathematical principles and theories concerning the optical system design are listed and discussed.

3.1 Basic Principles of laser beams and Their Propagation Characteristics

A laser is a device that emits light through a process of optical amplification based on the stimulated emission of photons. Lasers mainly consist of three parts, namely, the gain medium, the pumping mechanism and the optical cavity. The gain medium is the part where light of a specific wavelength that passes through it is amplified by stimulated emission. Normally controlled over its purity, size, concentration, and shape, the material of the gain medium can be of any state: gas (plasma), liquid (dye), solid (semiconductor or crystal). For the gain medium to amplify light, energy needs to be supplied. This process is called pumping. The optical cavity, also known as optical resonator, is usually made from a pair of mirrors on either end of the gain medium,

providing optical feedback so that light bounces back and forth between the mirrors, and the beam gains energy continuously.

In order for the lasers to operate, it is necessary to create a population inversion. The gain medium absorbs pump energy which raises some electrons into higher-energy (excited) quantum states. When the number of particles in one excited state exceeds the number of particles in some lower-energy state, populating inversion is achieved. The amount of stimulated emission due to light that passes through is larger than the amount of absorption by the material itself [16]. At this point, the light generated by stimulated emission and the amplified beam are the same in terms of wavelength, phase and polarization. This is why laser light has good characteristics coherence, uniform polarization and great monochromaticity. The gain medium will amplify any photons passing through it, regardless of direction, but only the photons in a spatial mode supported by the resonator will pass more than once through the medium; this is why laser lights usually have better directionality than other light sources.

When laser beams travel in free space or an isotropic media rather than waveguides, they form Gaussian beam and exhibit the minimum divergence for a given diameter due to diffraction. Some high power lasers may even be multimode, with the transverse modes often approximated using Hermit-Gaussian or Laguerre-Gaussian functions [17]. The simplest and lowest order mode is called the fundamental Gaussian beam which is the most stable and preferred beam type in many applications.

This research is interested in the type of semiconductor diode laser which has the profile of elliptical Gaussian beam. Therefore, in this section, only the basics of the

fundamental Gaussian beam analysis are presented [18]. A complete understanding of laser beam propagation requires a treatment based on Maxwell's Equations.

3.2. Mathematical theory of wave propagation

Maxwell's equations govern all electric, magnetic, electromagnetic and optical phenomena. In the field of optical electronics and optical communications, one often deals with the transmission and propagation of electromagnetic radiation in regions where both charge density and current density are zero.

Maxwell equations in charge free and isotropic media:

$$\nabla \times \vec{E} = -\mu \frac{\partial \vec{H}}{\partial t} \tag{3.1}$$

$$\nabla \times \vec{H} = \varepsilon \frac{\partial \vec{E}}{\partial t} \tag{3.2}$$

$$\nabla \cdot \vec{E} = 0 \tag{3.3}$$

$$\nabla \cdot \vec{H} = 0 \tag{3.4}$$

To derive the wave equation, we first take the curl of equation (3.1) and eliminate $\nabla \times \vec{H}$ by using equation (3.2). This leads to

$$\nabla \times (\nabla \times \vec{E}) = -\mu \cdot \nabla \times (\frac{\partial \vec{H}}{\partial t}) = -\mu \frac{\partial (\nabla \times \vec{H})}{\partial t} = -\mu\varepsilon \frac{\partial^2 \vec{E}}{\partial t^2} \tag{3.5}$$

The left hand side of the equation can be expanded and rewritten as

$$\nabla \times (\nabla \times \vec{E}) = \nabla (\nabla \cdot \vec{E}) - \nabla^2 \vec{E} = -\mu\varepsilon \frac{\partial^2 \vec{E}}{\partial t^2} \tag{3.6}$$

Using equation (3.3), the equation (3.6) becomes

$$\nabla^2 \vec{E} - \mu\varepsilon \frac{\partial^2 \vec{E}}{\partial t^2} = 0 \tag{3.7}$$

This is the wave equation for the electric field vector $\vec{E}$ in homogeneous and isotropic media. A similar equation for the magnetic field vector $\vec{H}$ can be easily shown, thus we only use electric field to demonstrate the process. Equation (3.7) is the standard electromagnetic wave equations. It satisfys the well-known monochromatic plane wave solution

$$\vec{E} = \vec{a}Ae^{i(\omega t - \vec{k}\vec{r})} \tag{3.8}$$

Where A is a constant and called the amplitude and $\vec{a}$ is the unit vector representing the polarization state of the E-field. The parameter $\vec{k}$ is the wave vector and ω is the angular frequency, where

$$\left|\vec{k}\right| = \omega\sqrt{\mu\varepsilon} \tag{3.9}$$

Substituting equation (3.9) in (3.8), we get another form of wave equation for harmonic field with a time dependence of $\exp(i\omega t)$:

$$\nabla^2 \vec{E} + k^2 \vec{E} = 0 \tag{3.10}$$

This equation can be applied to obtain a more complete wave description of the beams produced by lasers Because most optical beams propagating in free space are almost pure TEM (transverse electric and magnetic), we can assume the propagation direction is parallel to the z direction in the cylindrical coordinates, and thus the vector field components lie in the plane perpendicular to the direction of propagation z. In fact, we are looking for a solution of the form of equation (3.10)

$$\vec{E} = \hat{a}E_0\psi(r,z)e^{-jkz} \tag{3.11}$$

The factor E_0 is the customary amplitude factor expressing the intensity of the wave (in the development below it is set equal to 1); the factor $\exp(-jkz)$ expresses that the wave propagates more-or-less as a uniform plane wave; and the factor ψ measures how the beam deviates from a uniform plane wave [16].

We limit our derivation to the solution of the field with cylindrical symmetry, so that the Laplacian ∇^2 can be written in cylindrical coordinates

$$\nabla^2 = \frac{\partial^2}{\partial r^2} + \frac{1}{r^2}\frac{\partial^2}{\partial \theta^2} + \frac{\partial^2}{\partial z^2} \tag{3.12}$$

Substituting equations (3.11) and (3.12) into equation (3.10) leads to

$$\frac{\partial^2 \psi}{\partial r^2} + \frac{\partial^2 \psi}{\partial z^2} - j2k\frac{\partial \psi}{\partial z} = 0 \tag{3.13}$$

We assume that the variation of the field amplitude is slow enough, so that

$$\frac{\partial^2 \psi}{\partial z^2} << k\frac{\partial \psi}{\partial z} \tag{3.14}$$

This approximation is known as the slowly varying amplitude (SVA) approximation and legitimate when the transverse dimension of the beam is much larger than the wavelength. This is true for most laser beams. Therefore, equation (3.13) can be reduced to a scalar differential equation:

$$\frac{\partial^2 \psi}{\partial r^2} - j2k\frac{\partial \psi}{\partial z} = 0 \tag{3.15}$$

It is convenient to introduce two complex functions $P(z)$ and $q(z)$ to solve the differential equation such that ψ is in the form of

$$\psi = \exp[-j(p(z) + \frac{k}{2q(z)}r^2)] \tag{3.16}$$

Now, we need to find $P(z)$ and $q(z)$ so that equation (3.16) is a solution of equation (3.15). Use equation (3.12), we obtain

$$\frac{\partial^2\psi}{\partial r^2}=\frac{\partial}{\partial r}[\psi\cdot(-j\frac{k}{2q(z)})\cdot 2r]=\psi(-j\frac{k}{2q(z)}2r)^2+\psi(-j\frac{k}{q(z)}) \tag{3.17}$$

$$j2k\frac{\partial\psi}{\partial z}=j2k\psi(-j)\frac{\partial p}{\partial z}+k^2r^2\psi(\frac{1}{q})' \tag{3.18}$$

Substituting equation (3.17) and (3.18) into equation (3.15), results in

$$\frac{\partial^2\psi}{\partial r^2}-j2k\frac{\partial\psi}{\partial z}=\psi\times(-j\frac{k}{2q(z)}2r)^2+\psi\times(-j\frac{k}{q(z)})-j2k\psi\times(-j)\frac{\partial p}{\partial z}-k^2r^2\psi\times(\frac{1}{q})'=0$$

The above equation can be simplified to

$$-(\frac{k}{q})^2r^2-2j\frac{k}{q}-k^2r^2(\frac{1}{q})'-2kp'=0 \tag{3.19}$$

Where the "prime" in this equation indicates differentiation with respect to z. If equation (3.19) holds for all r, the coefficient of the different powers of r must be equal to zero. This leads to

$$(\frac{1}{q})^2+(\frac{1}{q})'=0 \qquad\qquad p'=\frac{-j}{q} \tag{3.20}$$

The problem now has been reduced to solve these two coupled deferential equations. In order to solve them, we introduce a function $u(z)$ by the relation

$$\frac{1}{q}=\frac{1}{u}\frac{du}{dz} \tag{3.21}$$

Thus,

$$\begin{cases}(\frac{1}{q})'=\frac{-1}{u^2}(\frac{du}{dz})^2+\frac{1}{u}\frac{d^2u}{dz^2}\\ (\frac{1}{q})^2=\frac{1}{u^2}(\frac{du}{dz})^2\end{cases} \tag{3.22}$$

By substituting equation (3.22) into the first equation of (3.20), we can easily obtain

$$\frac{d^2u}{dz^2} = 0 \tag{3.23}$$

The general solution for the above equation can be written as

$$u = az + b \tag{3.24}$$

Where a and b are arbitrary constants. The beam parameter $q(z)$ can be written, according to equation (3.21), as

$$\frac{1}{q} = \frac{a}{az+b} \qquad\qquad q = z + \frac{b}{a} = z + q_0 \tag{3.25}$$

Where q_0 is a constant ($q_0 = q(0) = b/a$), the other beam parameter $P(z)$ can be obtained from equation (3.20) and (3.25) as:

$$p' = -j\frac{1}{z+q_0} \tag{3.26}$$

So that, upon integration, one obtains:

$$p = -j\ln(1+\frac{z}{q_0}) \tag{3.27}$$

Combining Equations (3.25) and (3.27) in Equation (3.16), we obtain the following cylindrically symmetric solution:

$$\psi = \exp[-j(\ln(1+\frac{z}{q_0}) + \frac{k}{2(z+q_0)}r^2)] = \frac{q_0}{q_0+z}\exp(-i\frac{k}{2(z+q_0)}r^2) \tag{3.28}$$

One notes that the solution in Equation (3.28) is the solution to Helmholtz equation in equation (3.15). In equation (3.28), if we substitute $z = 0$, the amplitude distribution factor ψ becomes:

$$\psi(z=0) = \exp(-\frac{dr^2}{2z_0})\exp(-jp(z=0)) \tag{3.29}$$

Then we express q_0 in terms of a new constant ω_0, where or

$$\omega_0^2 = \frac{2z_0}{k} = \frac{\lambda_0 z_0}{n\pi} \qquad \text{or} \qquad z_0 = \frac{n\pi\omega_0^2}{\lambda_0} \tag{3.30}$$

This is important because ω_0 appears to be a measure of the beam spot at $z = 0$.

So rearranging parameters by using parameters that characterizes the beam, we have:

$$q_0 = j\frac{\pi w_0^2 n}{\lambda} = j\frac{kw_0^2}{2} = iz_0 \tag{3.29}$$

We now define two new parameters:

$$R(z) = z(1+\frac{z_0^2}{z^2}) = z\left[1+(\frac{\pi w_0^2 n}{\lambda z})^2\right] \tag{3.30}$$

$$w(z) = w_0\sqrt{1+\frac{z^2}{z_0^2}} = w_0\sqrt{1+(\frac{\lambda z}{\pi w_0^2 n})^2} \tag{3.31}$$

It turns out that $R(z)$ is the radius of curvature of the wavefront and $w(z)$ is the beam spot size at any z. By expressing the equation (3.28) in terms of these two new parameters in equations (3.29), (3.30), and (3.31), we obtain the solution to the wave equation as:

$$\psi = \{\frac{w_0}{w(z)}\exp[-\frac{r^2}{w^2(z)}]\}\times\exp[j\tan^{-1}(\frac{z}{z_0})]\times\exp[-j\frac{kr^2}{2R(z)}] \tag{3.32}$$

Thus,

$$\frac{E(x,y,z)}{E_0} = \{\frac{w_0}{w(z)}\exp[-\frac{r^2}{w^2(z)}]\} \qquad \text{Amplitude factor}$$

$$\times\exp\{-j[kz-\tan^{-1}(\frac{z}{z_0})]\} \qquad \text{Longitudinal phase factor}$$

$$\times\exp[-j\frac{kr^2}{2R(z)}] \qquad \text{Radial phase factor} \tag{3.33}$$

This is the complete mathematical expression of the fundamental mode of the Gaussian laser beam. This expression shows the characteristics of a laser beam from the analytical point of view. Higher order modes are expressed as the superposition of fundamental Gaussian function, and Laguerre polynomial are used to express higher order modes for lasers with circular symmetry. On the other hand, the superposition of Gaussian function and Hermite polynomials is used to express lasers with rectangular symmetry.

Figure 3.1 shows the characteristic parameters of a Gaussian beam of fundamental TEM_{00} mode.

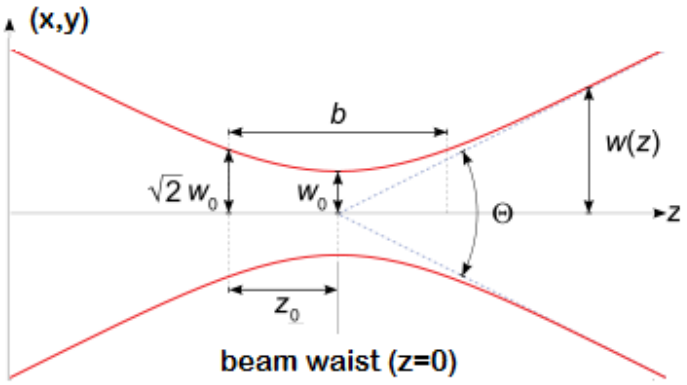

Figure 3.1: the characteristic parameters of a Gaussian beam

Z_0 is the Rayleigh range and defined as the distance in propagation direction of a beam from waist to the place where the area of the cross section is doubled. b is the confocal parameter. The divergence of a Gaussian beam in the far-field region is given by the beam divergence half angle

Near the beam waist, the beam is highly collimated ($R(z) = 0$); the wavefront are planar, normal to the direction of propagation, with no beam divergence at that point. However, that can only remain true well within the Rayleigh range. The beam of a single

transverse mode laser eventually diverges at an angle which varies inversely with the beam diameter. The divergence of a Gaussian beam in the far-field region is given by:

$$\theta \approx \frac{w(z)}{z} \approx \frac{w_0}{z_0} = \frac{\lambda}{\pi w_0} \tag{3.34}$$

Therefore, the beam shaping becomes necessary; otherwise a common laser would spread out to a size of hundreds of kilometers.

3.3 Beam shaping in the general sense

Beam shaping is a process of redistributing irradiance and phase of a beam of optical radiation through an optical system. Shape of a beam is defined by spatial irradiance distribution of the beam. Laser beam shaping is the simplest technique for matching the laser beam to part features. The phase of the shaped beam is a major factor in determining the propagation properties of the beam profile. For example, a collimated and reasonably large beam with a uniform phase front will maintain its shape over a considerable propagation distance; this is why the beam collimation is preferable and usually required. Figure 3.2 illustrates the general beam shaping problem. A beam is incident upon an optical system that may consist of one or more elements. The optical system must operate upon the beam to produce the desired output.

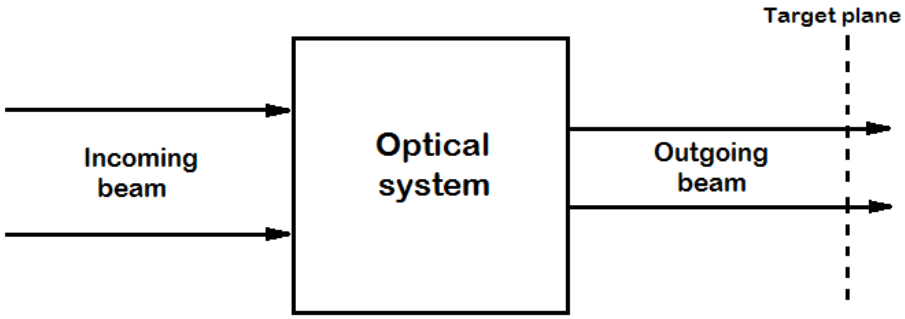

Figure 3.2: General beam shaping system

Basically, the goal of the beam shaping is to design an optimal and practical optical system that can transform the incoming beam so that the outgoing beam will have the desired beam distribution on the Target plane. The optical system can be composed of different types of optical components such as mirrors [19], lenses, prisms [20], gratings [21], or gradient lens/fiber[15]; Furthermore, the surface shape of each optical component can also be different, such as biconic lens, binary optics, cylindrical lens, asphere and others. Therefore, the optical design can be very diverse and interesting. On the other hand, having these many options increases the complexity of the optical designing systems and adds difficulty to the problem. With the development of laser industry and applications, the laser beaming shaping has become more and more important and necessary and attracted more and more scientific attention into this field.

The optical system is usually simpler if the design only requires a certain spatial irradiance distribution at the target plane and the “foot-print” of the beam shape is left unconstrained. Complications arise if both beam shape and irradiance profiles are specified. It is easy to manipulate the propagation of the light beams to achieve the desire irradiance distribution, because each individual light ray can be manipulated individually. But when the shape is concerned, the beam must be treated as a whole and thus many options would be limited. In fact, Laser beam shaping techniques are grouped into two basic types: field mappers and beam integrators. Field mappers work only for beams with a known field distribution, such as single-mode beams, and they are generally highly sensitive to alignment and beam dimensions. Integrators work for both coherent and multimode beams, where the input field distribution may not be known, and they are much less sensitive to alignment and beam size. Like many optical problems, there is no

single beam shaping method that addresses all situations. The nature of the input beam, the system geometry, and the quality of the desired output beam and others affect the choice of shaping technique.

In the optical problem concerned in this research, the input beam consists of individual elliptically shaped beams from several laser diodes forming a laser array. The quality of the desired output includes forming a single beam that is collimated, and has uniform irradiance and rectangular beam shape. The task is to find and design an optical system that could achieve these demands. The difficulty of the design of this beam shaping system comes from the fact that the source is a multi-laser array sources. First, we have to face the complexity of the incoming beam which contains several elliptical Gaussian laser beams; second, we have to merge the beams into a single beam with rectangular beam shape and uniform phase and amplitude.

The author will propose a four lens systems which can treat individual laser beam separately in perpendicular plane and parallel plane. With the help of the lenslet, this optical system can be easily applied to the multi laser diode sources. Figure 3.3 shows the model of this system generated by ZEMAX. Each surface is either aspherical or cylindrical. The following chapters will demonstrate in detail the operation of this system and its design parameters.

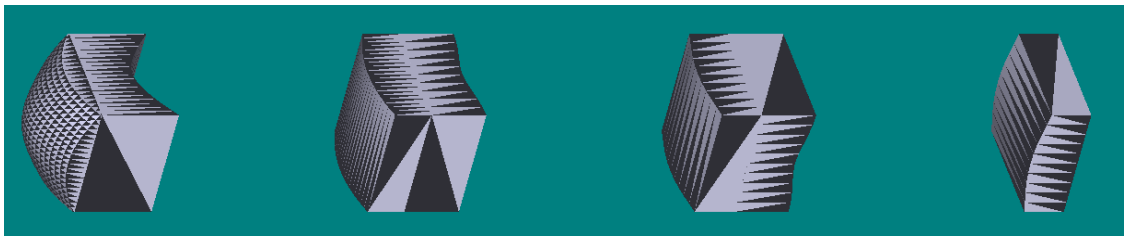

Figure 3.3: The proposed four lenses optical system.

3.4 Lenslet technology

A lenslet is literally a small lens, and is a part of a lenslet array. A lenslet array consists of a set of lenslets in the same plane. Each lenslet in an array normally has the same focal length, as shown in Figure 3.4. Ordinarily speaking, the lenslets are manufactured identically and arrayed on one substrate, as shown in Figure 3.5. In another words, lenslet arrays are substrates covered with set of micro lenses. Lenslet technology actually is a type of manufacturing engineering that allows the manufactures to build lenslets of micro-size on a substrate. The size of the whole substrate (fused silica) in Figure 3.5 is only 1.5 mm. The lenslet arrays perform as diffusers or used for local focusing and sampling. There are mainly two types of lenslet arrays, diffractive and refractive. This research uses refractive lenslet to shape the beam. There are many specifications to evaluate a lenslet array such as surface roughness, array pitch, and; most importantly, fill factor. Higher fill factor means higher extent to which the substrate is covered by the lenslet and more control over the whole beam.

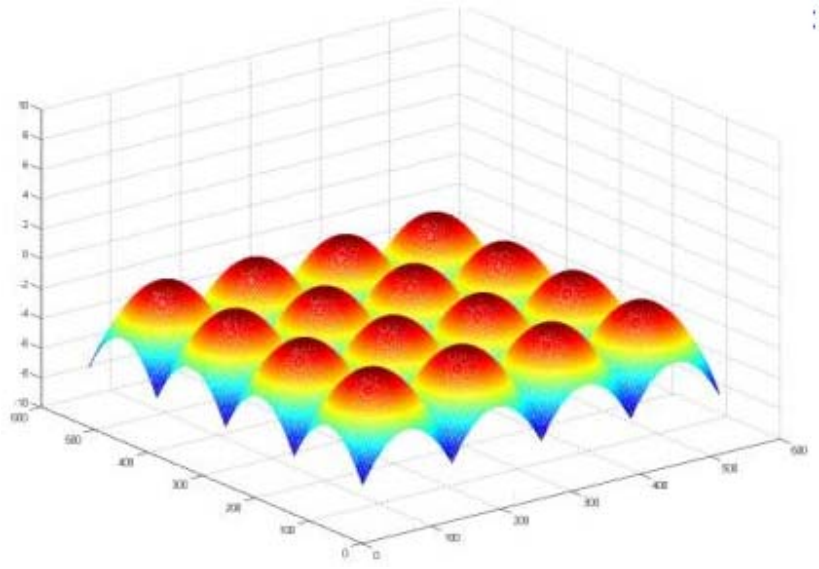

Figure 3.4: The model of lenslet array simulated by MATLAB [22]

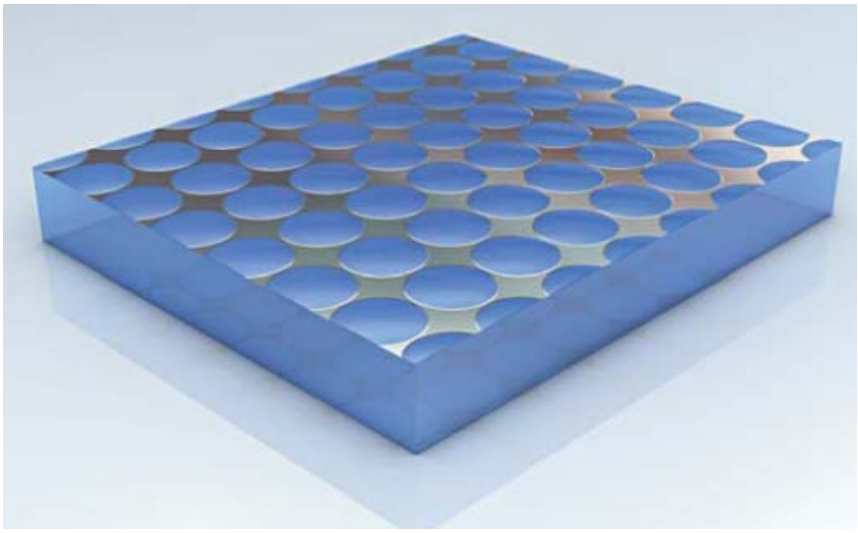

Figure 3.5: The actual product of a type of lenslet array [23]

This thesis only gives some introduction to the lenslet technology, because we are more concerned about designing and utilizing the lenslet array rather than practically manufacturing. Figure 3.3 shows the proposed four-lens system. And Figure 3.6 shows the proposed optical system including four lenslet arrays each of which are specified by the corresponding lens shown in Figure 3.3. The aperture of each lenslet is made to be equal to the spacing of the laser diode array so that each diode laser could be treated identically and that the outgoing beam would become a single bundle of beam .

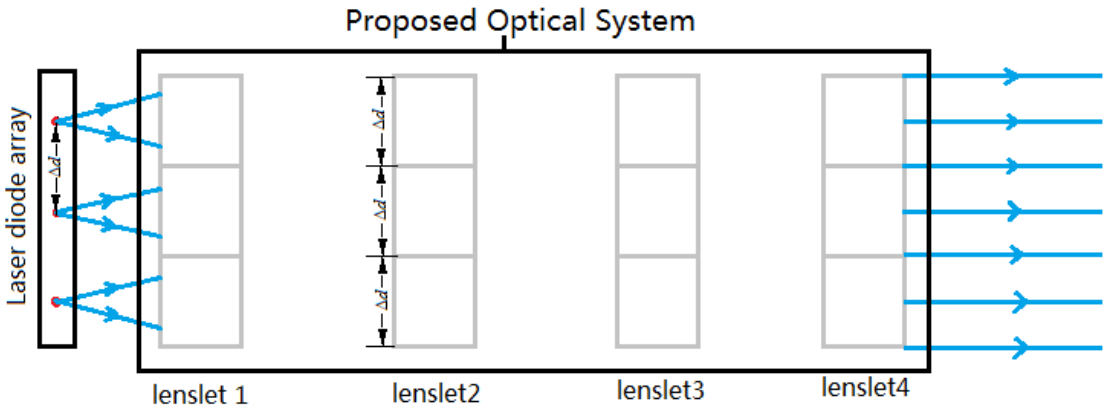

Figure 3.6: The proposed optical system including four lenslet arrays in two-demention

3.5 The mathematical preliminaries for the laser beam shaping

This section gives the mathematical background of the design process and explains the effectiveness of the geometrical optics approximation, the surface types used in optical system design, the idea of surface fitting, and the constant optical length condition which is commonly used in problems of geometrical optics.

3.5.1 Geometrical Optics Approximation

Geometrical optics, or ray optics, describes light propagation in terms of "rays" and is treated by the method of light rays. The "ray" in geometric optics is an abstraction and is a line or curve that is perpendicular to the light's wavefront. Rays generally characterize the direction of the flow or propagation of radiant energy, except near the focus or an edge point where interference and diffraction takes place. Optical design of a beam shaper can be achieved by using either physical or geometrical ray optics [8]. It is customary to design an optical system with geometrical ray optics instead of physical optics when the wavelength is very small compared with the size of structures in which the light interacts. A dimensionless parameter, β, is used to determine if Geometrical optics approximation is valid in treating the beam shaping problem. For a given wavelength λ of the light and the image distance f from the aperture, the dimensionless parameter is written as [24]

$$\beta = \frac{2\pi w_i w_o}{f\lambda} \tag{3.35}$$

Where w_i and w_o are the incoming beam radius and the beam radius at the target plane. This dimensionless parameter is very important to understand beam shaping technique. Generally, for simple output geometries such as circles and rectangles, if $\beta < 4$, a beam

shaping system will not produce acceptable results; geometrical optics is not valid. For $4 < \beta < 32$, diffraction effects are significant and should be included in the development of the beam shaping system. For $\beta > 32$, diffraction effects will not significantly degrade the overall shape of the output beam, and geometrical optics is valid. Therefore it is clear that we need β to be large in order for geometrical optics to hold. If β is large, it is relatively simple to work beam shaping problem using geometrical optics, but if it is small, the results are hard to control due to diffraction. As an example, a circular Gaussian beam in Figure 3.7 has been transformed analytically into a flat top shape as shown in Figure 3.8 for different β values. We see that for $\beta = 2$ the result does not look at all like a square pulse, while for $\beta = 32$ the result starting to look close to a square shape.

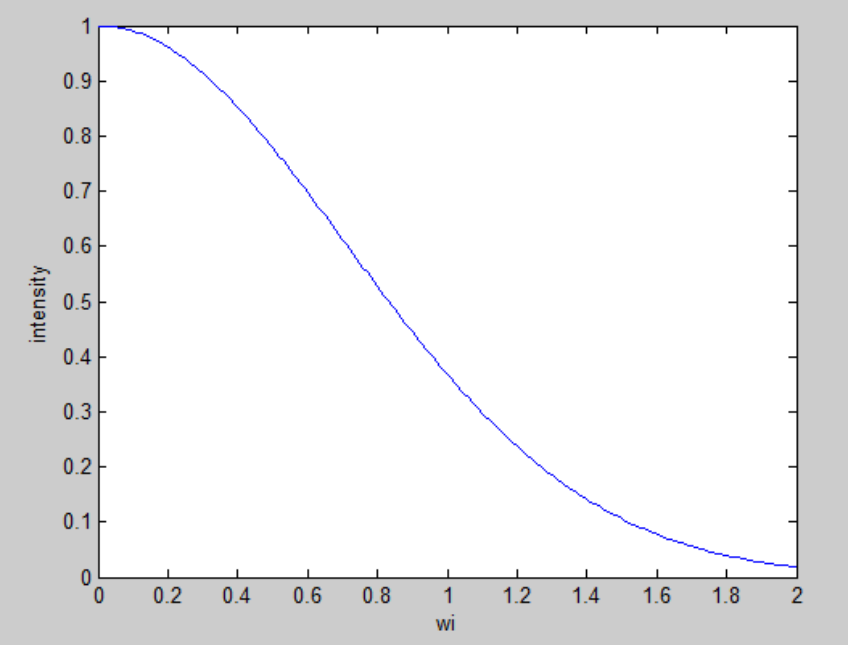

Figure 3.7: The Gaussian input beam

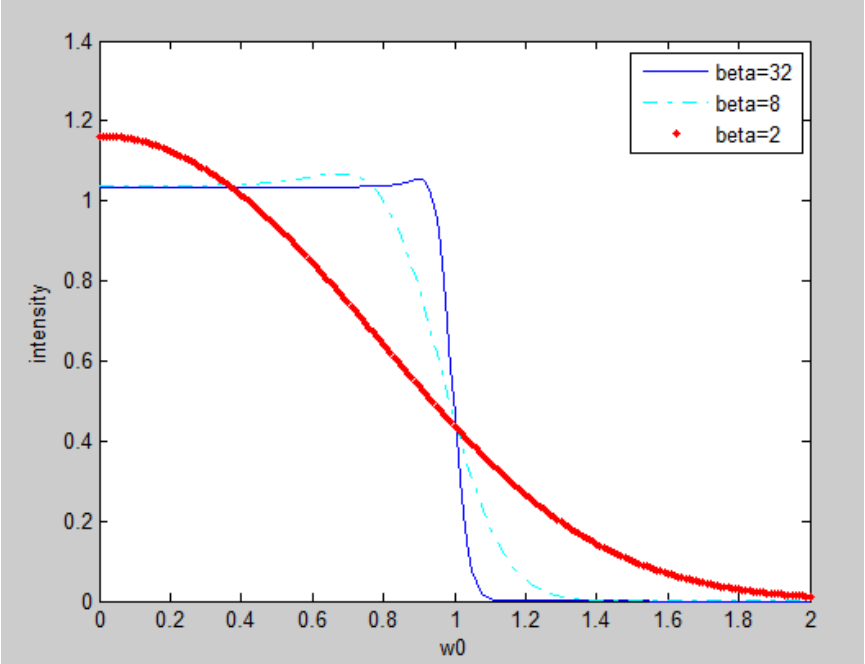

Figure 3.8: The output beam with flat-top intensity profile for different β

3.5.2 Spherical and aspheric surfaces in beam shaping optical systems

An optical system is composed of one or several optical components, and each optical component is defined and determined by different optical surfaces. If the surface is refractive and separates two mediums with different refractive indices on each side, then it changes the direction of the light propagating from one side to the other side. In fact, an optical surface has many other ways to manipulate the light propagating through it. Therefore, the problem of beam shaping usually turns out to be choosing and designing the proper optical surfaces. There are mainly two types of commonly employed optical surfaces, such as spherical and aspherical.

A spherical surface is defined by only one parameter, the radius or the curvature of the surface. Optical components with this type of surfaces are simple to design and easy to manufacture. This type of surface also has high controllability over the paraxial

light rays. Actually, the entire theory of applied optics is based on the assumption that light propagates in the paraxial region of the spherical surface, i.e. Paraxial Approximation. Paraxial Approximation works very well in the cases of small Field of View and sources with small divergence. However, spherical surface has the property that the rate of change of the surface slope is exactly the same everywhere on the surface, and thus the aberration is inevitable with the increased radial distance from the main axis of an optical system. Aspherical surface has the property that the slope of the surface is gradually reduced toward the outer periphery of the surface in order to flatten the shape in the region surrounding the outer rays, as shown in Figure 3.9 [25].

The important parameter of optical surface is the “surface sag”, which is illustrated in Figure 3.10. Surface sag is the distance between the vertex of the surface to the projected point of the corresponding surface point determined by the radial height r. Therefore, Surface sag z is actually a function of the radial height r

$$z = z(r) \tag{3.36}$$

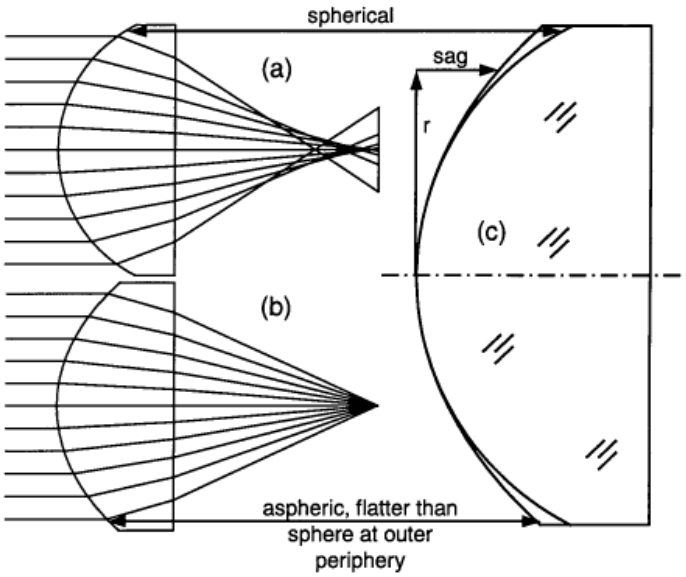

Figure 3.9: The comparison of a spherical (a) and aspherical (b) lens, (c) Surface sag

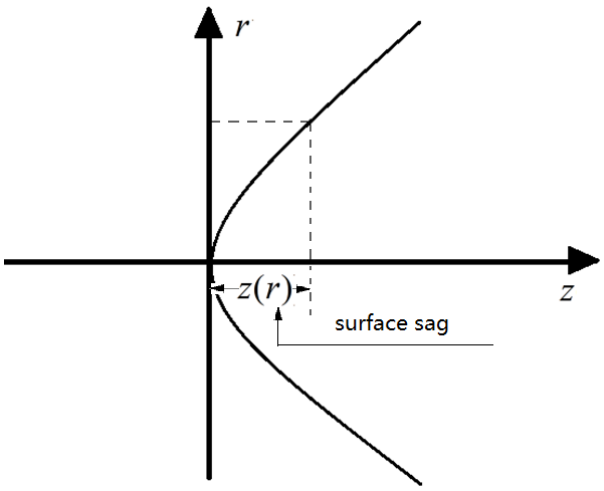

Figure 3.10: Illustration of the surface sag

Different surfaces have different surface sag function, but the most commonly used optics surface equation can be written in the form

$$z(r) = \frac{cr^2}{1+\sqrt{1-(1+k)c^2r^2}} + \sum_{i=1}^{N} A_{2i} r^{2i} \tag{3.37}$$

Where z is the surface sag, r is the coordinate in one of the transverse directions, c is the curvature (the reciprocal of the radius of curvature), k is the conic constant, and A_{2i} are the coefficients of the polynomial deformation terms. Different combinations of k and A_{2i} may have the same impact on the surface sag function. Theoretically, the coefficient number i can be as large as possible, but from a numerical point of view, it is desirable to use the least number of deformation terms in order to simplify the surface manufacturing. If there are no deformation terms and all the polynomial terms are equal to 0, we come to another type of aspherical surface called conic surface whose surface sag function is written as

$$z(r) = \frac{cr^2}{1+\sqrt{1-(1+k)c^2r^2}} \tag{3.38}$$

For a hyperbola $k < -1$, for a parabola $k = 1$, for an ellipse $-1 < k < 0$, and for a circle $k = 0$

3.5.3 Constant optical path condition

Optical path length (OPL) or optical distance is the product of the geometric length of the path the ray travels, and the index of refraction of the medium through which light propagates. For a uniform index media, the OPL of a ray passing through an optical system is the sum of the geometrical path length of a specific ray times the index of refraction of the component of the system. OPL is an extremely useful measure of the performance of an imaging optical system. Light ray propagation is commonly described by wavefronts described as the surfaces of constant phase of the wave or optical path length from the source or reference surface. In order for the output wavefront to have the same shape as the input plane wavefront, it is necessary for all rays passing through the optical system to have the same optical path length.

Optical Path Length Condition (OPLC) is that the optical path length of every light ray between two wavefronts of this ray bundle will be equal to each other. A simple convex-plano lens system collimating the rays of a point source is shown in Figure 3.11. The optical path length $(OPL)_0$ of a ray passing along the optical axis from source to the reference plane is

$$(OPL)_0 = n_0 d + nt \tag{3.39}$$

For an arbitrary ray of height r, the optical path length is

$$(OPL)_r = n_0 \sqrt{r^2 + z^2} + n(d + t - z) \tag{3.40}$$

The constant optical path length condition is satisfied for this optical system by requiring

$$(OPL)_0 = (OPL)_r \tag{3.41}$$

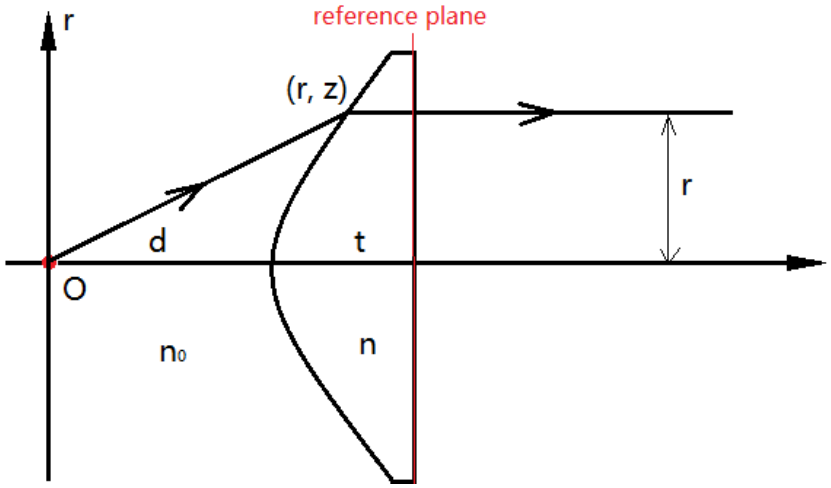

Figure 3.11: Illustration of OPLC for a convex-plano lens

3.5.4 Surface fitting

In the process of optical system design, you often meet some fairly complicated problems, such as the situations that only aspheric surfaces can satisfy the demand. If the high-order deformation terms are needed, the situation will get even worse; because it is very difficult to derive the equations for the coefficients A_{2i} of the deformation terms in the surface equation (3.37) and direct calculation. The common way of solving this type of problems is to use equation (3.37) to fit the desired surface equation with the help of certain fitting method. First, we need to use ray tracing method to trace a number of rays so that these rays will spread in the same way as the required outgoing beams propagate. Second, using the energy conservation principle, constant optical path condition and trigonometric relationships, we employ the inverse method to calculate the surface sag z at every radial height r determined by the corresponding light ray traced. Eventually, we will get a series of points, that: a curve is formed by connecting these points. This curve

should have the same shape as the actual surface shape we desire. Finally, we use fitting method to fit the curve with the surface equation and calculate the best combination of the k and A_{2i} that specify the surface. The more light rays we trace, the more points we obtain, the more similarity the curve formed by these points has with the actual surface shape, the less difference there would be between the shape of the surface fitted by the fitting method and that of the surface we desire. Theoretically, it is encouraging to trace as many rays as we can in order to pursue the best results. However, there exists a tradeoff between the number of rays traced and computing time needed. Usually, we trace just number of rays so that we do not waste an enormous amount of time on an insignificant improvement.

Actually, the performance of the whole fitting process largely hinges on the selection of a right fitting method. There are several fitting methods available now days, such as fit using unconstrained optimization, fit using simplex search, fit using nonlinear least squares (Levenberg-Marquardt), fit using minimax optimization and fit using genetic algorithm. Fit using genetic algorithm is the best one if accuracy is the only requirement. However, in this research, we use fit using simplex search, because this fitting method usually can achieve relatively good performance with less computing time.

Fit using simplex search is a fitting method that uses simplex method for function minimization [26] to find the minimum point of the merit function of the problem. Here, we hope that the surface equation can fit those sets of (r, z) points perfectly. That means the merit function should represent the difference between the resultant surface from the surface equation and the actual surface we desire and that the merit function should be as small as possible. Therefore, we choose the merit function (MF) to have the form:

$$MF = \sqrt{\frac{\sum_{i=1}^{N} (z_i' - z_i)^2}{N}} \tag{3.42}$$

Where N is the number of rays traced. z_i' is the surface sag calculated through surface equation (3.37), z_i is the actual surface sag calculated through ray tracing. This MF is the mean square error of the difference between z_i' and z_i ; the smaller MF is, the better surface we can get. MF is a function of the surface parameters k and A_{2i}

$$MF = MF(k, A_{2i}) \tag{3.43}$$

We need to search the best combination of k and A_{2i} to make the MF the smallest. As mentioned earlier, we are going to use simplex search to find the minimum of the MF. Simplex method is a method for function minimization. It is described for the minimization of a function of n variables, which depends on the comparison of function values at the (n+1) vertices of a general simplex, followed by the replacement of the vertex with the highest value by another point. The simplex adapts itself to the local landscape, and contracts on to the final minimum. This method is known to be effective and computationally compact. In MATLAB, this method is described as fminsearch. In appendix, the entire MATLAB codes are shown.

3.5.5 The relationship between aperture size and the beam size

In lens designing problem, a must-do step is to decide the aperture size of the lens (in an optical system). If the aperture size is too small, the beam would be truncated, causing the truncation effects [27]. The two obvious disadvantage caused by the truncation effect is the loss of energy and the increased diffraction effect which could largely degrade the output beam quality. If the aperture size is too large, the whole size of the system has to be expanded with the result of potential fewer applications. It is also a waste of material at a certain level. Therefore, to choose a right aperture size is very important. In order to reduce aperture diffraction effects while minimizing the lens sizes, only the portions of the lenses where approximately 99.78% of the beam irradiance is refracted are assumed to be the surface diameter. To determine the lens aperture radius, the power transmission equation [17] is used:

$$\frac{P_a}{P_T} = 1 - e^{-2a^2/w^2(z)} \tag{3.44}$$

Where, a is the aperture radius, $w(z)$ is the beam spot radius at position z, P_T is the total power of the input beam, and P_a is the transmitted power through the aperture. For 99.78% power transmission, the following equation is required:

$$a = 1.75 w_f \tag{3.45}$$

Where w_f is the beam spot radius after circularization in this research.

CHAPTER 4

METHODOLOGY

This chapter demonstrates the step by step design procedures and derivations of the equations and surface parameters for each surface individually. Geometrical ray optics method is used in the design as introduced in Chapter 3.

4.1 Overview of the system operation

As stated in Chapter 3, a four-lens system shown in Figure 3.3 is proposed to collimate the beams from laser diodes, transform the irradiance distribution to a uniform radiance, and make the beam spot rectangular. This system is applied to the laser diode arrays to combine the beams into one single beam with the rectangular shape and uniform amplitude. In this chapter, system operation is explained and each surface's functionality with respect to beam propagation is shown. Because each incoming beams have different divergence angle in the perpendicular and parallel direction, we have to treat the light rays in these two orthogonal planes respectively, and thus the surface shape must be designed differently in each planes. In optics, it is common and convenient to use a line segment to represent a surface and to demonstrate the function of that surface, as shown in Figure 4.1. The number 1-8 means that there are 8 surfaces in sequence and each number represents a surface. The angles $\theta_{\perp}$ and $\theta_{\parallel}$ denotes the two different divergence angles of the laser sources in perpendicular and parallel transverse direction.

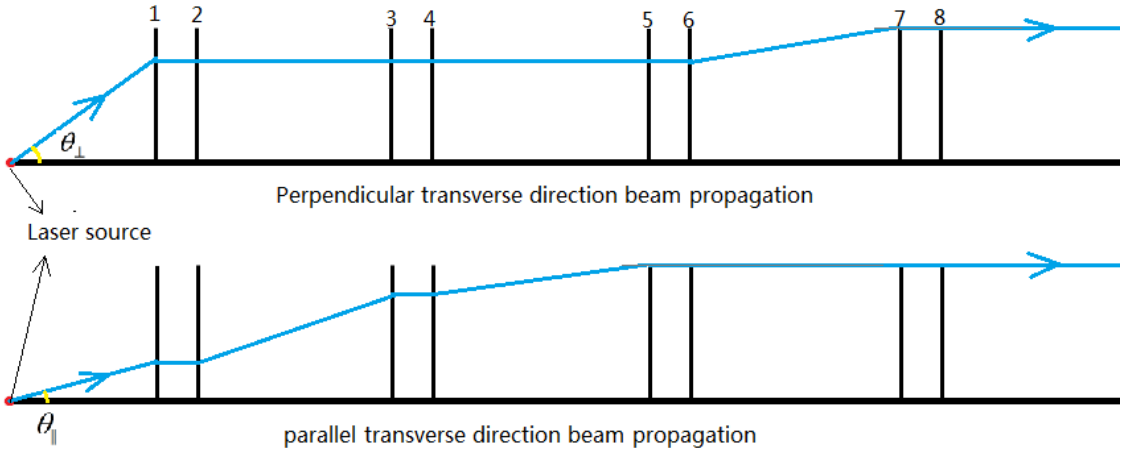

Figure 4.1: A schematic diagram of four-lens system

Only the up half of the lens system is shown in the above figure, because the system is symmetric about the optical axis in both directions. From this figure, we can see clearly how light rays are expected to propagate in each plane. In fact, this figure is a ray tracing of the marginal rays in two orthogonal directions; after surface 8, these two marginal rays propagate parallel to the optical axis and have the same radial height. To describe the ray propagation, we refer to the light rays in perpendicular and parallel planes as TLR (transverse light ray) and PLR (parallel light ray) respectively.

First, the incoming beam from laser source meets surface 1 which collimates TLR and PLR simultaneously. The rays will have different radial height after being refracted by surface 1 due to the different divergent angle $\theta_{\perp}$ and $\theta_{\parallel}$. The beam at this stage still has the elliptical shape while propagating within the lens. In order to circularize the beam spot, the beam width in parallel plane must be expanded so that it is the same as the one in perpendicular plane. Therefore, only the beam in the parallel transverse direction is allowed to diverge at the back surface of the first lens (surface 2) while the beam in the perpendicular transverse direction propagates with no refraction. The second lens is

positioned at a distance from the first where TLR and PLR have the same radial height and the beam shape becomes circular, as shown in Figure 4.2.

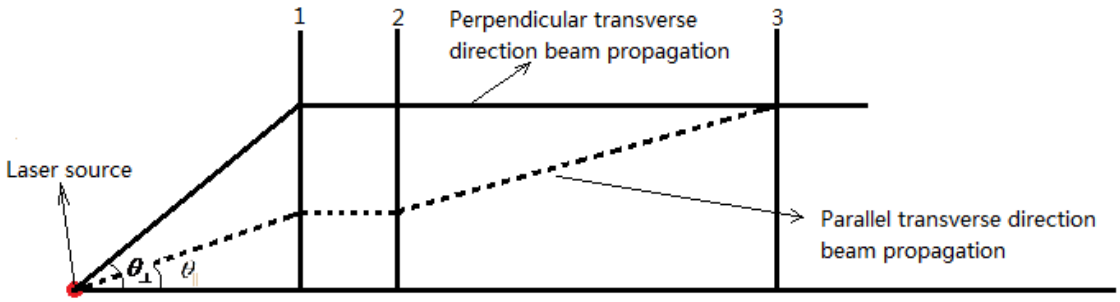

Figure 4.2: A schematic diagram of the first three surfaces.

The surface 3 is designed to collimate the beam only in the parallel perpendicular beam allowing the beam to continue to propagate as a collimated circular beam in both transverse directions. Thus, at this stage the beam has been expanded, circularized and collimated. The next step is to uniform the energy distribution and make the beam spot rectangular. Once this is achieved, combining several rays having the same features at this stage is easy and convenient.

As mentioned earlier, the beam profile is modeled as two independent 2-D Gaussian beams propagating along the two orthogonal planes (the x-z and the y-z planes). Therefore, the beam shaper is designed separately in these two orthogonal planes to achieve a rectangular, collimated and uniform beam at the output plane. As shown in Figure 4.1 surface 4 and surface 5 transforms PLRs and surface 6 and 7 transforms TLRs. Because the beam spot are shaped to be identical in perpendicular and parallel planes after surface 3, surface 4&6 and surface 5&7 can be designed identically and achieve the same functions. Unlike surface 2, surface 4&6 not only expands the beam but also refracts the beam in a way that the density of the light rays are evenly incident on the surface 5&7, meaning that the designing process transforms the density of light rays of

the incoming beam into a uniformly distributed form. Finally, surface 5&7 collimates the beam. Surface 8 is flat in both transverse directions and does not participate in beam shaping since at this surface the beam already has the desired profile.

According to the above descriptions about the functions of each surface, surface 1 is rotationally symmetric about the optical axis of the system; surface 2-7 are cylindrical shape whose cylindrical axis is perpendicular to the optical axis of the system; surface 8 is flat. The whole system can be divided into two parts: the first part, containing the first three surfaces, expands the beam to achieve collimation and circularization, and the second part, containing the remaining surfaces, further expands while achieving uniform irradiance and rectangular shape. The second part is to evenly spread the light rays in both planes, to ensure that the resultant light ray densities in perpendicular and parallel planes are the same thus to make the irradiance uniform.

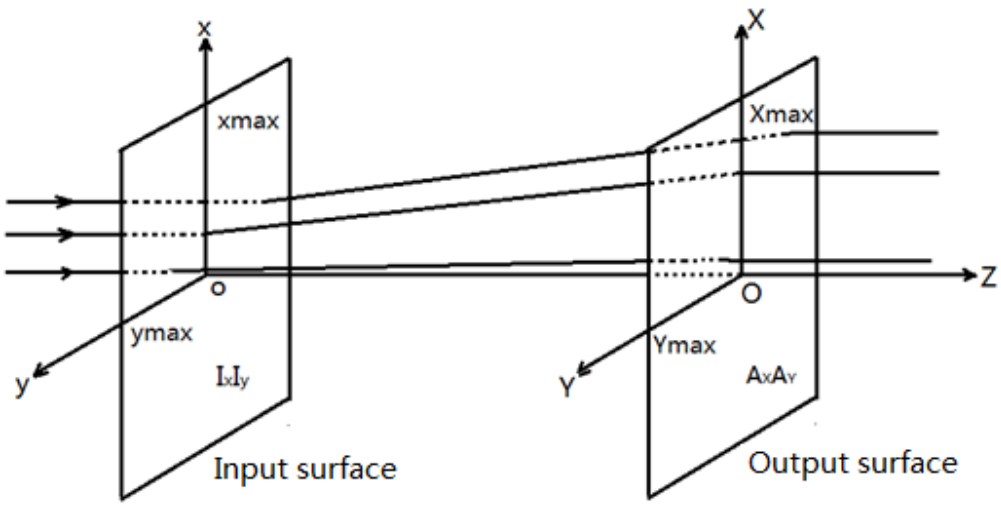

Figure 4.3: A simplified mode of two surfaces making the irradiance uniform

During the whole process, the step of beam circulation by the first part is very important, because the second part only works when the beam has the same energy

profiles in two orthogonal planes; we can prove this necessity of circularization from the simple mathematical point, as shown in Figure 4.3. Lower case x and y are used for the first surface and upper case X and Y are used for the second surface. For our concern, both surfaces have the same aperture size, so

$$x\max = X\max \quad \text{and} \quad y\max = Y\max \tag{4.1}$$

The beam first meets Input surface and has an irradiance distribution function on this surface given by:

$$I_{in} = I_0 I_x I_y \tag{4.2}$$

Then, refracted by this Input surface, the beam propagates toward Output surface and has an irradiance distribution function on this surface given by:

$$I_{out} = A_X A_Y \tag{4.3}$$

Where I_0 is the arbitrary amplitude of the input beam, A_X and A_Y are the constant values of irradiance in the perpendicular and parallel transverse directions. I_0 is chosen to be unity (1) here. Because we want to achieve a uniform irradiance profile on the second surface, we have:

$$A_X = A_Y \tag{4.4}$$

As stated in Section 3.3.6, the aperture is large enough to avoid beam truncation and conserve the energy. Therefore, the energy passing through the first surface is the same as that passing through the second surface, so

$$E_{in} = \int_{-x\max}^{x\max} I_x dx \int_{-y\max}^{y\max} I_y dy = E_{out} = \int_{-X\max}^{X\max} A_X dX \int_{-Y\max}^{Y\max} A_Y dY \tag{4.5}$$

Where E_{in} and E_{out} are the input and output energies. Because the x and y coordinates are independent of each other and the beam propagation is decoupled into two orthogonal

planes, the x and y coordinate variables can be calculated independently in equation (4.5). Rewrite equation (4.5) and using equation (4.4), we have:

$$\int_{-x\max}^{x\max} I_x dx = \int_{-X\max}^{X\max} A_X dX = \int_{-Y\max}^{Y\max} A_Y dY = \int_{-y\max}^{y\max} I_y dy \tag{4.6}$$

Substitute equation (4.1) into equation (4.6), we conclude that:

$$I_x = I_y \tag{4.7}$$

Above equations assumes the initial beam has the same irradiance distribution in both orthogonal planes. In our case, the source diode produces elliptical Gaussian beam, therefore, we first circularize the beam to obtain circular Gaussian beam profile and thus the energy distribution is the same in both x-z and y-z planes.

4.2 Lens design method

The model of the proposed system and the functions of each surface have been described in the foregoing section. In this section, surface equation $z(r)$ of each surface is defined. In order to solve this problem, we first define parameters clearly. In Section 4.2.1, the known input parameters are shown. According to these known parameters, the surface function for each surface is derived in the following three sections.

4.2.1 Known parameters

The first two known parameters, inherent of the laser source itself, are the divergent angles $\theta_{\perp}$ and $\theta_{\parallel}$ in the two orthogonal planes. For applications using monochromatic laser beams, there are no chromatic aberrations present, and it is satisfactory to use the same material (index of refraction) for all four lenses, so we choose

all lenses to have the same refractive index n. Because the beam propagations inside the lenses are always designed to be parallel to the main axis, the thickness of each lens has no direct effect on the beam propagation and can be chosen in a way that the edges of the front and back surface of each lens do not intersect with each other within the chosen aperture size of each lens; The output beam diameter is required and is set to have the same value as the space between two laser diode sources in order to apply this system to the laser diode arrays using lenslet technology; Then according to the equation (3.45), the beam radius after the first part of the system is known.

$$w_f = \Delta d / (2 \cdot 1.75) \tag{4.8}$$

To sum up, as shown in Figure 4.4, the known parameters are:

1. The refractive index of each lens: n;
2. The divergence angle of the laser diode sources: $\theta_{\perp}$ and $\theta_{\parallel}$;
3. The desired output beam spot diameter: Δd;
4. The beam spot radius after surface 4: w_f;
5. The thickness of each lens: t_1, t_2, t_3 and t_4;
6. The distances between each lens: d_3 and d_5;

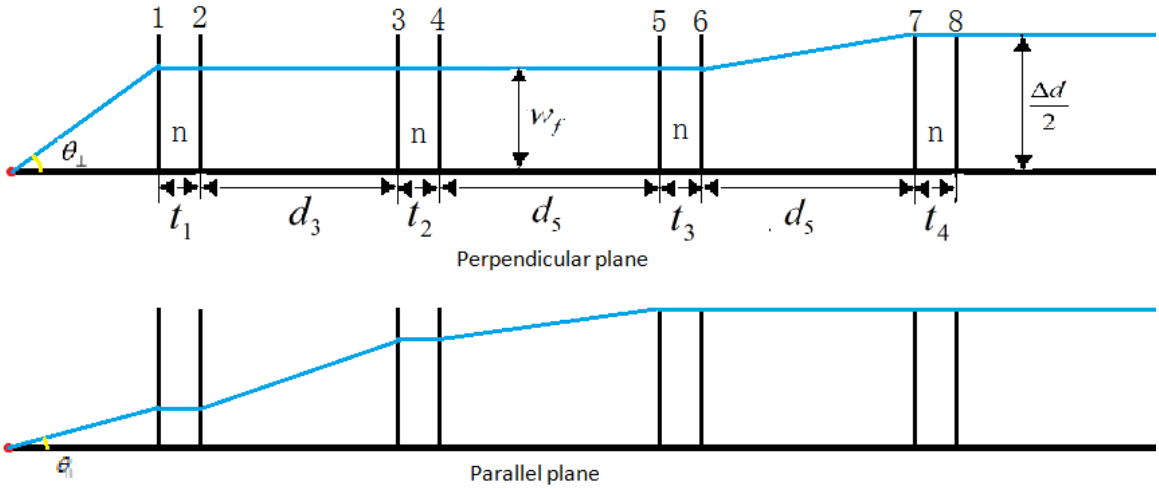

Figure 4.4: The illustration of the known parameters

4.2.2 The design of surface 1

As a first step, the front surface of the first lens (surface 1) is designed. Figure 4.5 shows a representation of the surface in the perpendicular transverse direction (x-z plane) and variables used to calculate lens parameters for the front surface of the first lens. Because surface 1 is a rotationally symmetric surface, the surface shape in parallel transverse direction is the same as that in perpendicular direction, and the cylindrical coordinate is used for derivation. Furthermore, throughout this research, r is used for the radial height of a light ray. As stated earlier, our goal is to derive the sag function $z(r)$ of each surface. As shown in Figure 4.5, $z(w_f)$ represents the surface sag at the radial height of w_f. Point A represents laser diode source, and it acts like the focal point of the surface 1. Point B represents the point of intersection of a light ray and surface. Point C is the projection point of B on the main axis z. d_1 is the distance between point A and the

surface vertex (vertex is the point where the optical axis crosses the surface). The distance between the surface vertex and point C is the surface sag $z(w_f)$.

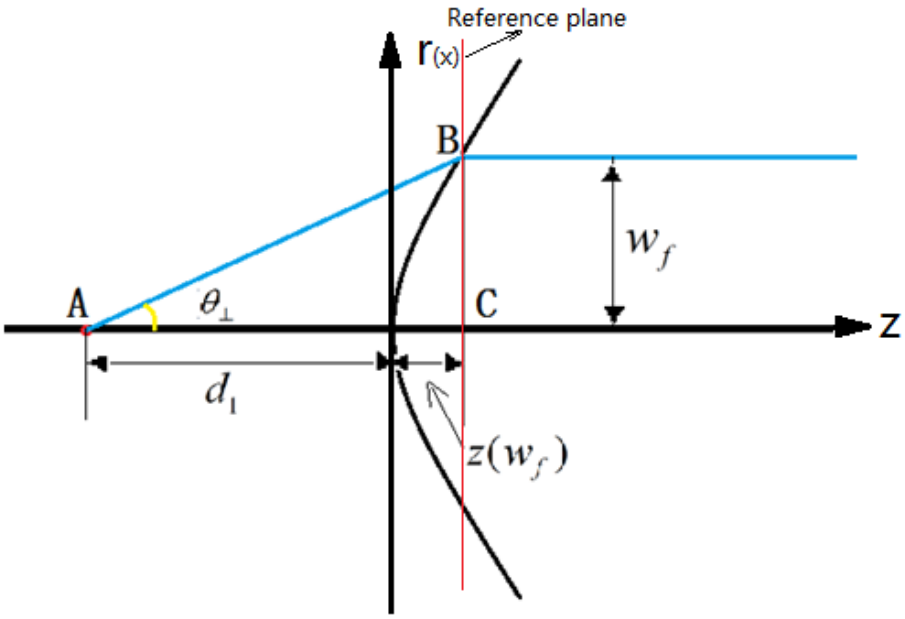

Figure 4.5: A schematic representation of surface 1 in the x-z plane

The surface 1 is a rotationally symmetric surface, and only the x-z plane calculations are shown in this section. The y-z plane calculations are the same as x-z plane

In triangular ABC, we use the trigonometric relation:

$$\tan(\theta_\perp) = \frac{w_f}{d_1 + z(w_f)} \tag{4.9}$$

The rays are emanated from the point A and propagate parallel to the optical axis after surface 1, so a plane wavefront is formed by surface 1 and the light rays have the same phase at the reference plane as shown in Figure 4.5. Therefore, according to the constant optical path length condition (COPLC), as stated in chapter 3, we have:

$$\begin{cases} (OPL)_{AB} = \sqrt{w_f^2 + (d_1 + z(w_f))^2} \\ (OPL)_{AC} = d_1 + n \cdot z(w_f) \\ (OPL)_{AB} = (OPL)_{AC} \end{cases} \tag{4.10}$$

Solving simultaneously Equation (4.9) and equation (4.10) provides the numeric value of the distance d_1

$$d_1 = \frac{\sqrt{w_f^2 + (\frac{w_f}{\tan(\theta_\perp)})^2} - n \cdot \frac{w_f}{\tan(\theta_\perp)}}{1-n} \tag{4.11}$$

As long as d_1 is known, we apply the COPLC to all rays passing through the surface 1, to ensure that all rays have the same phase at the reference plane and thus become collimated. Applying COPLC to any light ray with the radial height r, we obtain:

$$\sqrt{r^2 + (d_1 + z(r))^2} = d_1 + n \cdot z(r) \tag{4.12}$$

Solving equation (4.12), we have

$$\begin{aligned} z(r) &= \frac{-2d_1(n-1) + \sqrt{4d_1^2(n-1)^2 + 4(n^2-1)r^2}}{2(n^2-1)} \\ &= \frac{2r^2}{(2d_1(n-1) + \sqrt{4d_1^2(n-1)^2 + 4(n^2-1)r^2})} \\ &= \frac{\frac{1}{d_1(n-1)} r^2}{(1 + \sqrt{1-(1-n^2)\frac{1}{d_1^2(n-1)^2} r^2})} \end{aligned} \tag{4.13}$$

We realize that the resultant surface sag $z(r)$ has the same form as equation (3.38)

$$z(r) = \frac{cr^2}{1 + \sqrt{1-(1+k)c^2r^2}}$$

Therefore, surface 1 is a common conic surface—a type of aspherical surface whose surface functions have no deformation terms. From these equations we define:

$$c_1 = \frac{1}{d_1(n-1)} \tag{4.14}$$

$$R_1 = d_1(n-1) \tag{4.15}$$

$$k_1 = -n^2 \tag{4.16}$$

Where c_1 is the surface curvature of surface 1; R_1 is the surface radius of surface 1; k_1 is the conic constant of surface 1. The feature of surface 1 is to collimate the beam from single point source with no geometrical aberration.

Next, the aperture diameter (physical diameter of the surface of the lenses in both transverse directions) and the lens thickness are determined using the energy transmission criteria of over 99% as stated earlier. For simplicity, the aperture sizes of all lenses are decided to be the same Δd which is required to be equal to the space between laser diode sources. The thickness of all lenses is reasonably determined in a way that the front surface of a lens does not intersect with the back surface of that lens.

4.2.3 The design of surface 2 and surface 3

Surface 1 is a rotationally symmetric surface, and the beam is collimated by this surface in both transverse directions, but not yet circularized. Therefore, surface 2 is designed to allow the beam to propagate without any refraction in the perpendicular direction while allowing it to diverge further in the parallel direction. That means, surface 2 is a cylindrical lens and only have optical power in parallel transverse direction. Surface 3 is positioned at a distance when the beam profile becomes circular in both

transverse directions (see Figure 4.2). The second lens, the surface 3, is also a cylindrical. The incoming beam for surface 2 is collimated and the outgoing beam after surface 3 should also be collimated, in order to achieve this requirement, the COPLC must be satisfied between reference plane 1 and reference plane 2 as shown in Figure 4.6, so the surface 2 and surface 3 have to be designed together. Because surface 2 and 3 are both designed to have optical power in the parallel transverse direction, only y-z plane is shown in Figure 4.6. The incoming beam for surface 2 has a radial height of w_{f1}, and the outgoing beam after surface 3 has a radial height of w_f, which is equal to the radial height in x-z plane, so the final beam spot is circular. During the propagation, the light meets surface 2 at point B and surface 3 at point D. Point C and E are the projection point of point B on the main axis z and on the reference plane 2 respectively, so the distance between the vertex of surface 2 and point C is the surface sag at radial height of w_{f1} denoted as $z_{22}(w_{f1})$. Similarly, $z_{31}(w_f)$ is the surface sag of surface 3 at radial height of w_f. If we reversely extend the light rays refracted by surface 2, they will come to a point (point A in Figure 4.6) as if all rays are radiated from this point. In fact, this is how a secondary focal point of a concave lens is defined. For surface 3, point A acts like a point source, then it is refracted into a parallel beam in the right side of surface 3, so point A is the primary focal point of the surface 3. The distance between point A and the vertex of surface 2 is denoted as d_2'. And the distance between the vertex of surface 2 and that of surface 3 is denoted as d_3.

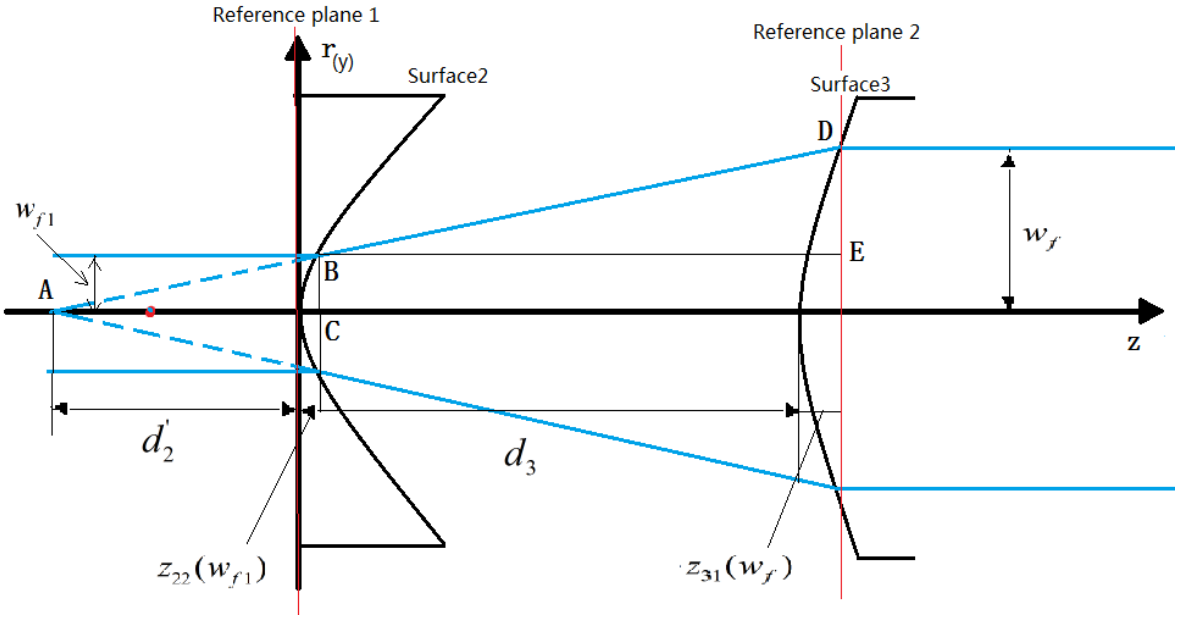

Figure 4.6: A schematic representation of surface 2 and surface 3 in the x-z plane

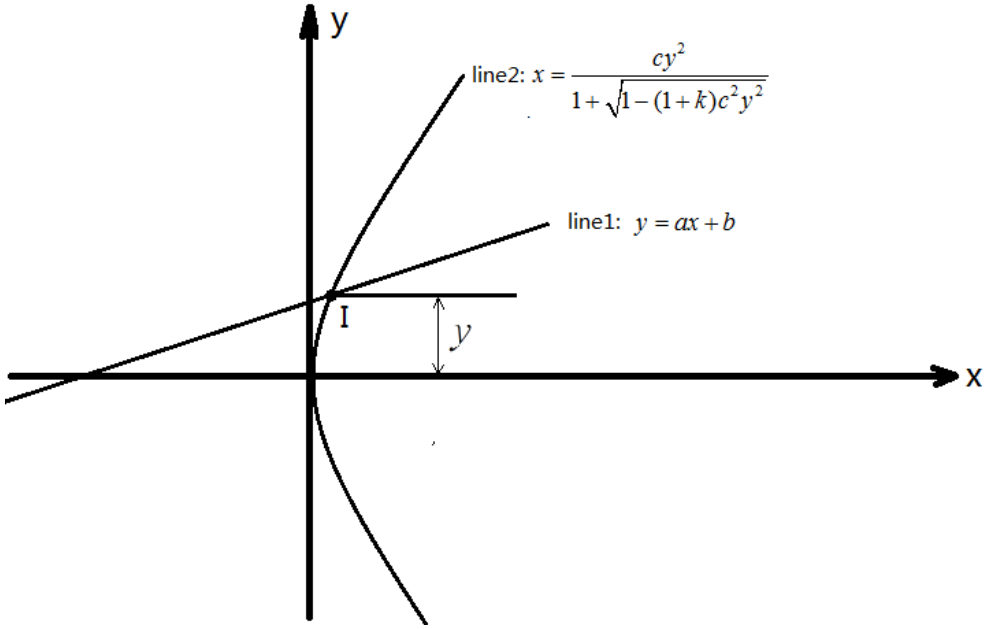

Figure 4.7: The x-y rectangular coordinate system calculating the intersection point of light ray and surface

As a first step, the incoming beam size w_{f1} must be determined, because its value directly affects the optical power and surface parameters of both surface 2 and surface 3.

In order to get the point where the light meets surface 2, a new coordinate is established as shown in Figure 4.7.

Line 1 represents a random ray with the line equation

$$y = ax + b \tag{4.17}$$

Where a is the slop, and b is the y- intercept distance. Line 2 represents the surface with the surface equation

$$x = \frac{cy^2}{1+\sqrt{1-(1+k)c^2y^2}} \tag{4.18}$$

Where c is the curvature of the surface and k is the conic constant of the surface. With the help of MATLAB, we can solve equation (4.17) and equation (4.18) simultaneously to generate the coordinate of the interception point $I(x, y)$. The coordinate y has the form:

$$y(a,b,c,k) = \frac{a+bc+bck}{(c+ck)} - \frac{a(k+1)(1-b^2c^2k-2abc-b^2c^2)^{1/2}+a^3+a^2bc+a^2bck}{(a^2+k+1)(c+ck)} \tag{4.19}$$

A MATLAB function $rlts(a,b,c,k)$ has been developed to specially calculate the equation (4.19) and to obtain the radial height of the intersection points between the line and the conic surface (see appendix). We calculate the beam spot size w_{f1} after surface 1 in x-z direction, as shown in Figure 4.7. In this case,

$$\begin{cases} a = \tan(\theta_{\parallel}) \\ b = d_1 \cdot \tan(\theta_{\parallel}) \\ c = c_1 \\ k = k_1 \end{cases} \tag{4.20}$$

Therefore,

$$w_{f1} = y(\tan(\theta_{\parallel}), d_1 \cdot \tan(\theta_{\parallel}), c_1, k_1) \tag{4.21}$$

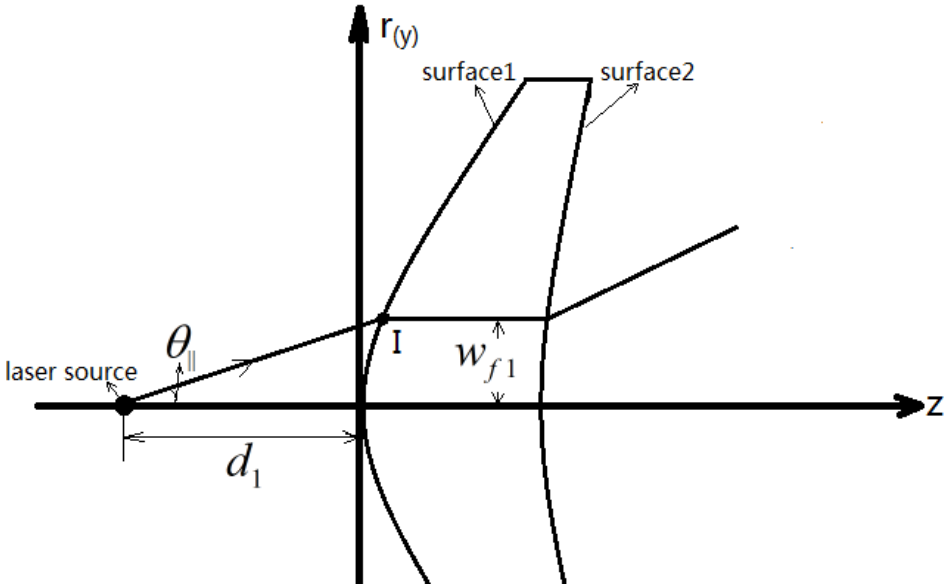

Figure 4.8: A schematic of a light ray emanated at divergent angle in parallel transverse direction

The second step is to know the value of distance d_2', just as we did in designing surface 1. Because basically point A serve the same function in Figure 4.5 as in Figure 4.6—point A is treated as the focal point of both surface 2 and surface 3. The equations for the parameters of surface 2 and 3 will have the same form as equations 4.14 through 4.16.

From the advanced trigonometric relation in triangular ABC and BDE in Figure 4.6:

$$\frac{DE}{BE} = \frac{BC}{AC} \tag{4.22}$$

Thus,

$$\frac{w_f - w_{f1}}{d_3 - z_{22}(w_{f1}) + z_{31}(w_f)} = \frac{w_{f1}}{d_2^{'} + z_{22}(w_{f1})} \tag{4.23}$$

For surface 2, between point A and reference plane formed by BC, using COPLC, we obatin:

$$\begin{cases} (OPL)_{AC} = d_2^{'} + n \cdot z_{22}(w_{f1}) \\ (OPL)_{AB} = \sqrt{w_{f1}^2 + (d_2^{'} + z_{22}(w_{f1}))^2} \\ (OPL)_{AC} = (OPL)_{AB} \end{cases} \tag{4.24}$$

Similarly, for surface 3, between reference plane 1 and reference plane 2, using COPLC, we have:

$$n \cdot z_{22}(w_{f1}) + \sqrt{(d_3 - z_{22}(w_{f1}) + z_{31}(w_f))^2 + (w_f - w_{f1})^2} = d_3 + n \cdot z_{31}(w_f) \tag{4.25}$$

In equations (4.23) to (4.25), there are 3 unknowns namely $d_2^{'}$, $z_{22}(w_{f1})$ and $z_{31}(w_f)$ and there equations. Solving these three equations simultaneously, $d_2^{'}$ can be solved analytically. Again MATLAB codes are written to obtain the expression for $d_2^{'}$ due to its Complexity as:

```
(d3*n*wf1-d3*wf1+(wf1^2*((n^2*wf^2+n^2*wf1^2+d3^2*n^2+d3^2-2*n^2*wf*wf1-
2*d3^2*n-(2*d3*(n*((d3^2*n-d3^2+n*wf^2+wf^2+n*wf1^2+wf1^2-2*n*wf*wf1-
2*wf*wf1)/(n-1))^(1/2)+d3))/(n+1)+(2*d3*n*(n*((d3^2*n - d3^2 + n*wf^2+wf^2+
n*wf1^2+wf1^2-2*n*wf*wf1-2*wf*wf1)/(n-1))^(1/2)+d3))/(n+1))/(n^2-1))^(1/2))
/(wf-wf1)+(wf1*(n*((d3^2*n-d3^2+n*wf^2+wf^2+n*wf1^2+wf1^2-2*n*wf*wf1-
2*wf*wf1)/(n-1))^(1/2)+d3))/(n+1)-(wf*wf1*((n^2*wf^2+n^2*wf1^2+d3^2*n^2+
d3^2-2*n^2*wf*wf1-2*d3^2*n-(2*d3*(n*((d3^2*n-d3^2+n*wf^2+wf^2+n*wf1^2+wf1^2
-2*n*wf*wf1-2*wf*wf1)/(n-1))^(1/2)+d3))/(n+1)+(2*d3*n*(n*((d3^2*n-d3^2+
n*wf^2+wf^2+n*wf1^2+wf1^2-2*n*wf*wf1-2*wf*wf1)/(n-1))^(1/2)+d3))/(n+1))
/(n^2-1))^(1/2))/(wf-wf1))/(n*wf-wf-n*wf1+wf1)
```

(4.26)

As expected, $d_2^{'}$ is very complicated and it is very difficult to solve by hand. However, if MATLAB is used to solve one or more equations and it results a real expression, it means that these equations are solvable and the answer does exist. Generally speaking, unlike the results obtained from the numerical method, a complete

MATLAB expression means that the answer can be accurately and precisely calculated. Therefore, we can use the resultant $d_2^{'}$ and equation (4.14) to (4.16) to determine the surface parameters for surface2:

$$\begin{cases} c_2 = \dfrac{1}{d_2^{'}(n-1)} \\ R_2 = d_2^{'}(n-1) \\ k_2 = -n^2 \end{cases} \tag{4.27}$$

And for surface 3:

$$\begin{cases} c_3 = \dfrac{1}{(d_2^{'} + d3)(n-1)} \\ R_3 = (d_2^{'} + d3)(n-1) \\ k_3 = -n^2 \end{cases} \tag{4.28}$$

4.2.4 The design of surface 4&6 and surface 5&7

In this section, the design of surface 4&6 and surface 5&7 is presented. After surface 3, the beam is collimated and reshaped from elliptical Gaussian beam to circular Gaussian beam. As stated earlier, surface 6 and surface 7 are designed to further shape the beam in perpendicular transverse direction so that the outgoing beam propagate as a collimated beam and have uniform irradiance profile with rectangular beam spot. Surface 6 is to expand the beam; and at the same time transform the light rays of different radial height to evenly distributed rays incident on surface 7 so that the irradiance profile is uniformed. The incoming beam for surface 6 and the outgoing beam after surface 7 are all required to be collimated, so the COPLC must be satisfied to ensure the feature of plane wave of the beam before surface 6 and after surface 7. Therefore, these two

surfaces must also be designed together, just as we did in section 4.2.3. Remember, surface 4 and 5 are identical with surface 6 and 7 except that surface 4 and 5 transform the beam parallel direction, so there is no difference in the design of these two groups of surfaces. Here, for the convenient sake, we are going to pick x-z plane for derivation. Before we actually start to solve the surface equations for these surfaces and modulate the irradiance distribution of the beam after surface 3, we first study the irradiance distribution and mathematical function of this incoming beam.

For this purpose, we start from the irradiance of the laser diode itself. In industrial world, the diode model can be used to define one diode, a 1D array of diodes, or a 2D array of diodes; and each diode has an intensity distribution given by [29]:

$$I(\theta_x, \theta_y) = I_0 e^{-2((\frac{\theta_x}{\alpha_x})^{2G_x} + (\frac{\theta_y}{\alpha_y})^{2G_y})} \tag{4.29}$$

Where α_x is the XZ divergence angle in degrees, G_x is the "supergaussian" factor for the x direction, with similar definitions for the y subscripted values. If G_x is 1.0, then the expression gives a typical Gaussian distribution. If G_x is greater than 1.0, then the distribution becomes more "square". Therefore, both G_x and G_y must be greater than or equal to 1.0. Most laser diode manufacturers specify the far field divergence angles as the full width of the distribution between the half power points, θ_{fwhm}. For a true Gaussian distribution as in our case ($G_x = 1$), setting the left hand side of the equation (4.29) to $\frac{1}{2} I_0$, setting θ_y to zero, substituting for θ_x the value of $\frac{1}{2}\theta_{fwhm}$, then solving equation, we have:

$$\frac{1}{2}I_0 = I_0 e^{-2((\frac{\frac{1}{2}\theta_{fwhm}}{\alpha_x})^2} \tag{4.30}$$

Then this gives:

$$\alpha_x = \frac{\theta_{fwhm}}{\sqrt{2\ln(2)}}, or \quad \alpha_x = (0.8493218)\theta_{fwhm} \tag{4.31}$$

For example, a diode with a θ_{fwhm} in the x direction of 10 degrees, the value for α_x would be 8.493218 degrees. A similar conversion applies in the y direction.

Now, we can use equation (4.29) to get the irradiance distribution expression of laser diode in the perpendicular transverse direction (x-z plane), in this case:

$$I(\theta_x) = I_0 e^{-2(\frac{\theta_x}{\alpha_x})^2} \tag{4.32}$$

The next step is to determine the irradiance distribution expression on surface 1, meaning that the intensity I must be expressed in terms of x or y coordinates. Figure 4.9 shows a schematic representation of the light rays of different angle of divergence θ_x incident on surface 1 in the perpendicular plane.

Once again from a trigonometric relation in triangular ABC, we have:

$$\tan(\theta_x) = \frac{x}{d_1 + z_1(x)} \tag{4.33}$$

Thus:

$$\theta_x = \arctan(\frac{x}{d_1 + z_1(x)}) \tag{4.34}$$

And,

$$I(x) = I_0 e^{-2(\frac{\arctan(\frac{x}{d_1+z_1(x)})}{\alpha_x})^2} \tag{4.35}$$

Where

$$\alpha_x = \theta_\perp \tag{4.36}$$

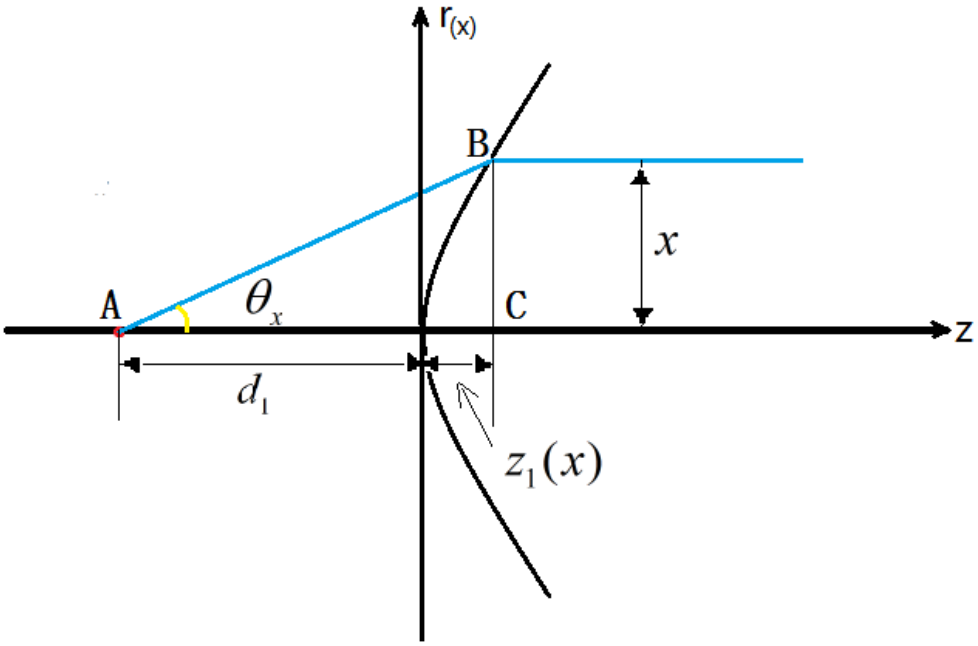

Figure 4.9: A schematic representation of the light rays of different divergence angle θ_x from the optical axis incident on surface 1 in the perpendicular plane

Because the beam is already collimated by surface 1 in x-z plane and there is no additional beam shaping done, after surface 3, the beam has the same irradiance profile as described by the equation (4.35). In addition, the beam is circularized by the first part of the system, so the irradiance profile in y-z plane and x-z plane has the same expression. Therefore, the problem is reduced to a one dimensional, and we focus our attention only on one transverse direction.

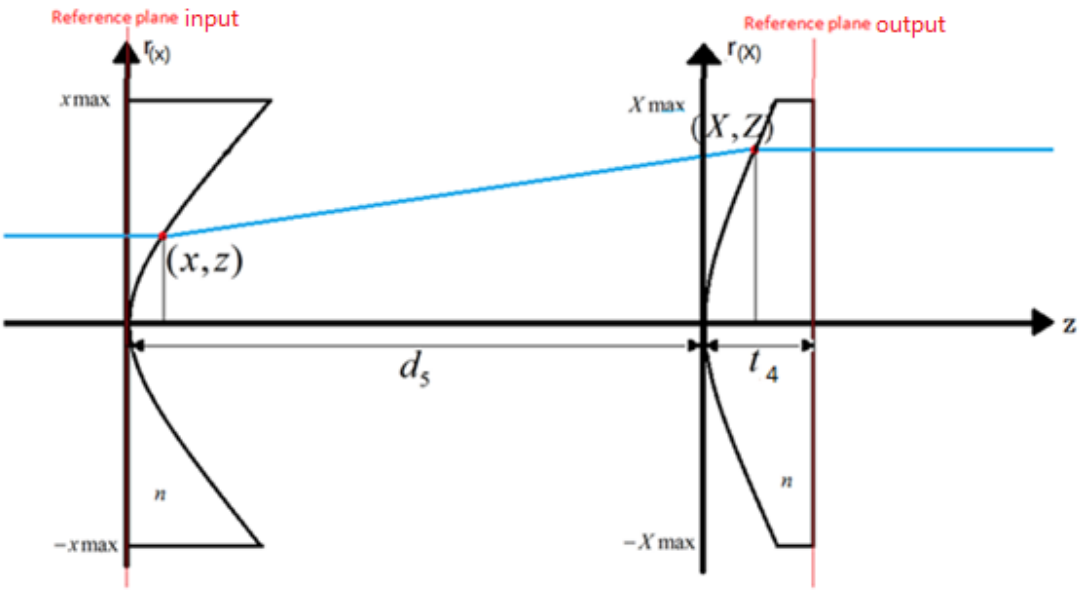

Figure 4.10: the illustration of the general design in the x-z plane

Figure 4.10 illustrate the general design in the x-z plane. (x, z) is the coordinate point where light ray meets surface 6 and (X, Z) is the coordinate point where light ray meets surface 7. $x\,\text{max}$ and X max are the aperture size. As stated in the section 4.2.1,

$$x\,\text{max} = X\ \text{max} = \frac{\Delta d}{2} = 1.75 w_f \tag{4.37}$$

The important task to achieve the uniform irradiance is to determine the locations of each light ray's coordinates. In another word, we need to find a relationship between (x, z) and (X, Z) so that the light rays will evenly redistribute on the back surface. Besides, the characteristic of beam collimation is desired to be maintained. Unfortunately, the only known variable is the incoming ray height x, meaning that the first surface sag z, the outgoing ray height X and the second surface sag Z have to be expressed in terms of x. As long as $X(x)$, $z(x)$ and $Z(x)$ are solved, we can trace a reasonable amount of light rays with different ray height x and obtain a series of desired (x, z) and (X, Z) coordinate

points. Then use fitting method described in section 3.4.5 to determine the resultant surfaces constituted by these traced points.

First, we start with the energy distribution. The input irradiance distribution function in x-direction is given by equation (4.35). The desired output irradiance distribution function is given as:

$$I(X) = A_X \tag{4.38}$$

A_X is the constant value of the square-pulse function in the perpendicular transverse direction. Using the energy conservation principle given by equation (4.6), and substituting equation (4.35) and equation (4.38) into equation (4.6), we have:

$$\int_{-x\max}^{x\max} e^{-2\left(\frac{\arctan\left(\frac{x}{d_1+z_1(x)}\right)}{\alpha_x}\right)^2} dx = \int_{-X\max}^{X\max} A_X\, dX \tag{4.39}$$

Then Solving for A_X , we have

$$A_X = \frac{1}{2X\max} \cdot \int_{-x\max}^{x\max} e^{-2\left(\frac{\arctan\left(\frac{x}{d_1+z_1(x)}\right)}{\alpha_x}\right)^2} dx \tag{4.40}$$

Conservation of energy principle also provides a relationship for any two corresponding surface areas [28]. In Figure 4.10, this relationship can be described as

$$\int_{0}^{x} e^{-2\left(\frac{\arctan\left(\frac{x}{d_1+z_1(x)}\right)}{\alpha_x}\right)^2} dx = \int_{0}^{X} A_X\, dX \tag{4.41}$$

Solving equation (4.40) results the relationship between x and X ,

$$X(x) = 2X \max \frac{\int_0^x e^{-2\left(\frac{\arctan\left(\frac{x}{d_1+z_1(x)}\right)}{\alpha_x}\right)^2} dx}{\int_{-x\max}^{x\max} e^{-2\left(\frac{\arctan\left(\frac{x}{d_1+z_1(x)}\right)}{\alpha_x}\right)^2} dx} \tag{4.42}$$

In order for the reference plane 2 to have the same phasefront as the reference plane 1, it is necessary for all rays traced between these planes to have the same optical path length according to the COPLC.

The optical path length of a ray passing along the optical axis is, as shown in Figure 4.10:

$$(OPL)_0 = d_5 + nt_4 \tag{4.43}$$

The optical path length of an arbitrary ray crossing the x-coordinate at a point (x, z) is given by:

$$(OPL)_x = nz + \sqrt{(X-x)^2 + (Z-z)^2} + n(d_5 + t_4 - Z) \tag{4.44}$$

The COPLC requires that

$$(OPL)_0 = (OPL)_x \tag{4.45}$$

Solve equation (4.43)-(4.45) simultaneously, an equation for $(Z-z)$ in terms of $(X-x)$ is obtained and is given by:

$$(Z-z) = \frac{n(n-1)d_5 + \sqrt{(n-1)^2 d_5^2 + (n^2-1)(X-x)^2}}{n^2-1} \tag{4.46}$$

Finally, the Snell's law must be obeyed by any rays traced. Snell's law is a formula used to describe the relationship between the angles of incidence and refraction, when referring to light passing through a boundary between two different isotropic media. Figure 4.11 shows the refraction phenomena of a light ray incident on point (x, z).

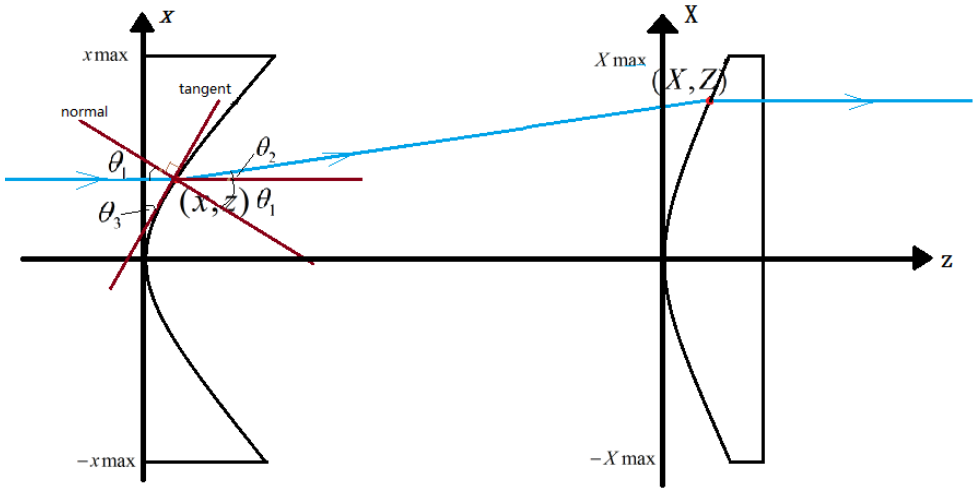

Figure 4.11: Illustration of refraction at point (x, z)

A line tangent to the surface and a line normal to the surface are drawn in the figure. An angle θ_1 is subtended by the normal line and the incident light ray; The angle θ_2 is subtended by the incident light ray and the refracted light ray; The angle θ_3 is subtended by the x axis and the tangent line.

From the trigonometric relation, we have:

$$\tan\theta_2 = \frac{X - x}{Z - z} \tag{4.47}$$

According to the Snell's law, we have:

$$n\sin\theta_1 = \sin(\theta_1 + \theta_2) \tag{4.48}$$

Using MATLAB, we solve the above two equations for θ_1 as:

$\theta_1(x)$ = -(log(-(X+deltaz*i-x-deltaz*n*((X^2-2*X*x+deltaz^2+x^2)/deltaz^2)^(1/2)*i)/(X-deltaz*i –x +deltaz*n*((X^2-2*X*x+deltaz^2+x^2)/deltaz^2)^(1/2)*i))*i)/2; (4.49)

Furthermore, through careful observation, we can find that there is a relationship between the slope of the surface sag z and θ_1:

$$z' = \tan\theta_3 = \tan\theta_1 = z'(x) \tag{4.50}$$

Then according to the definition of definite integral,

$$z(x) = \int_0^x z'(x)dx + z(0) = \int_0^x z'(x)dx \tag{4.51}$$

We solve for $Z(x)$ by substituting equation (4.51) into equation (4.46):

$$Z(x) = (Z - z)\big|_x + z(x) \tag{4.52}$$

Until now the surface sag z of the first surface, the X coordinate and the surface sag Z of the second surface have all been expressed in terms of the incoming ray height x. Therefore, we are able to trace a series of light rays with different ray heights x, and then use equation (4.51) to get the required surface sag z at each height. Using equation (4.42) we obtain the corresponding X coordinates at the second surface and using equation (4.52) we obtain the desired surface sag Z at each ray height X. Eventually, we calculate number of points $(x_1, z_1), (x_2, z_2), ..., (x_{i-1}, z_{i-1}), (x_i, z_i)$ on the first surface, and the same number of points $(X_1, Z_1), (X_2, Z_2), ..., (X_{i-1}, Z_{i-1}), (X_i, Z_i)$ on the second surface. Then, using surface fitting method, we find the corresponding fitted surface. Theoretically, if there was no error produced in the fitting process, the resultant surfaces would pass through every traced point and have the exactly same surface shape as the desired surface.

CHAPTER 5

DESIGN EXAMPLES AND RESULTS

This chapter provides design examples to the systems discussed in chapter 4. The parameters of example are calculated with MATLAB code developed. The MATLAB and ZEMAX results are presented and discussed separately.

5.1 Design of the examples calculated using MATLAB

First, we list the values of the given parameters of our design example, as shown in Table 1.

Table 5.1 Parameters of Laser shaping system

Parameter	Value
Wavelength	870 nm
The perpendicular divergent angle	18 degrees
The parallel divergent angle	5 degrees
The laser diode spacing	0.5 mm
The glass used	BK7
The refractive index at the wavelength	1.509493
The thickness of each lenslet	0.4 cm
Space between lenslets	1mm

Second, we use the equations derived in chapter 4 to obtain the parameters of each surface. Because the shape of each surface is dependent on the shape of the surface before, we start from the surface 1.

1. Use equation (4.11) to obtain the primary focal length of the surface 1: d_1;
2. Use equation (4.14)-(4.16) to obtain the parameters for surface 1: c_1, R_1 and k_1;
3. Use equation (4.26) to determine the secondary focal length of the surface 2: $d_2^{'}$;
4. Use equation (4.27) to determine the parameters for surface 2: c_2, R_2 and k_2;
5. Use equation (4.28) to obtain the parameters for surface 3: c_3, R_3 and k_3;
6. Trace a number of rays with ray heights on surface 6 $(x_1, x_2, ..., x_{i-1}, x_i)$ to design surface 4&6 and 5&7. In this research, 2001 light rays are traced.
7. Use equation (4.43) to determine the corresponding ray heights on surface 7 $(X_1, X_2, ..., X_{i-1}, X_i)$;
8. Use equation (4.46) to determine the sag difference between surface 6 and surface 7 $((Z-z)_1, (Z-z)_2, ..., (Z-z)_{i-1}, (Z-z)_i)$;
9. Use equation (4.50) to obtain the slope of surface 6 at each traced ray height $(z'_1, z'_2, ..., z'_{i-1}, z'_i)$;
10. Use equation (4.51) to obtain the surface sag of surface 6 at each traced ray height $(z_1, z_2, ..., z_{i-1}, z_i)$;
11. Use equation (4.52) to obtain the surface sag of surface 7 at each traced ray height $(Z_1, Z_2, ..., Z_{i-1}, Z_i)$;
12. Use equation (3.42) to build the merit function.

13. Use the surface fitting method to fit the coordinates of surface points $(x_1, z_1), (x_2, z_2), ..., (x_{i-1}, z_{i-1}), (x_i, z_i)$ for surface 6 and $(X_1, Z_1), (X_2, Z_2), ..., (X_{i-1}, Z_{i-1}), (X_i, Z_i)$ for surface 7 with the surface sag function (3.37) and determine the parameters $(c, k, A_{2i})_6$ and $(c, k, A_{2i})_7$ of surface 6 and surface 7 respectively. In this research, we employ the fitting method using simplex minimization search.
14. Surface 4 has the same surface parameters as surface 6, and surface 5 is same as surface 7.

According to the above design steps, MATLAB codes are developed to solve each equation using the known parameters listed in Table 5.1. Table 5.2 and Table 5.3 lists the parameters of each surface calculated using MATLAB code.

Table 5.2: The parameters of surface 1-4 calculated by MATLAB

	First lenslet		Second lenslet	
Parameter	Surface 1	Surface 2	Surface 3	Surface 4
β	3684.71	1473.88	3684.71	1473.88
Thickness, t	0.4mm		0.4mm	
Vertex Radius	0.2014cm	0.1643cm	0.6738	0.159507cm
Surface Type	Aspherical	Cylindrical	Cylindrical	Cylindrical
Conic Constant	-2.2786	-2.2786	-2.2786	-3.27578
A2	--	--	--	-1.270823
A4	--	--	--	0.400731
A6	--	--	--	-1.245213e-003
A8	--	--	--	9.111077e-006

Table 5.3: The parameters of surface 5-8 calculated by MATLAB

	Third lenslet		Fourth lenslet	
Parameter	Surface 5	Surface 6	Surface 7	Surface 8
β	1.1284e05	4513.78	1.1284e05	
Thickness	0.4mm		0.4mm	
Vertex Radius	0.012072cm	0.159507cm	0.012072cm	Plane Surface
Surface Type	Cylindrical	Cylindrical	Cylindrical	
Conic Constant	-1.0001	-3.27578	-1.0001	
A2	-40.7258	-1.270823	-40.7258	
A4	1.6202	0.400731	1.6202	
A6	0.2132	-1.245213e-003	0.2132	
A8	1.4844e-05	9.111077e-006	1.4844e-05	

As stated earlier, in order to use fitting method, we traced 2001 light rays. That means, for each surface, we have 2001 intersection points generated on each surface by the incidence light rays. These points are treated as the sampled points of the desired surface. Connecting these "sampled" points together one by one forms a surface curve. The more point we sample, the more accurately the resultant curve will match the desired surface shape. In our case, two thousand and one sample points are enough to represent the right shape of the surface and errors are negligible. Figure 5.1 shows the curves of surface 6 and 7 generated by connecting the traced sample points. In general, the largest errors are most likely to occur during the surface fitting process. For example, when one uses different fitting method, one may get different results. In fact, using proper fitting method does not necessarily give error free result. Due to the limitation of computational

complexity and the random initial points, the errors are unavoidable, and the surface fitting step is very important.

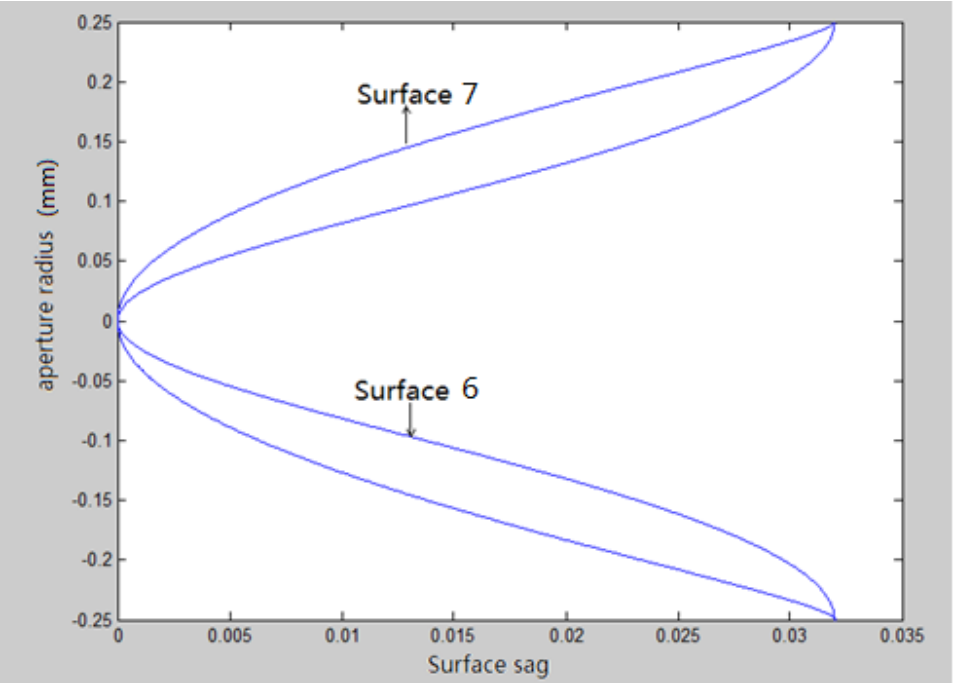

Figure 5.1: The curve of surface 6 and surface 7 formed by the traced rays

This research uses the simplex search fitting method. This method is known by its accuracy and computational speed, but its performance is largely dependent on the initial values chosen. Figure 5.2 shows the fitted curve (green) and the desired curve (red) of surface 6. From that figure, it is hard to tell the difference the two of them at first glance. Figure 5.3 is an expanded figure of Figure 5.2, showing a very small difference. This means that the error is very small. Figure 5.4 shows the fitting result for surface 7 and Figure 5.5 is the expanded plot of the insert in Figure 5.4. We can see that the performance is not as good as the surface 6 fitting. The merit function value for surface 6 is 3×10^{-7} and for surface 7 is 2.9×10^{-4} respectively. Therefore, as we can expect, surface 7 may produce a large percent of errors degrading the performance of the entire system.

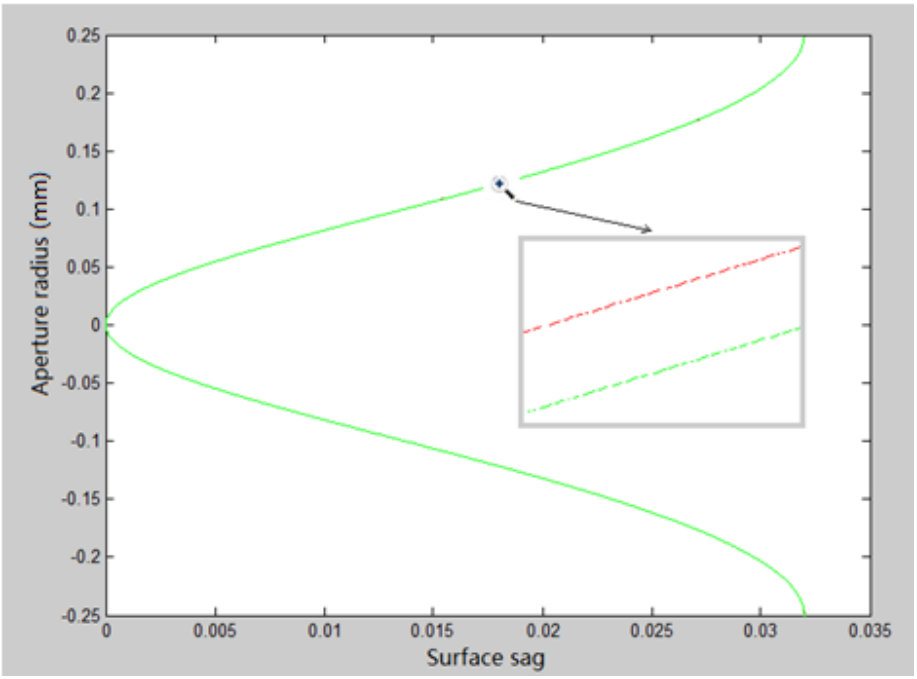

Figure 5.2: The fitted and traced curve of surface 6

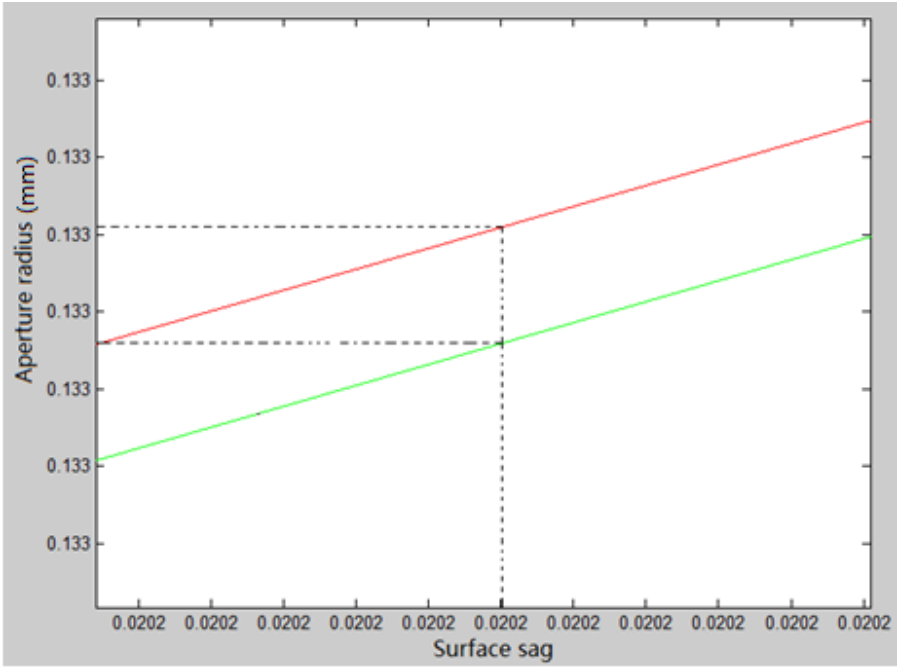

Figure 5.3: Expanded plot of the insert in Figure 5.2, showing the difference between the fitted and traced curve of surface 6

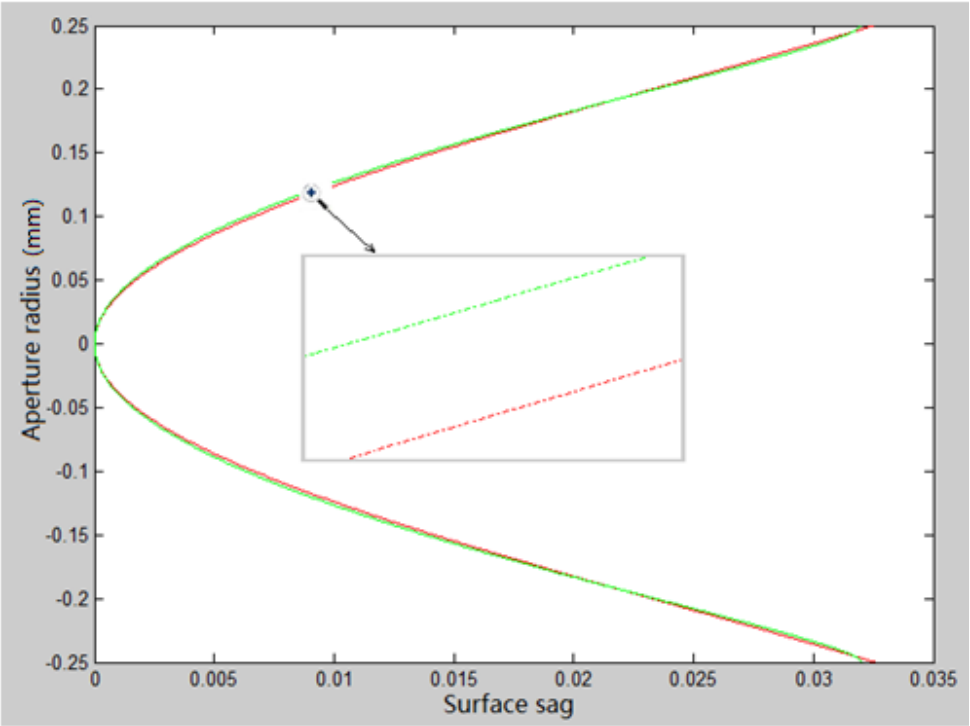

Figure 5.4: The fitted and traced curve of surface 7

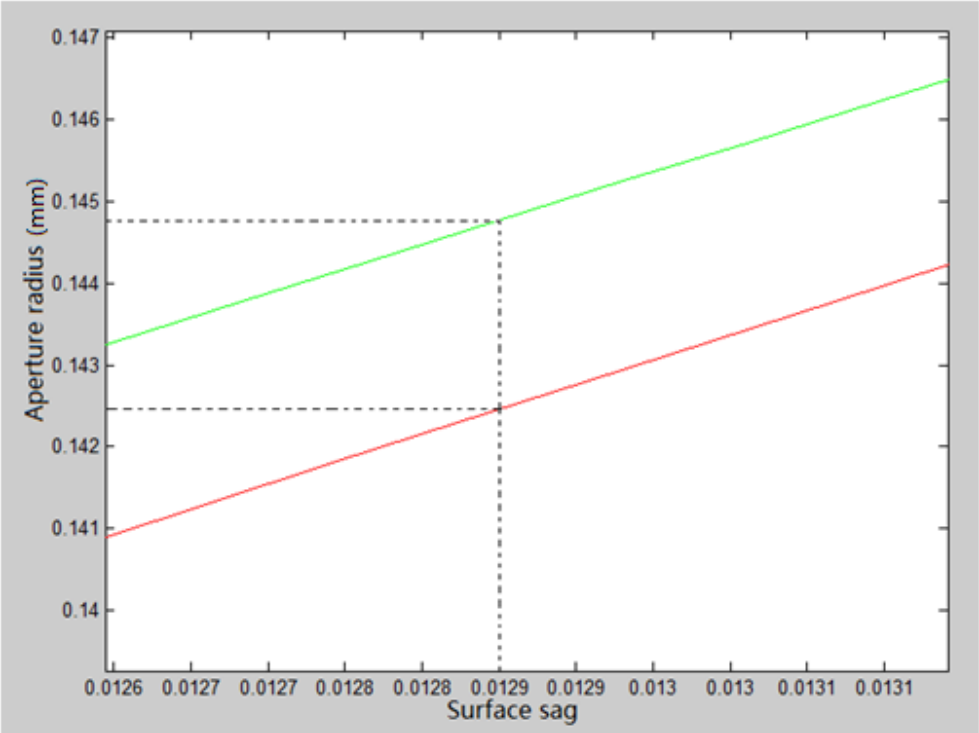

Figure 5.5: The difference between the fitted and traced curve surface 6

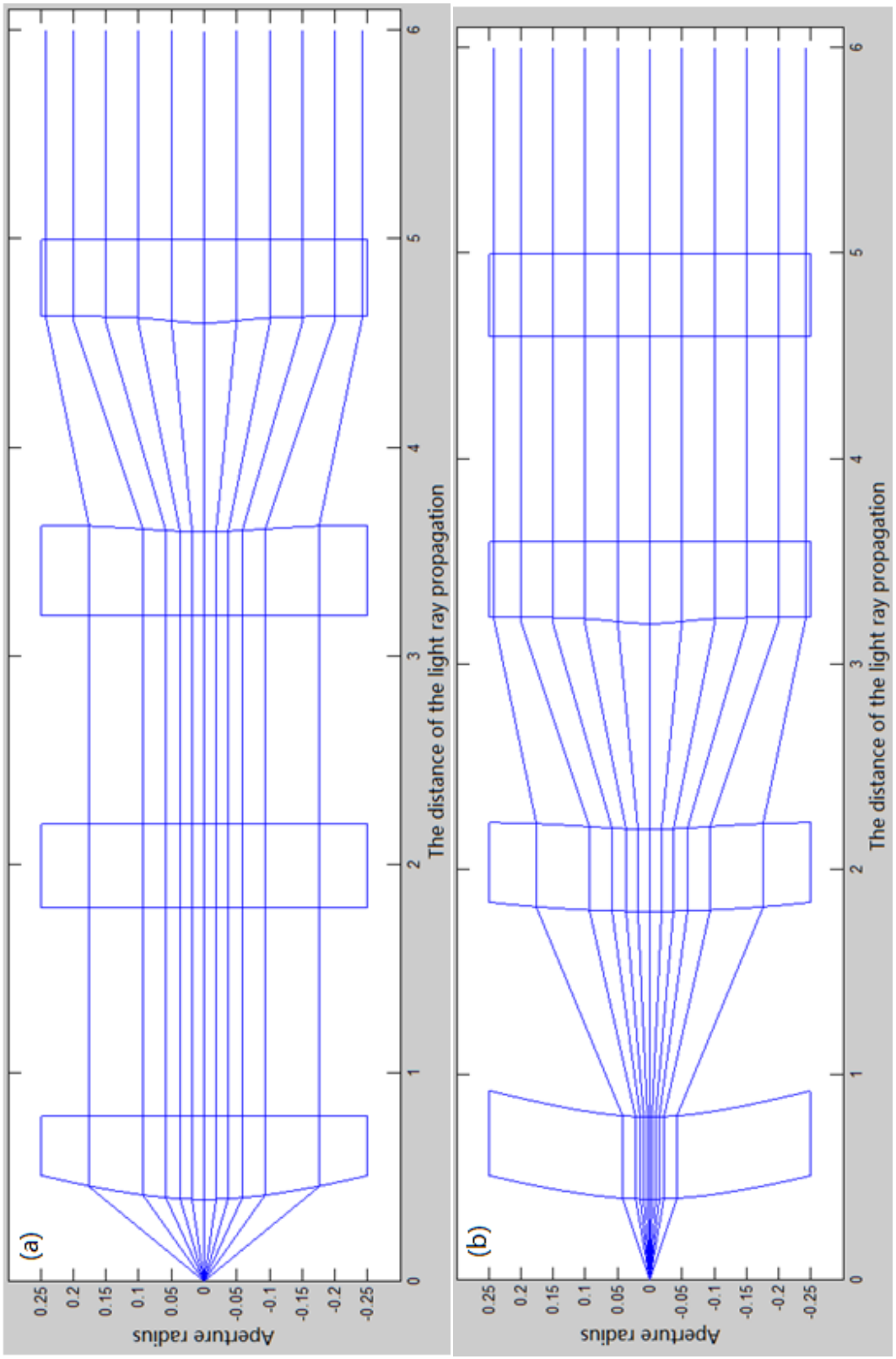

Figure 5.6: Ray tracing of the entire system using MATLAB simulation

5.2 Simulation of the system performance using MATLAB

In order to demonstrate the basic system performance, we traced only 10 light rays, initiated at the source and propagated through the system. Figure 5.6 is 10 rays traced through the system. Figure 5.6 (a) is the rays in the perpendicular transverse direction, and Figure 5.6 (b) is the rays in the parallel transverse direction. Comparing Figure 5.6 with Figure 4.1, we easily see that the traced rays are propagating the way as we expect: surface 1 collimates the beams in both directions; surface 2 and 3 expand and circularize the beam; surface 4&5 and surface 6&7 further expand the beam and redistribute the irradiance. These two figures confirm that the proposed system collimates the laser rays from the laser diode and uniformly distributes them as they emerge out of the last surface of the system.

In geometrical optics, irradiance distribution is represented by the ray density distribution. Therefore, we have to know the ray density in each region of the surface. In the simulation step, it is unlikely to get the actual and real energy distribution value at a given point. An alternative way is to sample the aperture of the optical surface and simulate the energy distribution of that region to find the irradiance distribution after that surface. In this research, we first traced 20001 light rays from the source. Then according to the equation (4.6) and (4.35), we derive an equation to calculate energy distribution in the region confined by two adjacent light rays:

$$dE_i = \frac{\int_{x_i}^{x_{i+1}} e^{-2\left(\frac{\arctan\left(\frac{x}{d_1+z_1(x)}\right)}{\alpha_x}\right)^2} dx}{\int_{x_1}^{x_{20001}} e^{-2\left(\frac{\arctan\left(\frac{x}{d_1+z_1(x)}\right)}{\alpha_x}\right)^2} dx} \tag{5.1}$$

Equation (5.1) is used to sample the irradiance distribution after surface 4&6. According to the energy conservation principle—the energy between any two light rays is the same. We use the ray tracing method to trace these 20001 rays and determine the ray distributions of these rays on each surface. Eventually, we are able to sample the irradiance distribution after each surface. As a second step, we divide each surface into 200 segments and integrate the energy distribution over each segment. A series of MATLAB codes are developed to complete the procedure and simulated the irradiance distribution after each functional surface, in Figure 5.7. Figure 5.11 shows the irradiance results.

To analyze the results, we first view the perpendicular transverse direction. Figure 5.7 shows the irradiance distribution after surface 1 which is a Gaussian shape. Figure 5.8 illustrates that the beam has been successfully transformed to a beam with a uniform irradiance distribution after surface 8. There is only a four percent fluctuation of the irradiance distribution, showing a reasonable uniformity. Figure 5.9 is the irradiance distribution after surface 1 for the parallel transverse direction. The beam has the Gaussian shape with a narrow beam spot. Figure 5.10 is the irradiance distribution after surface 3. Compared the Figure 5.7, the beam has the same distribution as in the perpendicular transverse case with the same beam spot size. This means that the surface 2 and 3 have successfully circularized the incoming elliptical beam from the laser diode. The surface 4 and 5 are designed to transform the beam irradiance distribution to uniformly distributed one in the parallel transverse direction. The irradiance distribution after surface 5, as shown in Figure 5.11, almost has a square-pulse shape. However, the level of uniformity in Figure 5.11 is not as good as that in Figure 5.8 for the

perpendicular direction case. This may be due to the sampling rate that is not sufficient to achieve the goals.

As a summery, Figure 5.7 and Figure 5.9 tell us that the laser diode beam is initially elliptical Gaussian beam with different beam spot size in two orthogonal directions; and then after being reshaped by the system, the beam becomes a rectangular shaped with the uniform irradiance distribution, as shown in Figure 5.8 and Figure 5.11.

The MATLAB simulations produce the system parameters. The next step is to verify the results simulated by MATLAB using ZEMAX simulation, and demonstrate the effectiveness and feasibility of this system.

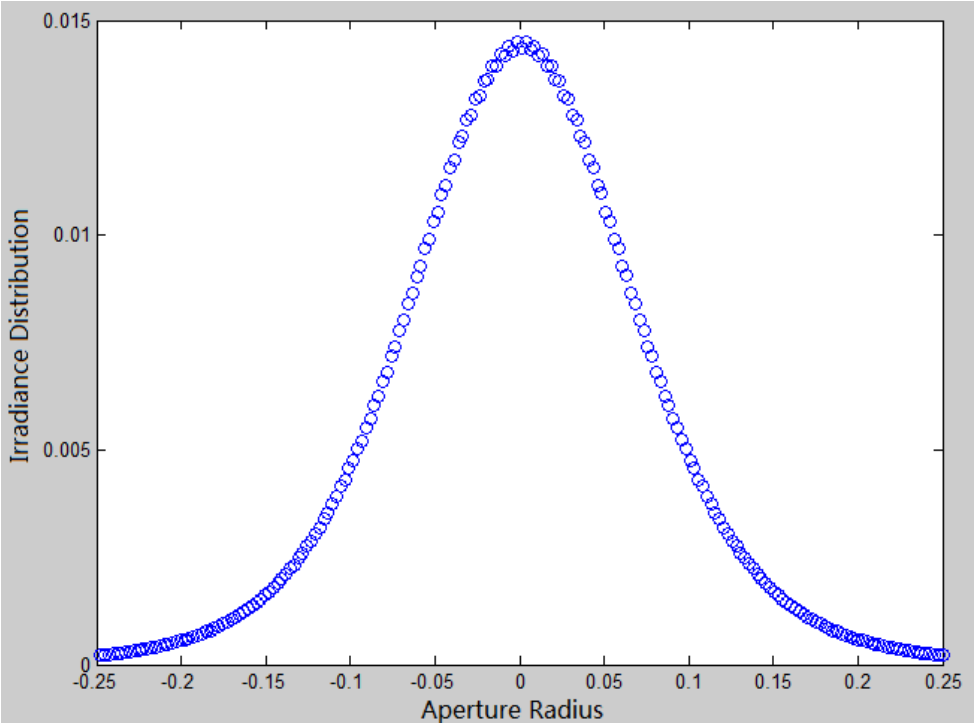

Figure 5.7: The irradiance distribution after surface 1 in the perpendicular direction

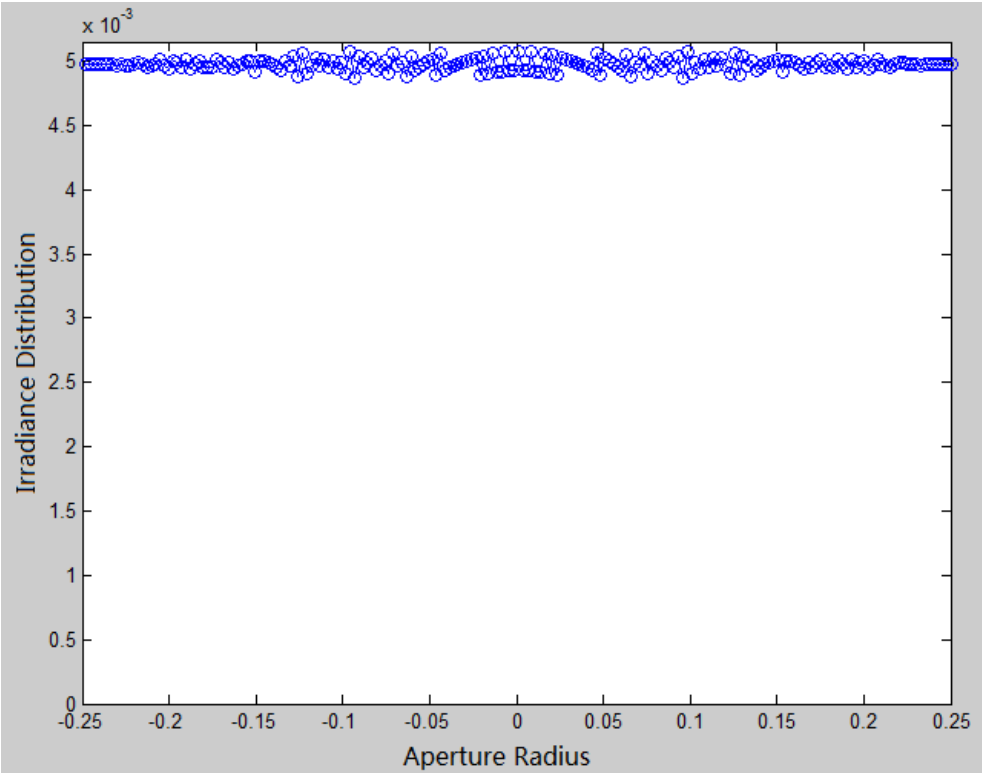

Figure 5.8: The irradiance distribution after surface 7 in the perpendicular direction

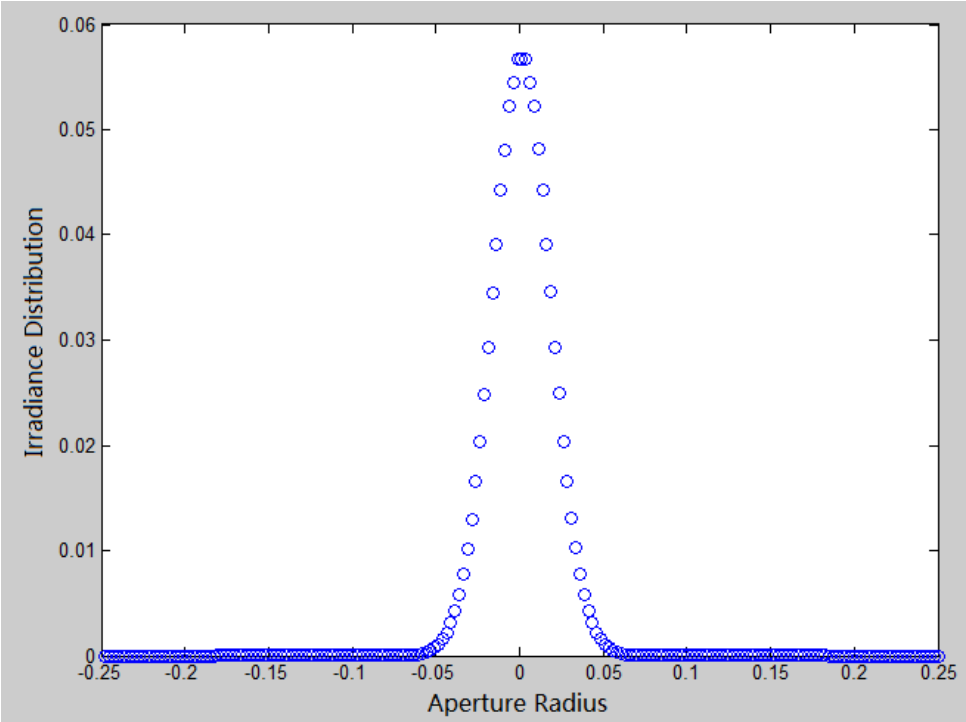

Figure 5.9: The irradiance distribution after surface 1 in the parallel direction

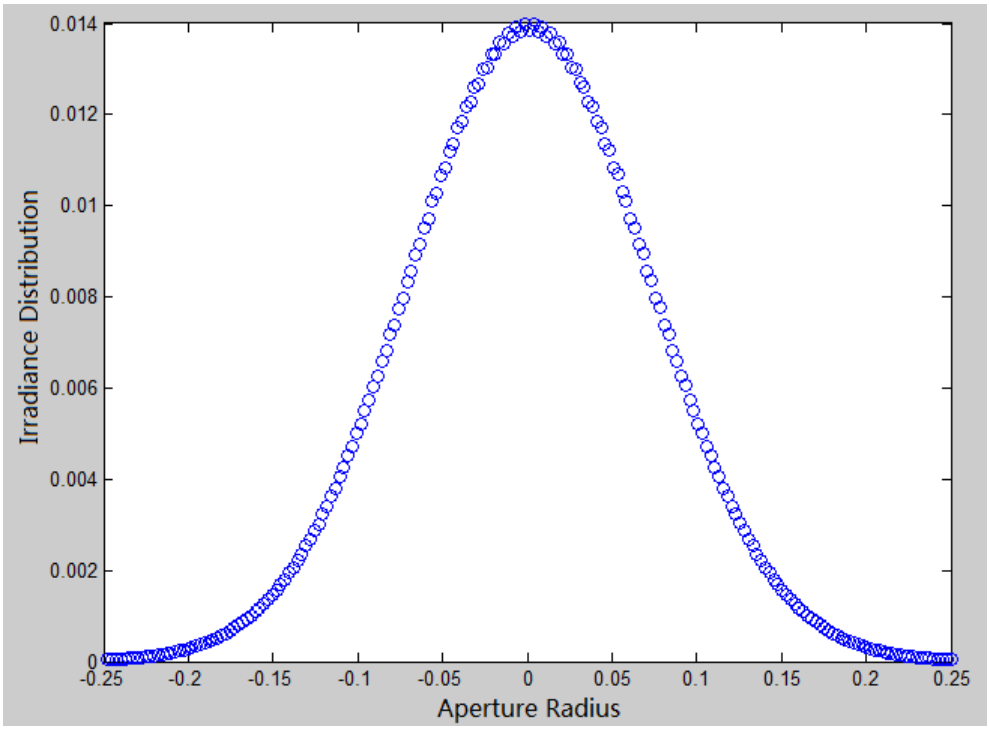

Figure 5.10: The irradiance distribution after surface 3 in the perpendicular direction

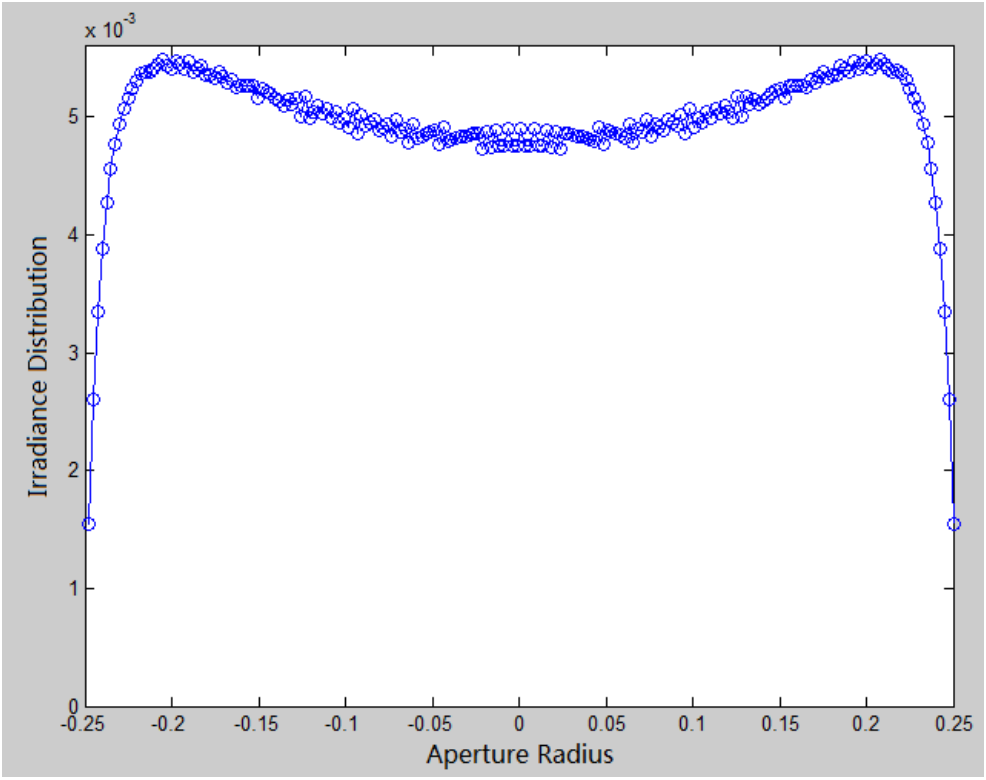

Figure 5.11: The irradiance distribution after surface 5 in the parallel direction

5.3 Optimization and Simulation using ZEMAX

ZEMAX is a widely-used optical design program which can model, analyze, and assist in design of optical systems. ZEMAX can perform standard sequential ray tracing through optical elements, non-sequential ray tracing for analysis of stray light, and physical optics beam propagation. It can model the propagation of rays through optical elements such as lenses, mirrors, and diffractive optical elements. It includes an extensive library of lenses from a variety of manufacturers. Additionally, ZEMAX has a powerful suite of optimization tools that can be used to optimize a lens design by automatically adjusting parameters to maximize performance and reduce aberrations.

The simulation using ZEMAX is commonly referred in industry as one of the most truly representation of the real light ray propagation, as it has more precise data base and considers many practical factors such as temperature, dispersion, scattering, diffraction and so on. Therefore, it is very common and necessary for optical designers to first use the optical theories and techniques to obtain the initial values of the parameters of each designed system, and then use ZEMAX to optimize values of parameters to maximize the performance and reduce aberrations. In section 5.1, we determined the initial values of the parameters for each surfaces, using MATLAB codes developed according to the design methodology proposed in Chapter 4. We use ZEMAX to test and optimize these values.

5.3.1 The optimization of each surface using ZEMAX

The ZEMAX user interface is composed of different types of windows, each of which serves a different purpose. In this section, we mainly use three types of windows,

namely, the main window, the lens data editor, and the merit function edit. The main window is where we enter the background information of the design such as wavelength, entrance pupil, system units, and other initiate conditions. The lens data editor is the primary window where the majority of the lens data will be entered. This data includes the radius of curvature, thickness, and glass type for each surface in the system. The merit function editor is used to define, modify, and review the system merit function which is used for optimization.

5.3.1.1 The optimization of surface 1

The data of surface 1 calculated using MATLAB is entered in the lens data edit as shown in Figure 5.12. In this figure, object is located at $d_1 = 0.3953mm$,the radius is $r_1 = 0.2014mm$, and the conic constant is $k_1 = -2.2786$. As stated in section 4.2.2, surface 1 collimates the beam in both perpendicular and parallel planes and has the radial symmetric about the optical axis. To optimize the actual performance of surface 1, a merit function as shown in Figure 5.13 is built. Operator REAY denotes the real ray in y-coordinate in lens units at the surface "surf". In this case, it says the ray at the standardized pupil height 1 (marginal ray) has a ray height of 0.142857mm (w_f). The operator RAED denotes the real ray angle of the exit, which is the angle in degrees between the surface normal and the ray after refraction or reflection from the surface; The smaller this angle is, the more this ray is collimated, if the surface is selected to be perpendicular to the main axis. In this case, we use eleven RAED operators to separately obtain the exit angles at the eleven rays of different entrance pupil locations from 0 to 1 with the spacing of 0.1. From the "Value" column, we can see that the average exit angle,

on the order of 10^{-5} degree, is relatively small; which in turn proves the effectiveness of the equations derived for surface 1 in section 4.2.2. However, it is still necessary to do the optimization in order to reduce the aberration and improve the performance, as much as possible.

	Surf:Type	Comment	Radius	Thickness	Glass	Semi-Diameter	Conic
OBJ	Standard		Infinity	0.395300		0.000000	0.000000
STO*	Standard		0.201400	0.400000	BK7	0.250000 U	-2.278600
2*	Standard		Infinity	1.000000		0.250000 U	0.000000
IMA	Standard		Infinity	-		0.250000 U	0.000000

Figure 5.12: The lens data calculated by MATLAB

Merit Function Editor: 0.000000E+000

Edit Tools Help

Oper #	Type									Target	Weight	Value
1	REAY	1	1	0.000000	0.000000	0.000000	1.000000	0.142857	0.000000			0.142872
2	RAED	3	1	0.000000	0.000000	0.000000	1.000000	0.000000	0.000000			6.836589E-005
3	RAED	3	1	0.000000	0.000000	0.000000	0.900000	0.000000	0.000000			8.597293E-005
4	RAED	3	1	0.000000	0.000000	0.000000	0.800000	0.000000	0.000000			9.719905E-005
5	RAED	3	1	0.000000	0.000000	0.000000	0.700000	0.000000	0.000000			1.021000E-004
6	RAED	3	1	0.000000	0.000000	0.000000	0.600000	0.000000	0.000000			1.008465E-004
7	RAED	3	1	0.000000	0.000000	0.000000	0.500000	0.000000	0.000000			9.386075E-005
8	RAED	3	1	0.000000	0.000000	0.000000	0.400000	0.000000	0.000000			8.177529E-005
9	RAED	3	1	0.000000	0.000000	0.000000	0.300000	0.000000	0.000000			6.533461E-005
10	RAED	3	1	0.000000	0.000000	0.000000	0.200000	0.000000	0.000000			4.549100E-005
11	RAED	3	1	0.000000	0.000000	0.000000	0.100000	0.000000	0.000000			2.335036E-005
12	RAED	1	1	0.000000	0.000000	0.000000	0.000000	0.000000	0.000000			8.537737E-007

Figure 5.13: The merit function editor for surface 1

This first parameter we need to optimize is d_1 which determines the beam spot size after surface 1 according to equation (4.11). According to the equation (4.8) $w_f = \Delta d / (2 \cdot 1.75) = 0.5 / (2 \cdot 1.75) = 0.1428571420 mm$. Give this value to the REAY operator, we set the weights of it to be 1 and set the thickness of the first surface in lens editor to be variable. This setting is to tell ZEMAX to optimize the parameter d_1 to achieve the target value of w_f . Then we use the optimization program in ZEMAX to optimize and obtain $d_1 = 0.395263 \text{mm}$, as shown in Figure 5.14.

The next step is to optimize the surface parameters to make the exit angles sampled as small as possible. So we set the radius and the conic constant to be variables; the target value of RAED operator to be 0; and the weights to be 1. Through optimization, we obtain $r_1 = 0.201384 mm$ and $k_1 = -2.278568$, as shown in Figure 5.15. Furthermore, the value of RAED operator has been decreased to the order of 10^{-14}. This is a great improvement of the level of parallelism. Because any small errors occurring at this step.is accumulative and results in large aberrations at the last surface. This improvement is very important to the performance of the whole system. The plot of the optimized surface 1 is shown in Figure 5.16.

Lens data editor

	Surf:Type	Comment	Radius	Thickness		Glass		Semi-Diameter		Conic
OBJ	Standard		Infinity	0.395263	V			0.000000		0.000000
STO*	Standard		0.201400	0.400000		BK7		0.250000	U	-2.278600
2*	Standard		Infinity	1.000000				0.250000	U	0.000000
IMA	Standard		Infinity		-			0.250000	U	0.000000

Merit function editor

Oper #	Type							Target	Weight	Value	% Contrib
1	REAY	1	1	0.000000	0.000000	0.000000	1.000000	0.142857	1.000000	0.142857	100.000000
2	RAED	3	1	0.000000	0.000000	0.000000	1.000000	0.000000	0.000000	1.044163E-003	0.000000
3	RAED	3	1	0.000000	0.000000	0.000000	0.900000	0.000000	0.000000	1.001786E-003	0.000000
4	RAED	3	1	0.000000	0.000000	0.000000	0.800000	0.000000	0.000000	9.428236E-004	0.000000
5	RAED	3	1	0.000000	0.000000	0.000000	0.700000	0.000000	0.000000	8.675622E-004	0.000000
6	RAED	3	1	0.000000	0.000000	0.000000	0.600000	0.000000	0.000000	7.767473E-004	0.000000
7	RAED	3	1	0.000000	0.000000	0.000000	0.500000	0.000000	0.000000	6.715808E-004	0.000000
8	RAED	3	1	0.000000	0.000000	0.000000	0.400000	0.000000	0.000000	5.536957E-004	0.000000
9	RAED	3	1	0.000000	0.000000	0.000000	0.300000	0.000000	0.000000	4.251090E-004	0.000000
10	RAED	3	1	0.000000	0.000000	0.000000	0.200000	0.000000	0.000000	2.881862E-004	0.000000
11	RAED	3	1	0.000000	0.000000	0.000000	0.100000	0.000000	0.000000	1.455452E-004	0.000000
12	RAED	1	1	0.000000	0.000000	0.000000	0.000000	0.000000	0.000000	8.537737E-007	0.000000

Figure 5.14: The optimization setting and result of d_1

Lens data editor

	Surf:Type		Comment	Radius		Thickness	Glass		Semi-Diameter		Conic	
OBJ	Standard			Infinity		0.395263			0.000000		0.000000	
STO*	Standard			0.201384	V	0.400000	BK7		0.250000	U	-2.278568	V
2*	Standard			Infinity		1.000000			0.250000	U	0.000000	
IMA	Standard			Infinity		-			0.250000	U	0.000000	

Merit function editor

Oper #	Type							Target	Weight	Value	% Contrib
1	REAY	1	1	0.000000	0.000000	0.000000	1.000000	0.142857	0.000000	0.142858	0.000000
2	RAED	3	1	0.000000	0.000000	0.000000	1.000000	0.000000	1.000000	1.478779E-006	100.000000
3	RAED	3	1	0.000000	0.000000	0.000000	0.900000	0.000000	1.000000	5.684342E-014	1.477589E-013
4	RAED	3	1	0.000000	0.000000	0.000000	0.800000	0.000000	1.000000	5.684342E-014	1.477589E-013
5	RAED	3	1	0.000000	0.000000	0.000000	0.700000	0.000000	1.000000	5.684342E-014	1.477589E-013
6	RAED	3	1	0.000000	0.000000	0.000000	0.600000	0.000000	1.000000	5.684342E-014	1.477589E-013
7	RAED	3	1	0.000000	0.000000	0.000000	0.500000	0.000000	1.000000	5.684342E-014	1.477589E-013
8	RAED	3	1	0.000000	0.000000	0.000000	0.400000	0.000000	1.000000	5.684342E-014	1.477589E-013
9	RAED	3	1	0.000000	0.000000	0.000000	0.300000	0.000000	1.000000	5.684342E-014	1.477589E-013
10	RAED	3	1	0.000000	0.000000	0.000000	0.200000	0.000000	1.000000	5.684342E-014	1.477589E-013
11	RAED	3	1	0.000000	0.000000	0.000000	0.100000	0.000000	1.000000	5.684342E-014	1.477589E-013
12	RAED	1	1	0.000000	0.000000	0.000000	0.000000	0.000000	1.000000	5.684342E-014	1.477589E-013

Figure 5.15: The optimization setting and results of surface 1

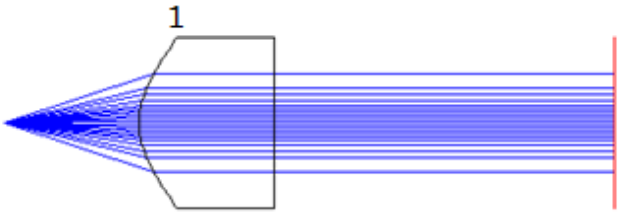

Figure 5.16: The layout of surface 1

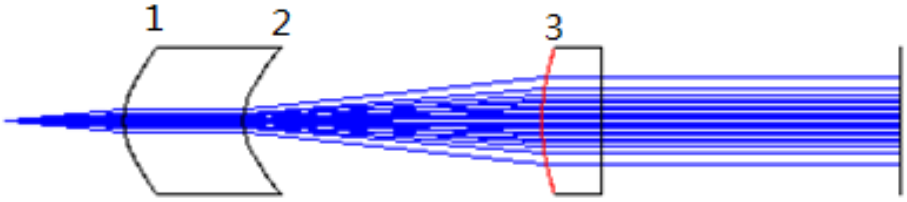

Figure 5.17: The layout of the first three surfaces in the parallel direction

Lens data editor

	Surf:Type		Comment	Radius	Thickness	Glass		Semi-Diameter		Conic
OBJ	Standard			Infinity	0.395263			0.000000		0.000000
STO*	Standard			0.201384	0.400000	BK7		0.250000	U	-2.278568
2*	Standard			0.164300	1.000000			0.250000	U	-2.278600
3*	Standard			0.673800	0.200000	BK7		0.250000	U	-2.278600
4	Standard			Infinity	1.000000			0.142888		0.000000
IMA	Standard			Infinity	-			0.250000	U	0.000000

Merit function editor

Oper #	Type							Target	Weight	Value	% Contrib
1	REAY	3	1	0.000000	0.000000	0.000000	1.000000	0.142857	0.000000	0.142888	0.000000
2	RAED	4	1	0.000000	0.000000	0.000000	1.000000	0.000000	0.000000	6.252981E-005	25.914295
3	RAED	4	1	0.000000	0.000000	0.000000	0.900000	0.000000	0.000000	5.631024E-005	21.015508
4	RAED	4	1	0.000000	0.000000	0.000000	0.800000	0.000000	0.000000	5.008239E-005	16.623991
5	RAED	4	1	0.000000	0.000000	0.000000	0.700000	0.000000	0.000000	4.385938E-005	12.749408
6	RAED	4	1	0.000000	0.000000	0.000000	0.600000	0.000000	0.000000	3.757574E-005	9.357940
7	RAED	4	1	0.000000	0.000000	0.000000	0.500000	0.000000	0.000000	3.135803E-005	6.517223
8	RAED	4	1	0.000000	0.000000	0.000000	0.400000	0.000000	0.000000	2.506665E-005	4.164452
9	RAED	4	1	0.000000	0.000000	0.000000	0.300000	0.000000	0.000000	1.876361E-005	2.333446
10	RAED	4	1	0.000000	0.000000	0.000000	0.200000	0.000000	0.000000	1.263470E-005	1.058022
11	RAED	4	1	0.000000	0.000000	0.000000	0.100000	0.000000	0.000000	6.331755E-006	0.265713
12	RAED	4	1	0.000000	0.000000	0.000000	0.000000	0.000000	0.000000	5.684342E-014	2.141537E-017

Figure 5.18: The lens datas and merit function for the first three surfaces

5.3.1.2 The optimization of surface 2 and 3

Surface 2 and surface 3 are cylindrical in the parallel direction. Their function is to circularize and collimate the beam after surface 1. As stated in section 4.2.3, they should be designed together to satisfy the constant phase front of the beam. Furthermore, in order to minimize the accumulative errors, we should optimize the first three surfaces as a whole. Figure 5.17 shows the layout of the first three surfaces in the parallel transverse direction. Figure 5.18 shows the lens editor where we entered the calculated values of parameters for surface 2 and surface 3, and the merit function editor where we entered the operators we need to optimize. The current value of operator REAY (the beam size w_f after surface 3) is 0.142888mm, and the current value of the operator RAED is on the order of 10^{-5}. We desire to optimize the surface parameters to make $w_f = 0.1428571420mm$ so that the beam is circularized, and to decrease the REAY values to collimate the beam. Therefore, we set the radius and conic constant of surface 2 and 3 to be variables, and set the target value of REAY to be 0.142857 and RAED to be 0. Using the same optimization techniques, we obtain a new set of surface parameters $r_2 = 0.164432mm$, $k_2 = -2.255340$, $r_3 = 0.673925mm$, $k_3 = -2.272907$, as shown in Figure 5.19. The REAY has been optimized to the target value; and the RAED is on the order of 10^{-14}. Comparing the results in Figure 5.19 and in Figure 5.15, we conclude that the beam has been successfully collimated and circularized with the same REAY value.

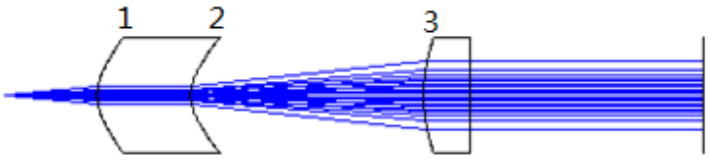

Figure 5.19: the layout of the first three surfaces optimized

Lens data editor

Surf:Type		Comment	Radius		Thickness		Glass	Semi-Diameter		Conic	
OBJ	Standard		Infinity		0.395263			0.000000		0.000000	
STO*	Standard		0.201384		0.400000		BK7	0.250000	U	-2.278568	
2*	Standard		0.164432	V	1.000000			0.250000	U	-2.255340	V
3*	Standard		0.673925	V	0.200000		BK7	0.250000	U	-2.272907	V
4	Standard		Infinity		1.000000			0.142857		0.000000	
IMA	Standard		Infinity		-			0.250000	U	0.000000	

Merit function editor

Oper #	Type								Target	Weight	Value	% Contrib
1	REAY	3	1	0.000000	0.000000	0.000000	1.000000		0.142857	1.000000	0.142857	3.740940E-003
2	RAED	4	1	0.000000	0.000000	0.000000	1.000000		0.000000	1.000000	5.684342E-014	5.540751E-014
3	RAED	4	1	0.000000	0.000000	0.000000	0.900000		0.000000	1.000000	5.684342E-014	5.540751E-014
4	RAED	4	1	0.000000	0.000000	0.000000	0.800000		0.000000	1.000000	5.684342E-014	5.540751E-014
5	RAED	4	1	0.000000	0.000000	0.000000	0.700000		0.000000	1.000000	1.909096E-006	62.497662
6	RAED	4	1	0.000000	0.000000	0.000000	0.600000		0.000000	1.000000	5.684342E-014	5.540751E-014
7	RAED	4	1	0.000000	0.000000	0.000000	0.500000		0.000000	1.000000	1.478779E-006	37.498597
8	RAED	4	1	0.000000	0.000000	0.000000	0.400000		0.000000	1.000000	5.684342E-014	5.540751E-014
9	RAED	4	1	0.000000	0.000000	0.000000	0.300000		0.000000	1.000000	5.684342E-014	5.540751E-014
10	RAED	4	1	0.000000	0.000000	0.000000	0.200000		0.000000	1.000000	5.684342E-014	5.540751E-014
11	RAED	4	1	0.000000	0.000000	0.000000	0.100000		0.000000	1.000000	5.684342E-014	5.540751E-014
12	RAED	4	1	0.000000	0.000000	0.000000	0.000000		0.000000	1.000000	5.684342E-014	5.540751E-014

Figure 5.20: The optimization settings and results of surface 2 and 3

5.3.1.3 The optimization of surface 6 and 7

Surface 6 and surface 7 are to transform the irradiance distribution to uniform irradiance and to collimate the beam in the perpendicular transverse direction. In section 4.2.4, we introduced the design method which is different from the design of the first three surfaces. In section 5.2, we demonstrated the MATLAB simulations proving the effectiveness of the proposed design. In this section, we use the values of the parameter calculated in section 5.1 for these surfaces as the initial values to further optimize surface 6 and surface 7. First, we enter the initial values of surface 6 and 7 into the lens data editor as shown in Figure 5.22, and obtain the 2-D layout as shown in Figure 5.21. As seen, we find that the outgoing light is not parallel to each other as they diverge away from the main axis after surface 8. This phenomenon actually explains why there is an energy increase in the border region in Figure 5.11.

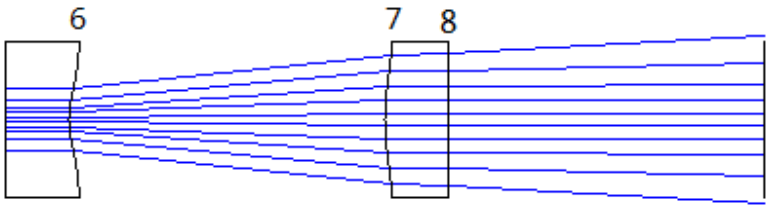

Figure 5.21: The simulation of surface 6 and 7 using ZEMAX according to the initial values

Lens data editor

	Surf:Type	Comment	Radius	Thickness	Glass	Semi-Diameter		Conic
OBJ	Standard		Infinity	Infinity		0.000000		0.000000
STO*	Standard		Infinity	0.200000	BK7	0.250000	U	0.000000
2*	Even Asphere		0.159507	1.000000		0.250000	U	-3.275780
3*	Even Asphere		0.012072	0.200000	BK7	0.250000	U	-1.000100
4*	Standard		Infinity	1.000000		0.250000	U	0.000000
IMA	Standard		Infinity	-		0.250000	U	0.000000

Deformation coefficients

	Surf:Type	Par 0 (unused)	2th Order Term	4th Order Term	6th Order Term	8th Order Term	10th Order Term
OBJ	Standard						
STO*	Standard						
2*	Even Asphere		-1.270823	0.400731	-1.245213E-003	9.111077E-006	0.000000
3*	Even Asphere		-40.725800	1.620200	0.213200	1.484400E-005	0.000000
4*	Standard						
IMA	Standard						

Figure 5.22: The initial values of surface 6 and 7 calculated by MATLAB

The next step is to build the right and appropriate merit function to optimize the parameters of these two surfaces. The basic optimization idea is same as the design method discussed in section 4.2.4.

1. To ensure that the location, where the light rays meet surface 7, is determined by equation (4.42); so that the light rays would evenly distributed on surface 7.
2. To ensure that the equation (4.45) is satisfied, so that the plane phase front of the outgoing beam is achieved.

The ray tracing method is once again used here, just as we did during the process of designing surface 6 and 7. We traced a series of light rays with ray height x_i, and substituted the optimized surface parameters into equation (4.42) to obtain a new set of ray heights X_i. Then a number of operators REAY are used to ensure the light rays traced at different pupil location x_i to reach surface 7 at the corresponding ray heights X_i. Furthermore, a number of operators READ are used to ensure the parallelism of the light rays at each traced location X_i. The surfaces parameters of these two surfaces are all set to be variables for ZEMAX for optimization. Figure 5.23 and Figure 5.24 show the optimized results. In Figure 5.23, we see that the rays are parallel and almost evenly distributed after surface 8. This is a much better result than the one in Figure 5.21.

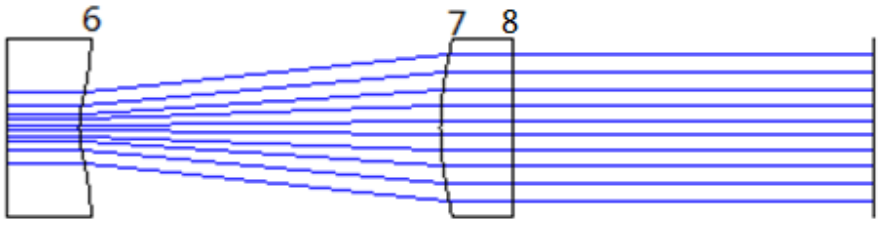

Figure 5.23: The layout of optimized surface 6 and 7

Lens data editor

	Surf:Type	Comment	Radius		Thickness	Glass	Semi-Diameter		Conic	
OBJ	Standard		Infinity		Infinity		0.000000		0.000000	
STO*	Standard		Infinity		0.200000	BK7	0.250000	U	0.000000	
2*	Even Asphere		0.150166	V	1.000000		0.250000	U	-2.886685	V
3*	Even Asphere		-3.989588	V	0.200000	BK7	0.250000	U	244.298486	V
4*	Standard		Infinity		1.000000		0.250000	U	0.000000	
IMA	Standard		Infinity		-		0.250000	U	0.000000	

Deformation coefficients

	Surf:Type	Par 0		Par 1		Par 2		Par 3		Par 4	
OBJ	Standard										
STO*	Standard										
2*	Even Asphere			-1.471824	V	1.626371	V	-7.148400	V	19.622770	V
3*	Even Asphere			0.767596	V	-0.724004	V	0.945536	V	-16.930721	V
4*	Standard										
IMA	Standard										

Figure 5.24: The optimization settings and results of surface 6 and 7

5.3.2 The simulation of overall system by ZEMAX

After optimizing each surfaces, we have obtained a new set of surface parameters as shown in Table 4 and 5. These values are more precise and can be used by the lens manufactures. As Figure 5.16, Figure 5.20, and Figure 5.24 show, each surface works as designed. Until now, all the simulations are done in the 2-D domain. ZEMAX has two working models, the sequential and non-sequential. The foregoing optimization is done in the sequential-model. In sequential mode, all ray propagation occurs through surfaes which are located using a local coordinate system. To demonstrate the system in 3D and simulate the light propagtion of laser diode arrays, we have to use the non-sequential mode of ZEMAX. In non-sequential mode, optical commponents are modeled as true three-demensional objects, either as surfaces or solid volumes. Each object is placed globally at an independent x, y, z coordinate with an independently defined orientation. Rays can propagate through the optical components in any order where total internal reflection ray paths can be accounted for. While sequential mode is limited to the analysis of imaging system, non-sequential mode can be used to analyze stray light, scattering, and illumination in both imaging and non-imaging systems. Also, it is much more easy to simulate the energy distribution and obtain intuitional irradiance distribution image at any location in non-squential mode.

Table 5.4: The parameters of surface 1-4 optimized by ZEMAX

	First lenslet		Second lenslet	
Parameter	Surface 1	Surface 2	Surface 3	Surface 4
Thickness	0.4mm		0.4mm	
Vertex Radius	0.201384*mm*	0.164432*mm*	0.673925*mm*	0.150166mm
Surface Type	Aspherical	Cylindrical	Cylindrical	Cylindrical
Conic Constant	–2.278568	–2.255340	–2.272907	-2.886685
A2	--	--	--	-1.471824
A4	--	--	--	1.626371
A6	--	--	--	-1.748400
A8	--	--	--	19.62277

Table 5.5: The parameters of surface 5-8 optimized by ZEMAX

	Third lenslet		Fourth lenslet	
Parameter	Surface 5	Surface 6	Surface 7	Surface 8
Thickness	0.4mm		0.4mm	
Vertex Radius	-3.989588mm	0.150166mm	-3.989588mm	Plane surface
Surface Type	Cylindrical(y)	Cylindrical(x)	Cylindrical(x)	
Conic Constant	244.298486	-2.886685	244.298486	
A2	0.767596	-1.471824	0.767596	
A4	-0.724004	1.626371	-0.724004	
A6	0.945536	-1.748400	0.945536	
A8	-16.930721	19.62277	-16.930721	

In this step, we enter the values in Table 5.4 and Table 5.5 into the non-sequantial mode and we obtain the 3-D illustration of the whole system, as shown in Figure 5.25. The source consists of 3 by 3 laser diode array. Each lenslet array is composed of 9 lenslet which is used to shape the corresponding laser diode. Figure 5.26 is the layout of the system in the perpendicular direction and Figure 5.27 is the layout in the parallel direction.

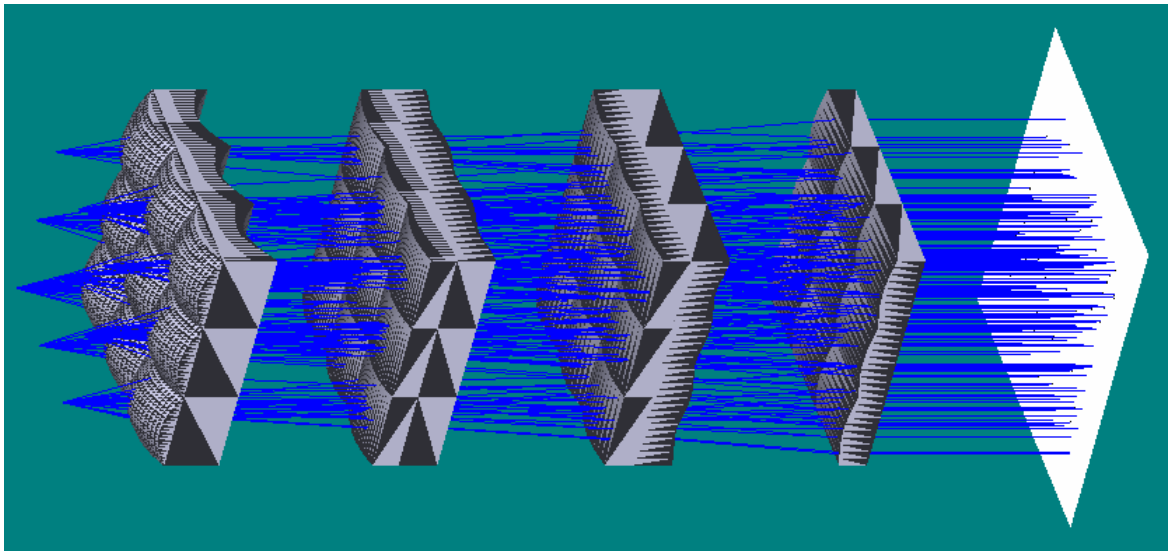

Figure 5.25: The 3-D illustration of the proposed system composed of lenslet arrays

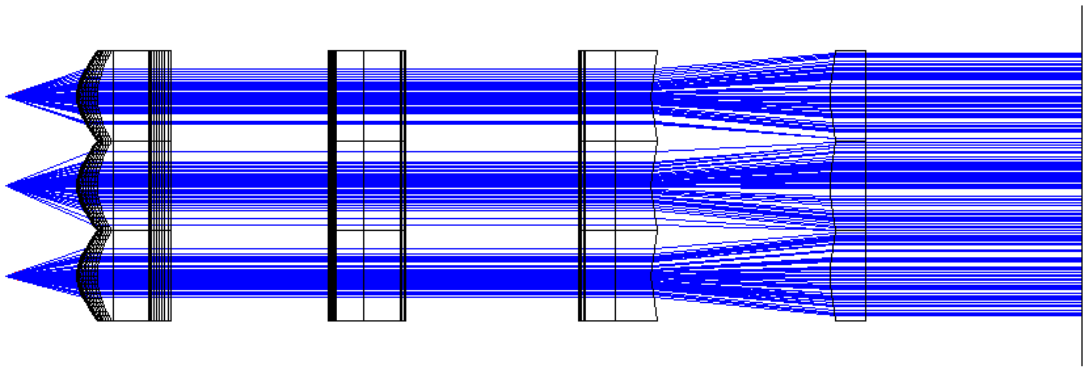

Figure 5.26: The layout of the system in perpendicular transverse direction

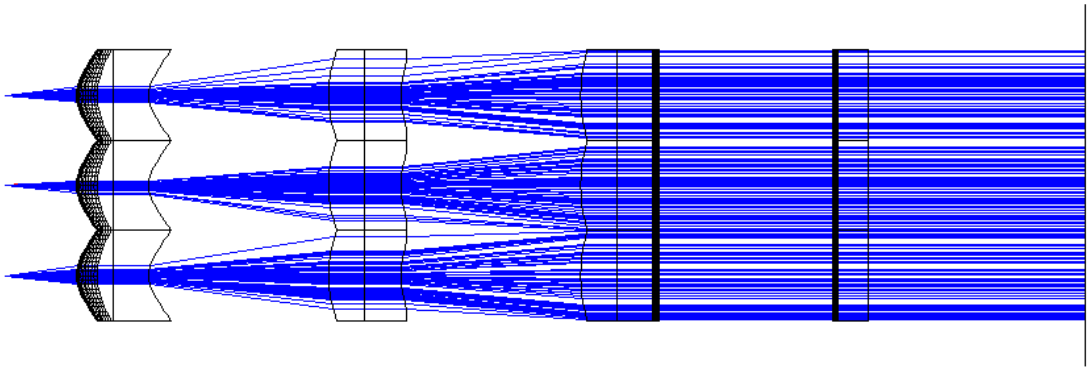

Figure 5.27: The layout of the system in parallel transverse direction

In Figure 5.26 and Figure 5.27, we can see that the beams are shaped respectively in each transverse direction; the sources have different divergent angle in each direction; but after being shaped by the system, the beams of each laser diode are expanded to fulfill the entire pupil diameter and collimated allowing to treat these beams as a single bundle of beam. These beams are propagating in the exact same way as we desired and simulated in the previous chapters. The exit angle of the outgoing beam after the whole system is on the order of 10^{-5}, which is relatively quite small. It is usually very difficult to achieve such a high level of parallelism.

Figure 5.28 shows the irradiance distribution before surface 1. Figure 5.29 shows the irradiance distribution after surface 3. Figure 5.30 and Figure 5.31 shows the irradiance distribution after surface 8. These four figures are the 2-D energy distribution and clearly show how the beam spots look like during the entire beam shaping process. The beam spot has been successfully shaped from the elliptical shape to the circular shape and finally to the rectangular shape. The irradiance distribution has been successfully shaped from Gaussian to uniform distribution.

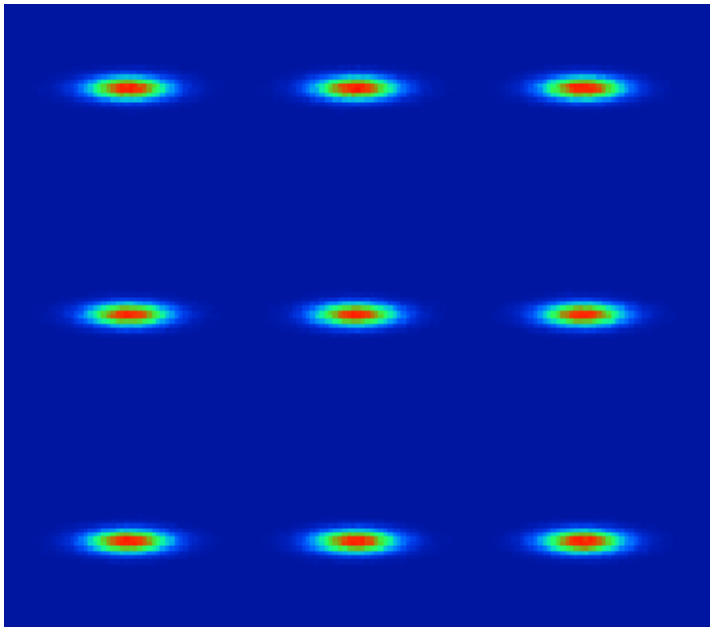

Figure 5.28: The irradiance distribution before surface 1

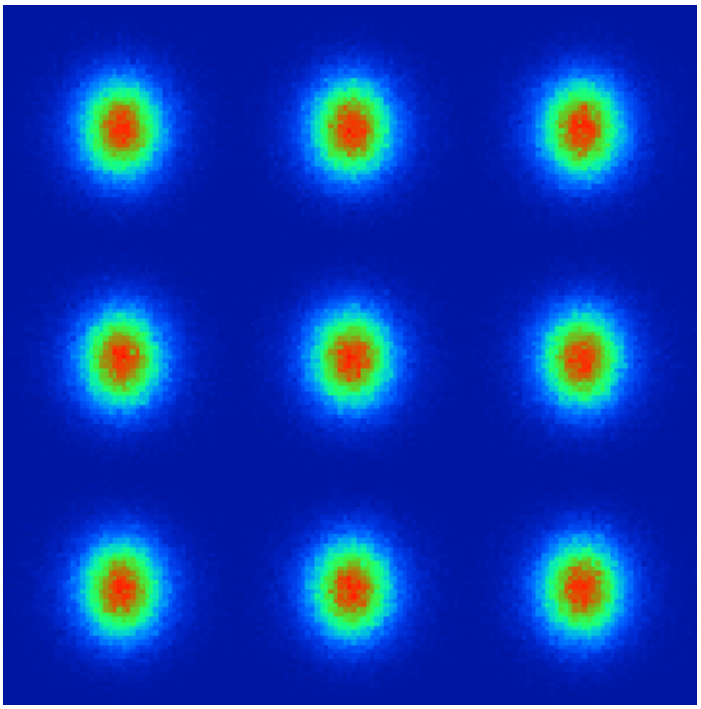

Figure 5.29: The irradiance distribution after surface 3

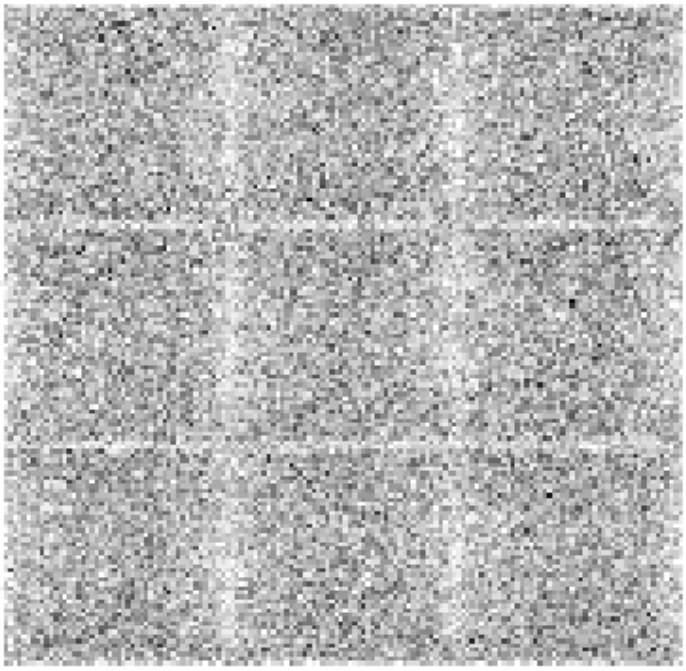

Figure 5.30: The irradiance distribution at the target plane in black and white

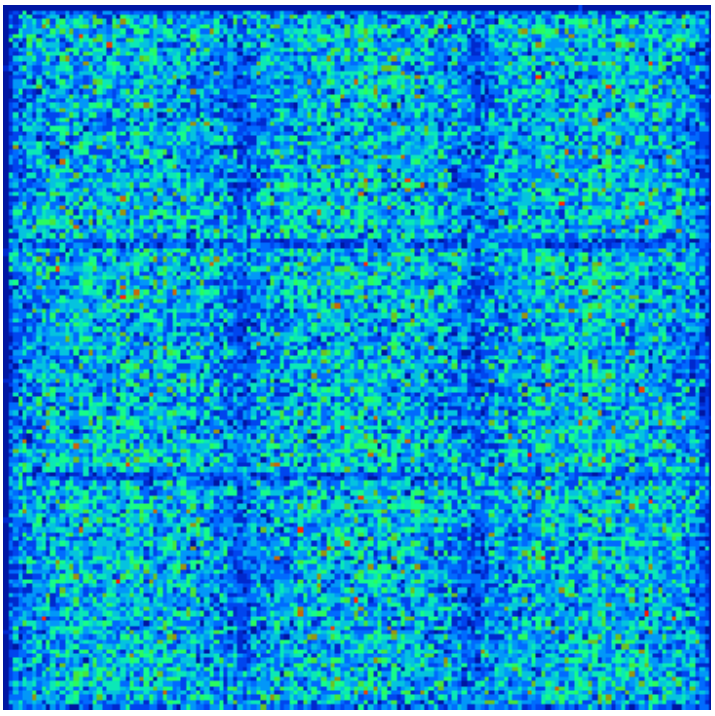

Figure 5.31: The irradiance distribution at the target plane in false color

CHAPTER 6

SUMMARY

Collimated beams with uniform energy profile and regular beam shape such as circular or rectangular are highly preferable in applications. This work mainly concentrates on shaping the beams from laser diode arrays having total 9 diode lasers to become a single beam with these attracting characteristics.

Laser diode arrays contain many laser diode sources. It is difficult to reshape and combine beams from multi-sources with the conventional optical lenses. Conventional optical lens has only one main axis so that only the on-axis laser diode source can be collimated parallel to the main axis. In this work, we use the lenslet arrays which are composed of many lenslets. The advantage of the lenslet array is that each lenslet can shape the corresponding laser diode source as long as we make the aperture size of the lenslet match to the spacing of the laser diode arrays. With the help of the lenslet technology, we can simplify the multi-sources beam shaping problem to a single laser diode beam shaping problem.

In section 3.3, a four sequential lens system is proposed. It has eight surfaces. The first surface is an aspherical surface which is radial symmetric about the main axis. The second to the seventh surfaces are cylindrical surfaces serving to reshape the beam in perpendicular and parallel transverse direction respectively. The last surface is a plane surface. The goal of this system is to collimate the beam and uniform the irradiance

distribution with the rectangular beam spot shape. The beams with these features can be easily added up and treated as a single beam.

In Chapter 4, a complete derivation of design method for each surface is discussed. These derivations are very important to further understand the working mechanism of the proposed system. Surface 1 is to collimate the beam in both transverse directions. Surface 2 and 3 are to expand and collimate the beam in parallel transverse direction so that the beam is circularized after surface 3. Surface 4&5 and 6&7 are to uniform the beam irradiance and collimate the beam respectively in both transverse directions, and results a rectangular beam spot shape. In section 5.1, a detailed procedure of the design is introduced, and an actual design example is proposed. According to the derived equations, a series of MATLAB codes are developed to calculate the parameters for each surface. This work uses both MATLAB and ZEMAX to simulate the calculated results. In section 5.2, the 2-D simulations by MATLAB are shown. In section 5.3, the 3-D simulations by ZEMAX are shown. All the simulations prove the effectiveness of the proposed system and design methods. Rays propagate in the same way, as shown in the ray tracing figures. The beam spot of each source is reshaped from the elliptical to the rectangular, as shown in the Figures (5.28)-(5.31). The irradiance distribution of the beam transformed from the Gaussian to the uniform, as shown in the energy simulation figures. The final collimation of the beam was high accuracy that the exit angle of the rays is on the order of 10^{-5}. The simulations results show that the multiple beams are reshaped to form a single beam. The only error is in the edges as shown in Figure 5.31. The author believes that they are caused by the diffraction which is inherent with the lenslet arrays.

References

[1] L.W. Casperson, A. Yariv, “Gain and Dispersion Focusing in a High Gain Laser,” applied Optics IP, vol. 11, Issue 2, pp. 462-466, 1972.

[2] S.M. Beck, J.A. Gelbwachs, D.A. Hinkley, D.W. Warren, and J.E. Wessel, “Aerospace Applications of Optical Sensing With Lidar,” in Proc. IEEE Aerospace Applications Conference, Aspen, CO, vol. 2, pp. 91-96, 1996.

[3] Mert Serkan, “Laser Beam Shaping Optical System Design Methods and Their Application In Edge-emitting Semiconductor Laser-based Lidar Systems,” Ph.D. dissertation, Auburn university, 2008.

[4] Computer Desktop Encyclopedia: laser diode. Retrieved from www.answers.com/topic/laser-diode, 2012 October.

[5] Y.B. Jiang, H.M. Yan, and X.D. Zhang, “Beam-Shaping Method for Uniform Illumination by Superposition of Tilted Gaussian Beams,” Opt. Eng. Vol.49, No. 4, April 2010. Doi: 10.1117/1.3407457.

[6] Anthony A. Tovar, “Propagation of Flat-topped Multi-Gaussian Laser Beams,” Opt. Soc. Vol.18, No.8, 2001.

[7] C. Pelliciari, L. Marinangeli, F. Critani, A. Baliva, I. Hutchinson, “Optimization of the MARS-XRD Collimator Using Converging Blades,” Proc. of SPIE Vol. 8076U-1 2011.

[8] F. M. Dickey and S. C. Holswade, *Laser Beam Shaping Theory and Techniques*, *Marcel Dekker*, New York, 2000.

[9] X. Gao, H. Ohashi, H. Okamoto, M. Takasaka, and K. Shinoda, “Beam-shaping technique for improving the beam quality of a high-power laser-diode stack,” Opt. Lett. Vol. 31 (11), 1645-1656 (2006).

[10] V. Sturm, H. G. Trensch, and P. Loosen, “Cylindrical microlenses for collimating high-power diode lasers,” Proc, SPIE 3097, 717-726 (1997).

[11] S. Heinemanna and L. Leininger, “Fiber coupled diode laser and Beam-shaped High-power stacks,” Proc. SPIE 3267, 116-124 (1998).

[12] S. Yamaguchi, “Collimation of emission from a high-power multi-stripe laser-diodebar with multiprism array coupling and focusing to a small spot,” Opt. Lett, 20(8), 898-900 (1995).

[13] LIMO company, retrieved from http://www.limo.de.October 2012.

[14] K. M. Nowak, H. J. Baker, and D. R. Hall, “Efficient laser polishing of silica micro-optic components,” Appl. Opt. 45(1), 162-171 (2006).

[15] Yu-Long Tang, Jin-Fu Niu, Yong Yang, Jian-Qiu Xu, “Beam collimation of high power laser array with graded-index fiber lens array”. Optical Engineering. 47(5), 054202 (May 01 2008); doi: 10.1117/1.2919782.

[16] K. J. Kuhn, *Laser Engineering*, Prentice Hall, New Jersey, 1998.

[17] C.-L. Chen, *Elements of Optoelectronics and Fiber Optics*, Times Mirror Higher Education Group, Chicago, 1996.

[18] Joseph T. Verdeyen, *Laser Electronics*, Prentice Hall, New Jersey, 1981.

[19] P. Hello, C. N. Man, “Design of a Low-Loss Off-Axis Beam Expander”, Appl. Opt., Vol. 35, no, 15, pp. 2534-2536, 1996.

[20] H. Hanada, “Beam Shaping Optical System”, United States Patent #4318594, 1982.

[21] G Borek, DR Brown, D Brown, R Clark. “High performance diffractive optics for beam shaping”. SPIE Proceedings 3633, San Jose, CA, January 1999.

[22] Holo/Or Ltd, retrieved from www.holoor.co.il/index.htm.

[23] www.axetris.com/fiber_micro_lens_arrays.htm.

[24] F. M. Dickey, S. C. Holswade, and D. L. Shealy, *Laser Beam Shaping Applications*, CRC Press, Inc., 2006.

[25] R. E. Ficher, Biljana Tadic-Galeb and P. R. Yoder, *Optical System Design*, McGraw-Hill, Inc., 2008

[26] J. A. Nelder and R. Mead, “A simple method for function minimization”, The computer Journal (1965) 7(4): 308-313; doi: 10.1093/comjnl/7.4.308.

[27] AE Siegman and Mill Valley, *Laser*, CA: University Science Books, Section 18.4, 1986.

[28] D. L. Shealy and S.-H. Chao, “ Geometric Optics-Based Design of Laser Beam shapers”, Opt. Eng., vol. 42, no. 11, pp. 3123-3128, 2003.

[29] *ZEMAX Optical Design Program User’s Guide*, pp.337.

Appendix Developed MALAB Codes Calculating the Parameters and Simulating the Results

```
function
[d1,c1,R1,k1,c22,R22,k22,c31,R31,k31,lam1,lam2,lens4,lens5]=draftns(the
tapp,thetahh,dd,nn,tt,d3,d55,stepss)
%thetapp is the e^(-2)divergence angle in the perpendicular plane;
%thetah  is the e^(-2)divergence angle in the parallel plane;
%dd is the spacing of the souce diodes (delta d)
%nn is the refractive index of the lenses;
%tt is the thickness of each lens;
%d3 is the distance between lenslet 1 and lenslet 2;
%d55 the distance between surface 4/6 and surface 5/7;
%stepss is the number of rays traced for surface 4&5 design;
format long
global n ymax Ymax y0 d5 thetap c1 k1 d1 thetah
%thetav is the e^(-2)divergence angle in the vertical plane (x-z)
%thetap is the e^(-2)divergence angle in the parallel plane (y-z)
%d3 is the spacing of the second and third lens
%-----------------------------------------------------------------
%parameters calculation
n=nn;
d5=d55;
thetap=thetapp;
thetah=thetahh;
thetap=thetap*pi/180;
thetah=thetah*pi/180;
wf=dd/(2*1.75);
%wf is the beam radius output of the lens combination for beam
circulization;
d1=(sqrt(wf^2+(wf/tan(thetap))^2)-n*wf/tan(thetap))/(1-n);
c1=1/(d1*(n-1));
R1=d1*(n-1);
k1=-n^2;
%c1, R1 and k1 are the curvature radius and conic constant of the first
surface;
wf1=rlts(tan(thetah),d1*tan(thetah),c1,k1);
% wf1 is the radis height where the energy drops to e^(-2) in y-z plane
after surface1;
```

```
d2p=(d3*n*wf1-d3*wf1+(wf1^2*((n^2*wf^2+n^2*wf1^2+d3^2*n^2+d3^2-
2*n^2*wf*wf1-2*d3^2*n-(2*d3*(n*((d3^2*n-d3^2+n*wf^2+wf^2+n*wf1^2+wf1^2-
2*n*wf*wf1-2*wf*wf1)/(n-1))^(1/2)+d3))/(n+1)+(2*d3*n*(n*((d3^2*n - d3^2
+ n*wf^2 + wf^2 + n*wf1^2 + wf1^2 - 2*n*wf*wf1 - 2*wf*wf1)/(n -
1))^(1/2) + d3))/(n + 1))/(n^2 -1))^(1/2))/(wf - wf1) +
(wf1*(n*((d3^2*n - d3^2 + n*wf^2 +wf^2 + n*wf1^2 +wf1^2 - 2*n*wf*wf1 -
2*wf*wf1)/(n - 1))^(1/2) + d3))/(n + 1) - (wf*wf1*((n^2*wf^2 +
n^2*wf1^2 + d3^2*n^2 + d3^2 - 2*n^2*wf*wf1 - 2*d3^2*n-(2*d3*(n*((d3^2*n
- d3^2 + n*wf^2 + wf^2 + n*wf1^2 + wf1^2 - 2*n*wf*wf1 - 2*wf*wf1)/(n -
1))^(1/2) + d3))/(n + 1) + (2*d3*n*(n*((d3^2*n - d3^2 + n*wf^2 + wf^2 +
n*wf1^2 + wf1^2 - 2*n*wf*wf1 - 2*wf*wf1)/(n -1))^(1/2) + d3))/(n
+1))/(n^2 -1))^(1/2))/(wf - wf1))/(n*wf - wf - n*wf1 + wf1);
%d2p is the effective focal length of the sencond surface;
c22=1/(d2p*(n-1));
R22=d2p*(n-1);
k22=-n^2;
%c22,R22,k22 are the curvature radius and conic constant of the second
surface;
c31=1/((d2p+d3)*(n-1));
R31=(d2p+d3)*(n-1);
k31=-n^2;
%c31,R31,k31 are the curvature radius and conic constant of the third
surface;
y0=wf;
ymax=dd/2;%working aperture of the lens4;
Ymax=dd/2;%working aperture of the lens5;
zzy=zeros((stepss+1),1);% the initial value of the z
errb=zeros(1,(stepss+1));% the ingetration error;
h=ymax/stepss; %the step segment of the integration
for i=1:stepss
  [T,Y]= quadgk(@rigid,0,i.*h,'RelTol',1e-13,'AbsTol',1e-14);
  zzy(i+1)=T;
  errb(i+1)=Y;
end
yy=h*(0:stepss);
yy=yy';
Ay=quadgk(@intensity,-ymax,ymax,'RelTol',1e-13,'AbsTol',1e-14);
YY2=zeros(length(yy),1);
for i=2:length(yy)
    YY21=(2*Ymax/Ay)*quadgk(@intensity,0,yy(i),'RelTol',1e-
13,'AbsTol',1e-14);
    YY2(i)=YY21;
end
one=ones(length(yy),1);
deltazZ=(n*d5*(n-1)*one+sqrt(d5^2*(n-1)^2*one+(n^2-1)*(YY2-
yy).^2))./(n^2-1);
ZZY2=zzy+deltazZ;
ZZY2=ZZY2-d5*one;
yy=[-yy(length(yy):-1:2,1);yy(1);yy(2:length(yy),1)];
zzy=[zzy(length(zzy):-1:2,1);zzy(1);zzy(2:length(zzy),1)];
YY2=[-YY2(length(YY2):-1:2,1);YY2(1);YY2(2:length(YY2),1)];
ZZY2=[ZZY2(length(ZZY2):-1:2,1);ZZY2(1);ZZY2(2:length(ZZY2),1)];
plot(zzy,yy);% the figure of the back surface of lens 4
hold on;
plot(ZZY2,YY2);% the figure of the front surface of lens 5
hold off;
lens4=[yy,zzy];
```

```
lens5=[YY2,ZZY2];
%------------------------------------------------------------------------
%------------------------------------------------------------------------
%Surface fitting
Data=[yy,zzy];
t = Data(:,1);
y = Data(:,2);
one=ones(length(t),1);
banana=@(lam) lamfunction(lam,Data)
options =
optimset('Display','iter','MaxIter',5000,'MaxFunEvals',100000,'TolFun',
1e-100,'TolX',1e-100);
[lam,fval]=fminsearch(banana,[0.01,0.01,0.001,0.0001,0.00001,0.00000001
],options);
lam1=lam;
figure;
plot(lamf(lam1,Data),t,'red',zzy,yy,'green');
Data=[YY2,ZZY2];
t = Data(:,1);
y = Data(:,2);
one=ones(length(t),1);
banana=@(lam) lamfunction(lam,Data)
options =
optimset('Display','iter','MaxIter',10000,'MaxFunEvals',100000,'TolFun'
,1e-100,'TolX',1e-100);
[lam,fval]=fminsearch(banana,[0.01,0.01,0.001,0.0001,0.00001,0.00000001
],options);
lam2=lam;
figure;
plot(lamf(lam2,Data),t,'red',ZZY2,YY2,'green')
%------------------------------------------------------------------------
%------------------------------------------------------------------------
%ray tracing in the perpendicular direction
figure;
ezplot('0',[0,d1+1.6+4]);
axis([0,d1+1.6+4+0.1,-0.3,0.3]);
hold on;
fh1p=@(x,y)  (x-d1)-c1*y^2/(1+sqrt(1-(1+k1)*c1^2*y^2))
ezplot(fh1p,[d1,d1+z1(dd/2,c1,k1),-0.25,0.25]);
line([d1+tt d1+tt],[-dd/2 dd/2]);
line([d1+z1(dd/2,c1,k1) d1+tt],[dd/2 dd/2]);
line([d1+z1(dd/2,c1,k1) d1+tt],[-dd/2 -dd/2]);
line([d1+tt+d3 d1+tt+d3],[-dd/2 dd/2]);
line([d1+2*tt+d3 d1+2*tt+d3],[-dd/2 dd/2]);
line([d1+tt+d3 d1+2*tt+d3],[-dd/2 -dd/2]);
line([d1+tt+d3 d1+2*tt+d3],[dd/2 dd/2]);
line([d1+tt+d3 d1+tt+d3],[-dd/2 dd/2]);
line([d1+2*tt+d3 d1+2*tt+d3],[-dd/2 dd/2]);
line([d1+tt+d3 d1+2*tt+d3],[-dd/2 -dd/2]);
line([d1+tt+d3 d1+2*tt+d3],[dd/2 dd/2]);
line([d1+2*tt+2*d3 d1+2*tt+2*d3],[-dd/2 dd/2]);
plot(zzy+(d1+3*tt+2*d3)*(zzy./zzy),yy);
line([d1+2*tt+2*d3 d1+3*tt+2*d3+zzy(length(zzy))],[-dd/2 -dd/2]);
line([d1+2*tt+2*d3 d1+3*tt+2*d3+zzy(length(zzy))],[dd/2 dd/2]);
plot(ZZY2+(d1+3*tt+3*d3)*(ZZY2./ZZY2),yy);
line([d1+4*tt+3*d3 d1+4*tt+3*d3],[-dd/2 dd/2]);
line([d1+3*tt+3*d3+ZZY2(length(ZZY2)) d1+4*tt+3*d3],[dd/2 dd/2]);
```

```
line([d1+3*tt+3*d3+ZZY2(length(ZZY2)) d1+4*tt+3*d3],[-dd/2 -dd/2]);
Tray6px=zeros(1,10); Tray6py=zeros(1,10);
Tray7px=zeros(1,10); Tray7py=zeros(1,10);
Tindex=[300 626 763 855 931 1071 1147 1239 1376 1702];
for i=1:10
    Tray6px(i)=d1+3*tt+2*d3+zzy(Tindex(i));
    Tray6py(i)=yy(Tindex(i));
    Tray7px(i)=d1+3*tt+3*d3+zzy(Tindex(i));
    Tray7py(i)=YY2(Tindex(i));
end
Tray1py=z1(Tray6py,c1,k1);
for i=1:10
    line([Tray7px(i) 6],[Tray7py(i) Tray7py(i)])
    line([Tray6px(i) Tray7px(i)],[Tray6py(i) Tray7py(i)]);
    line([d1+Tray1py(i) Tray6px(i)],[Tray6py(i) Tray6py(i)]);
    line([0 d1+Tray1py(i)],[0 Tray6py(i)]);
end
%-------------------------------------------------------------------------
%-------------------------------------------------------------------------
%ray tracing in the perpendicular direction
figure;
ezplot('0',[0,d1+1.6+4]);
axis([0,d1+1.6+4+0.1,-0.3,0.3]);
hold on;
fh1p=@(x,y)  (x-d1)-c1*y^2/(1+sqrt(1-(1+k1)*c1^2*y^2))
ezplot(fh1p,[d1,d1+z1(dd/2,c1,k1),-0.25,0.25]);
fh2h=@(x,y)  (x-d1-tt)-c22*y^2/(1+sqrt(1-(1+k22)*c22^2*y^2))
ezplot(fh2h,[d1+tt,d1+tt+z1(dd/2,c22,k22),-0.25,0.25]);
line([d1+z1(dd/2,c1,k1) d1+tt+z1(dd/2,c22,k22)],[dd/2 dd/2]);
line([d1+z1(dd/2,c1,k1) d1+tt+z1(dd/2,c22,k22)],[-dd/2 -dd/2]);
fh3h=@(x,y)  (x-d1-tt-d3)-c31*y^2/(1+sqrt(1-(1+k31)*c31^2*y^2))
ezplot(fh3h,[d1+tt+d3,d1+tt+d3+z1(dd/2,c31,k31),-0.25,0.25]);
plot(zzy+(d1+2*tt+d3)*(zzy./zzy),yy);
line([d1+tt+d3+z1(dd/2,c31,k31) d1+2*tt+d3+zzy(length(zzy))],[dd/2
dd/2]);
line([d1+tt+d3+z1(dd/2,c31,k31) d1+2*tt+d3+zzy(length(zzy))],[-dd/2 -
dd/2]);
plot(ZZY2+(d1+2*tt+2*d3)*(ZZY2./ZZY2),yy);
line([d1+3*tt+2*d3 d1+3*tt+2*d3],[-dd/2 dd/2]);
line([d1+2*tt+2*d3+ZZY2(length(ZZY2)) d1+3*tt+2*d3],[dd/2 dd/2]);
line([d1+2*tt+2*d3+ZZY2(length(ZZY2)) d1+3*tt+2*d3],[-dd/2 -dd/2]);
line([d1+3*tt+3*d3 d1+3*tt+3*d3],[-dd/2 dd/2]);
line([d1+4*tt+3*d3 d1+4*tt+3*d3],[-dd/2 dd/2]);
line([d1+3*tt+3*d3 d1+4*tt+3*d3],[dd/2 dd/2]);
line([d1+3*tt+3*d3 d1+4*tt+3*d3],[-dd/2 -dd/2]);
Tray4hx=zeros(1,10); Tray4hy=zeros(1,10);
Tray5hx=zeros(1,10); Tray5hy=zeros(1,10);
Tindex=[300 626 763 855 931 1071 1147 1239 1376 1702];
for i=1:10
    Tray4hx(i)=d1+2*tt+d3+zzy(Tindex(i));
    Tray4hy(i)=yy(Tindex(i));
    Tray5hx(i)=d1+2*tt+2*d3+zzy(Tindex(i));
    Tray5hy(i)=YY2(Tindex(i));
end
Tsag3h=z1(Tray4hy,c31,k31);
Tray3hx=d1+tt+d3+Tsag3h;
Tray2hy=zeros(1,10);
```

```
for i=1:10
    Tk3h=Tray4hy(i)/(d2p+d3+Tsag3h(i));
    fh2h=@(y) c22.*y.^2.*Tk3h./(1+sqrt(1-
(1+k22).*c22.^2.*y.^2))+Tk3h.*d2p-y;
    [x,fval]=fsolve(fh2h,[-0.25;0.25]);
    Tray2hy(i)=x(1);
end
Tray2hx=d1+tt+z1(Tray2hy,c22,k22);
Tray1hx=d1+z1(Tray2hy,c1,k1);
for i=1:10
    line([Tray5hx(i) 6],[Tray5hy(i) Tray5hy(i)])
    line([Tray4hx(i) Tray5hx(i)],[Tray4hy(i) Tray5hy(i)]);
    line([Tray3hx(i) Tray4hx(i)],[Tray4hy(i) Tray4hy(i)]);
    line([Tray2hx(i) Tray3hx(i)],[Tray2hy(i) Tray4hy(i)]);
    line([Tray1hx(i) Tray2hx(i)],[Tray2hy(i) Tray2hy(i)]);
    line([0 Tray1hx(i)],[0 Tray2hy(i)]);
end
%-------------------------------------------------------------------------
%-------------------------------------------------------------------------
%irradiance distribution after surface 1 in perpendicular direction;
duanshu=201;                  %number of segments in the surface
aperture;
duanju=dd/duanshu;            %the size of each segments;
duan=(-dd/2+duanju):duanju:(dd/2);  %the matrix of the segment
coordinate;
rayshu=20001;                 % the number of light traced for energy;
rayju=dd/(rayshu-1);   %the spacing between the original traced light
rays;
ray1p=(-dd/2):(rayju):(dd/2); % the matrix of the coordinate of the
original traced rays
%surface 1 in perpendicular direction;
Iray1p=ones(1,(rayshu-1));  % the intensity matrix;
for i=1:(rayshu-1)
    dIray1p=quadgk(@intensity,ray1p(i),ray1p(i+1),'RelTol',1e-
13,'AbsTol',1e-14);
    Iray1p(i)=dIray1p;
end
Iray1p=Iray1p/(quadgk(@intensity,ray1p(1),ray1p(rayshu),'RelTol',1e-
13,'AbsTol',1e-14));
Iduan1p=zeros(1,duanshu);
j=2;
for i=1:duanshu
        while (j<=rayshu)&&(ray1p(j))<=(duan(i))
        Iduan1p(i)=Iray1p(j-1)+Iduan1p(i);
        j=j+1;
        end
end
figure;
plot(duan,Iduan1p,'o')
%-------------------------------------------------------------------------
%-------------------------------------------------------------------------
%irradiance distribution after surface 8 in perpentdicular direction;
ray8p=zeros(1,rayshu);
Ay=quadgk(@intensity,-ymax,ymax,'RelTol',1e-13,'AbsTol',1e-14);
for i=1:rayshu
    dray8p=(2*Ymax/Ay)*quadgk(@intensity,0,ray1p(i),'RelTol',1e-
13,'AbsTol',1e-14);
```

```
    ray8p(i)=dray8p;
end
ray8p(10001)=0;
Iduan8p=zeros(1,duanshu);
j=2;
for i=1:duanshu
        while (j<=rayshu)&&(ray8p(j))<=(duan(i))
        Iduan8p(i)=Iray1p(j-1)+Iduan8p(i);
        j=j+1;
        end
end
figure;
plot(duan,Iduan8p,'-o')
axis([-0.25 0.25 0 5.15*10^(-3)]);
%-------------------------------------------------------------------------
%-------------------------------------------------------------------------
%irradiance distribution after surface 1 in parallel direction;
ray1h=(-dd/2):(rayju):(dd/2);% the matrix of the coordinate of the
original
%traced rays surface 1 in perpendicular direction;
Iray1h=ones(1,(rayshu-1));  % the intensity matrix for surface
1(parallel)
for i=1:(rayshu-1)
    dIray1h=quadgk(@intensityH,ray1h(i),ray1h(i+1),'RelTol',1e-
13,'AbsTol',1e-14);
    Iray1h(i)=dIray1h;
end
Iray1h=Iray1h/(quadgk(@intensityH,ray1h(1),ray1h(rayshu),'RelTol',1e-
13,'AbsTol',1e-14));
Iduan1h=zeros(1,duanshu);
j=2;
for i=1:duanshu
        while (j<=rayshu)&&(ray1h(j))<=(duan(i))
        Iduan1h(i)=Iray1h(j-1)+Iduan1h(i);
        j=j+1;
        end
end
figure;
plot(duan,Iduan1h,'o')
%-------------------------------------------------------------------------
%-------------------------------------------------------------------------
%irradiance distribution after surface 3;
ray3h=(-dd/2):(rayju):(dd/2);
sag3h=z1(ray3h,c31,k31);
ray2h=zeros(1,rayshu);
for i=1:rayshu
    k3h=ray3h(i)/(d2p+d3+sag3h(i));
    fh=@(y) c22.*y.^2.*k3h./(1+sqrt(1-(1+k22).*c22.^2.*y.^2))+k3h.*d2p-
y;
    [x,fval]=fsolve(fh,[-0.25;0.25]);
    ray2h(i)=x(1);
end
Iray2h=ones(1,(rayshu-1));
for i=1:(rayshu-1)
    dIray2h=quadgk(@intensityH,ray2h(i),ray2h(i+1),'RelTol',1e-
13,'AbsTol',1e-14);
    Iray2h(i)=dIray2h;
```

```
end
Iray2h=Iray2h/(quadgk(@intensityH,ray2h(1),ray2h(rayshu),'RelTol',1e-
13,'AbsTol',1e-14));
Iduan3h=zeros(1,duanshu);
j=2;
for i=1:duanshu
        while (j<=rayshu)&&(ray3h(j))<=(duan(i))
        Iduan3h(i)=Iray2h(j-1)+Iduan3h(i);
        j=j+1;
        end
end
figure;
plot(duan,Iduan3h,'o')
%-------------------------------------------------------------------------
%-------------------------------------------------------------------------
%irradiance distribution after surface 5
ray5h=zeros(1,rayshu);
Ay=quadgk(@intensity,-ymax,ymax,'RelTol',1e-13,'AbsTol',1e-14);
for i=1:rayshu
    dray5h=(2*Ymax/Ay)*quadgk(@intensity,0,ray3h(i),'RelTol',1e-
13,'AbsTol',1e-14);
    ray5h(i)=dray5h;
end
ray5h(10001)=0;
Iduan5h=zeros(1,duanshu);
j=2;
for i=1:duanshu
        while (j<=rayshu)&&(ray5h(j))<=(duan(i))
        Iduan5h(i)=Iray2h(j-1)+Iduan5h(i);
        j=j+1;
        end
end
figure;
plot(duan,Iduan5h,'-o')
axis([-0.25 0.25 0 5.6*10^(-3)]);
%-------------------------------------------------------------------------

end

function sag=z1(r,c,k)
% z1 is the sag functionof conic surface;
one=r./r;
sag=c*r.^2./(one+sqrt(one-(1+k)*c^2*r.^2));
end

function w=rlts(a,b,c,k)
% the y or x value of the intersection point between the line and the
% aspheric surface
w=(a + b*c + b*c*k - (a*(k*(1 - b^2*c^2*k - 2*a*b*c - b^2*c^2)^(1/2) +
(1 - b^2*c^2*k - 2*a*b*c - b^2*c^2)^(1/2) + a^2 + a*b*c +
a*b*c*k))/(a^2 + k + 1))/(c + c*k);
end

function dy=rigid(t)
% rigid is the derivative of the sag function of the surface 4;
% t is the matrix of the ray heights of the traced rays;
global n ymax Ymax d5
```

```
n0=1;
T=ones(t);
Ay=quadgk(@intensity,-ymax,ymax,'RelTol',1e-13,'AbsTol',1e-14);
for i=1:length(t)
    T1=(2*Ymax/Ay)*quadgk(@intensity,0,t(i),'RelTol',1e-13,'AbsTol',1e-
14);
    T(i)=T1;
end
deltaz=(n.*d5.*(n-n0)+n0.*sqrt(d5.^2.*(n-n0).^2+(n.^2-n0.^2).*(T-
t).^2))./(n.^2-n0.^2);
%one=ones(length(T));
%slopeangle=-(log(-(T + deltaz*1i - t*one - deltaz.*n.*((T.^2 - 2.*T.*t
+ deltaz.^2 + (t*one).^2)./deltaz.^2).^(1/2).*1i)./(T - deltaz*1i -
t*one + deltaz.*n.*((T.^2 - 2.*T.*t + deltaz.^2 +
(t*one).^2)./deltaz.^2).^(1/2).*1i)).*1i)./2;
%dy=tan(slopeangle);
dy=(-(T-t).*deltaz-n.*(T-t).*sqrt(deltaz.^2+(T-t).^2))./((1-
n.^2).*(deltaz).^2-n.^2.*(T-t).^2);

end

function f = lamfunction(x,Data)
% lamfunction is the merit function for fitting process
t = Data(:,1); y = Data(:,2);
one=ones(length(t),1);
yEst=x(1)*t.^(2)./(one+sqrt(one-(one+x(2)*one).*x(1)^2.*t.^(2)));
for i=3:length(x)
    yEst=yEst+x(i)*t.^(2*(i-2));
end
f=y-yEst;
f=f.^2;
f=10^5*sqrt(sum(f)/length(f));
end

function yEstimate = lamf(x,Data) % lamf is the even asphere sag
function
t = Data(:,1); y = Data(:,2);
one=ones(length(t),1);
yEstimate=x(1)*t.^(2)./(one+sqrt(one-(one+x(2)*one).*x(1)^2.*t.^(2)));
for i=3:length(x)
    yEstimate=yEstimate+x(i)*t.^(2*(i-2));
end
end

function I=intensity(x)% the intensity at ray height x in perpendicular
direction;
global c1 k1 d1 thetap
z11=z1(x,c1,k1);
one=z11./z11;
thetax=atan(x./(d1*one+z11));
I=exp(-2*(thetax/thetap).^2);
end

function I=intensityH(x)% the intensity at ray height x in parallel
direction;
global c1 k1 d1 thetah
z11=z1(x,c1,k1);
```

```
one=z11./z11;
thetax=atan(x./(d1*one+z11));
I=exp(-2*(thetax/thetah).^2);
end
```